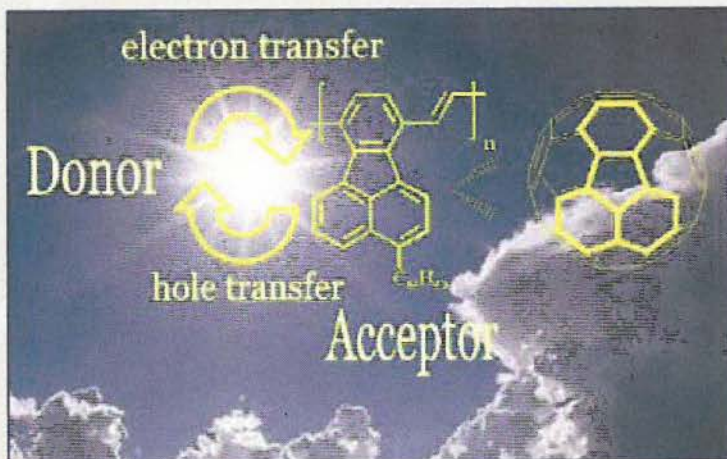


DOCTORAATSPROEFSCHRIFT

2008 | Faculteit Wetenschappen



Non-alternant cyclo-penta fused polycyclic aromatic hydrocarbons: Efficient structural elements to achieve n-type characteristics in conjugated polymers

Proefschrift voorgelegd tot het behalen van de graad van Doctor in de Wetenschappen, richting scheikunde, te verdedigen door:

Arne PALMAERTS

Promotor: Prof. dr. Thomas J. Cleij
Copromotor: Prof. dr. Dirk Vanderzande

 universiteit
hasselt


INSTITUUT VOOR
MATERIAALONDERZOEK

541.64

BIBLIOTHEEK UNIVERSITEIT HASSELT

03 04 0085216 3





541.64
PALM
2008

uhasselt

DOCTORAATSPROEFSCHRIFT

2008 | Faculteit Wetenschappen

Non-alternant cyclo-penta fused polycyclic aromatic hydrocarbons: Efficient structural elements to achieve n-type characteristics in conjugated polymers

Proefschrift voorgelegd tot het behalen van de graad van
Doctor in de Wetenschappen, richting scheikunde, te verdedigen door:

Arne PALMAERTS

Promotor: Prof. dr. Thomas J. Cleij
Copromotor: Prof. dr. Dirk Vanderzande



 universiteit
hasselt

INSTITUUT VOOR
MATERIAALONDERZOEK

D/2008/2451/40



Table of Contents

1. GENERAL INTRODUCTION	1
1.1. Introduction.....	2
1.2. Motivation for optoelectronic devices based on polymers.....	4
1.3. Applications of conjugated polymers.....	5
1.4. Plastic solar cells.....	7
1.4.1. <i>Physical processes in polymer:fullerene bulk heterojunction solar cells</i>	8
1.4.2. <i>Basic description of a photovoltaic device</i>	11
1.5. Aim and outline.....	14
1.6. Outline of this thesis.....	18
1.7. References.....	19
2. SYNTHESIS OF POLY(P-FLUORANTHENE VINYLENE)	25
2.1. Introduction.....	26
2.2. N-type materials.....	27
2.2.1. <i>Fullerenes</i>	27
2.2.2. <i>N-type polymers</i>	28
2.2.3. <i>Search for a new class of n-type conjugated polymers</i>	35
2.3. Synthesis.....	36
2.3.1. <i>Synthesis of the fluoranthene containing monomer</i>	36
2.3.2. <i>Polymerization</i>	38
2.4. Determination of the electrochemical and optical properties of poly(p-fluoranthene vinylene).....	39
2.4.1. <i>In situ UV-Vis spectroscopy and in situ FT-IR spectroscopy</i>	39
2.4.2. <i>cyclic voltammetry</i>	43
2.5. Conclusion.....	45
2.6. Experimental section.....	46
2.7. References.....	50
3. SYNTHESIS OF ALKYL-POLY(P-FLUORANTHENE VINYLENE)	55
3.1. Introduction.....	56
3.2. Synthesis.....	57
3.2.1. <i>Monomer Synthesis</i>	57
3.2.2. <i>Polymerization</i>	60
3.3. Determination of the electrochemical and optical properties of the poly(p-fluoranthene vinylene) derivatives.....	61
3.3.1. <i>Optical Properties</i>	61
3.3.2. <i>Electronic Properties</i>	67
3.3.3. <i>Mobility Measurements</i>	68
3.4. Conclusion.....	72
3.5. Experimental.....	73
3.6. References.....	83

4. COMPARING THE TRANSPORT PROPERTIES OF CONJUGATED POLYMERS WITH POLYCYCLIC AROMATIC HYDROCARBONS SUBSTRUCTURES IN THE BACKBONE	85
4.1. Introduction.....	86
4.1.1. Polycyclic Aromatic Hydrocarbons PAH.....	87
4.1.2. Charge transport.....	89
4.1.3. Hole only devices.....	90
4.1.4. LED devices.....	90
4.2. Synthesis.....	92
4.2.1. Dodecyl-PFV.....	92
4.2.2. Poly (2,7-Pyrene Vinylene) PPyV.....	92
4.3. Evaluation of the conversion process using <i>in situ</i> UV-Vis and FT-IR spectroscopy.....	93
4.4. Transport properties of PPyV and dodecyl-PFV.....	95
4.5. Conclusion.....	99
4.6. Experimental Section.....	100
4.7. References.....	105
5. TOWARDS COMPLEX ARCHITECTURES OF PPV TYPE POLYMERS FOR DEVICE APPLICATIONS	107
5.1. Introduction.....	108
5.2. Radical polymerization.....	111
5.2.1. The effect of temperature in the radical polymerization.....	113
5.2.2. The effect of concentration in the radical polymerization.....	115
5.3. Green light emitting copolymer with both conjugated and non-conjugated segments.....	118
5.3.1. Copolymerization.....	119
5.3.2. Device Fabrication and Characterization.....	124
5.4. Conclusion.....	128
5.5. Experimental.....	129
5.6. References.....	133
6. POLY(THIENYLENE VINYLENE)	135
6.1. Introduction.....	136
6.2. Transport properties of C ₈ -PTV and BOP-PTV.....	139
6.3. Cyclic Voltammetry.....	140
6.4. Solar cells.....	141
6.5. Absorption.....	143
6.6. Conclusion.....	145
6.7. Experimental Section.....	146
6.8. References.....	147
SUMMARY	149
SAMENVATTING	153
DANKWOORD	157

Chapter 1

General Introduction

Abstract

In the field of organic semiconductors, organic light-emitting diode (OLED) technology has already been commercialized. Although the photovoltaic industry has experienced a phenomenal annual 20% growth rate over the last decade, the general public has just started to realize its potential as an environmentally friendly and renewable energy source. The commercialization of plastic photovoltaic devices has yet to begin. From an overview of the advantages and disadvantages of the use of conjugated polymers, the significant industrial potential of these plastics becomes immediately obvious. As will be presented in the aim and outline of this thesis, we have a special interest in the design, synthesis and characterization of n-type conjugated polymers.

1.1. Introduction

Plastics, or polymers, are found throughout everyday life in applications ranging from food packaging to mobile phones. A wide variety of reasons can be identified explaining the popularity of polymers. Two of these reasons are especially of interest in the context of the research described in this thesis. First of all, there is an enormous array of potential structures, leading to a huge variety of properties. Secondly polymers are easy to process and shape, which results in simple manufacturing processes.

Another interesting class of materials consists of semiconductors, which are usually traditional inorganic materials such as Si and GaAs. They are used to make amongst others transistors, lasers and solar cells. They form the basis of modern electronics and optoelectronics. Semiconductive polymers combine typical semiconductor properties with the simple processing of polymers. Moreover, these semiconductive conjugated polymers can be dissolved in a wide range of solvents and printed as inks to make electronic devices.¹⁻³ This can be a large advantage over traditional semiconductors.

Polymers are usually long, chain-like molecules with a regular repeating unit, such as polyethylene, which is widely used in packaging materials. Semiconducting properties arise from using conjugated repeat units, *e.g.* a repeat unit in which there is a linear pattern of alternating single and double bonds. Some examples of conjugated polymers are shown in Figure 1. The alternating single and double bonds lead to one electron in a p orbital on each carbon atom. These p orbitals overlap, resulting in electron delocalization and semiconducting behaviour.⁴

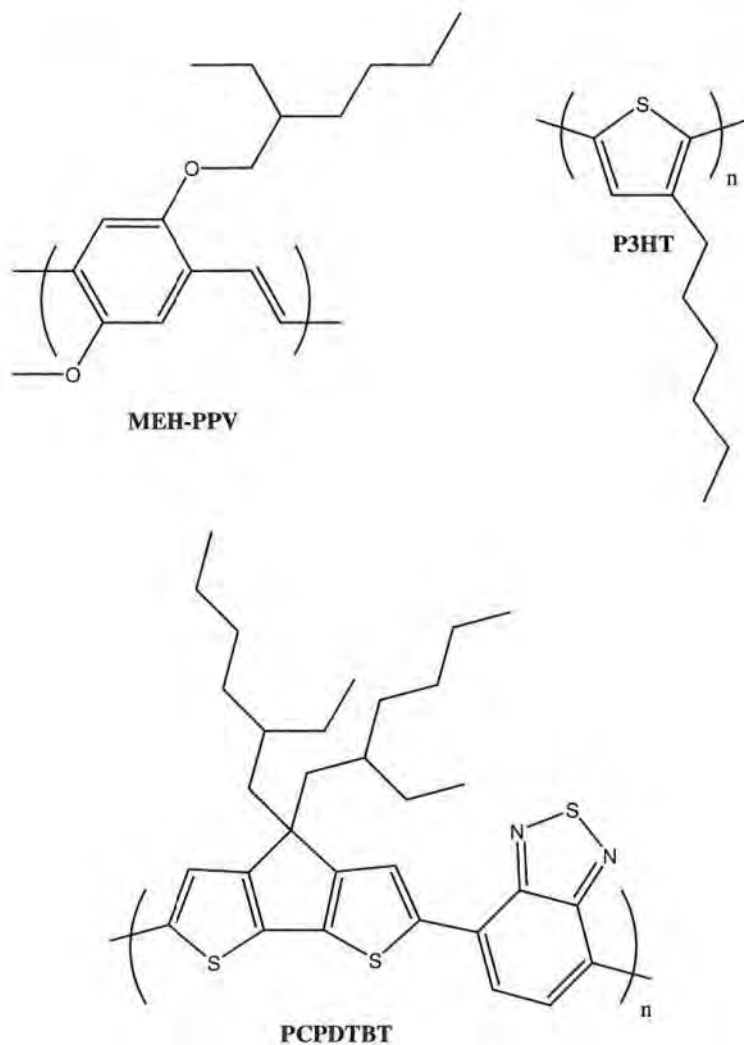


Figure 1. An overview of the molecular structures of some typical conjugated polymers. (a) poly(2-methoxy-5-(2'-ethyl-hexyloxy)-1,4-phenylene vinylene (**MEH-PPV**)⁵ (b) poly(3-hexylthiophene) (**P3HT**)⁶ and (c) poly[2,6-(4,4-bis-(2-ethylhexyl)-4H-cyclopenta[2,1-b;3,4-6']dithiophene)-alt-4,7-(2,1,3-benzothiadiazole)] (**PCPDTBT**).^{7,8}

1.2. Motivation for optoelectronic devices based on polymers

One major challenge for the large-scale application of photovoltaics at present is the high cost of commercially available inorganic semiconductor-based solar cells. In contrast, some of the important advantages of these so-called 'plastic' semiconducting materials include low cost of fabrication, large area production, low-energy operation, ease of processing, mechanical flexibility and versatility of chemical structure from advances in organic chemistry. Since these plastic materials can be processed from solution and printed onto plastic substrates, they offer the promise of being lightweight, bendable and inexpensive (Figure 2).⁹⁻¹⁴



Figure 2. a) polymer inks (BASF electronics®)¹⁵ b) roll to roll printing on flexible substrates (PolyIC®)¹⁶ c) a flexible and light weight organic solar cell. (Konarka's PowerPlastic®).¹⁷

1.3. Applications of conjugated polymers

The combination of electronic and optical properties of semi-conductors with the promising properties depicted above, makes conjugated polymers potentially useful for a wide range of applications such as light emitting diodes (LEDs),¹⁸⁻²¹ solar cells,^{9,10,13,14,22-26} transistors,^{20,27-29} biosensors,³⁰⁻³² smart windows^{33,34} and electronically pumped lasers.^{35,36}

So far, only the LEDs have been commercialized. The most challenging performance requirements for LED applications are full coverage of the color spectrum, a light-efficiency of at least 100 cd/m² and a lifetime over 10000 hours (5 years).³⁷ The development of LEDs based on conjugated polymers started only in 1990. Since then, the developments in this field have been rapid. Currently, it is possible to make polymer based full-color displays with a reasonable efficiency and lifetime. The first commercial application of OLEDs was launched in 2002 by Philips as the James Bond 007 shaver in Die Another Day (Figure 3a). Only 6 years later, Samsung showed a 31-Inch OLED with a thickness of just 4.3mm screen at the Consumer Electronics Show 2008 (Figure 3b). Other advantages of OLED TV's are the fast response times, wide viewing angles (178°), energy efficient, exceptional color reproduction, outstanding contrast levels and high brightness. The nature of its technology lends itself for extremely thin and lightweight designs along with the ability to use it in a variety of different applications as rollable displays (Figure 3c). The Dutch company Philips Polymer Vision has a leadership position in the area of rollable displays for the mobile-device industry.



Figure 3. (a) the James Bond 007 shaver with a OLED display (Philips®)³⁸ (b) 31-inch OLED TV (Samsung®)³⁹ and (c) Mobil phone with a integrated rollable OLED display (Polymer Vision®).⁴⁰

All other applications are thus far still rather academic. Conjugated polymers, which are now well established as materials for LEDs, also offer considerable potential as low-cost visible lasers. There are several reasons why semiconducting polymers could be attractive laser materials. The first reason is that there exists a range of polymers that can emit light across the visible spectrum. The polymers usually also have broad spectra, which provides a potential for making tunable lasers. In addition, they have very high absorption coefficients, which implies that there is the potential for extremely strong amplification of light. Furthermore, the absorption and fluorescence spectra are well separated, so that absorption of emitted light is weak. In many fluorescent organic molecules, light emission is severely quenched at high concentrations, such as typically found in solid films. In contrast, conjugated polymers can emit light as neat solid films and, in addition, are capable of charge transport, thereby providing the potential to make electrically pumped lasers in the future. Semiconducting polymers combine the specific advantages for lasing outlined above with the general advantages of polymers, namely the scope for tuning properties by changing the structure, simple fabrication, and the possibility of working with flexible substrates.^{35,36,41-43}

Organic Thin-film transistors (TFT) using semiconducting polymers are most likely to be used in low-performance applications such as displays⁴⁴ and potentially for low-performance radio-frequency identification transponders,⁴⁵ electronic barcodes, ferroelectric memories⁴⁶⁻⁴⁸ or in drivers for flexible displays and in smart sensors. These applications are considered “low performance” due to the low field-effect mobility of transistors in these devices relative to that of single crystalline silicon. The mobility defines the electrical resistance of a TFT and thereby the speed at which it can operate in a circuit. The mobility of semiconducting polymers is controlled both by molecular structure and by their microstructure in a thin film. It has been shown that semiconducting polymers can have a field-effect mobility that approaches that of amorphous silicon, which is used in most liquid crystal flat panel displays.⁴⁹

Since the polymers in this work were developed for possible use in plastic photovoltaics, a more detailed explanation of this application will be given in the following section.

1.4. Plastic solar cells

Nowadays, most of the energy is derived from fossil fuels and nuclear processes. However, these resources are limited and their use can have a serious environmental and political impact. Hence, a transition in energy consumption and production is desirable. In this respect, renewable energy sources are of considerable interest.⁵⁰ Several renewable energy sources are under development or have already been introduced onto the market. Notwithstanding, thus far they make up only a limited part of the total energy production.

Organic photovoltaics offer significant technological potential as an alternative source for electrical energy. Solar cells based on conjugated polymeric materials have several advantages, such as potential flexibility,

low manufacturing costs and straightforward processing. Currently, such solar cells can already reach efficiencies as high as 5.15%.⁵¹ In the energy market the competitive position of every solar technology is mainly determined by three factors, *i.e.* efficiency, lifetime and costs (per W_p). Efficiency and lifetime determine the cost/watt peak. The cost/watt peak is the dominant factor for commercialization.¹³ Although the overall power conversion efficiency of current organic solar cell is relatively low compared to that available from silicon technology, the efficiency can be improved through systematic molecular engineering and development of device architectures, which are optimally matched to the properties of these new photovoltaic materials. In high-power applications, today's organic photovoltaic devices will not be able to compete with crystalline Si solar cells, which have guaranteed lifetimes of tens of years. On the other hand, for many integrated product applications, the lifetime of the components does not necessarily need be significantly longer than the lifetime of the whole product. For the future, organic photovoltaics will most likely provide solutions in applications where price or/and large area challenges play an important role. Inorganic solar cells will most likely predominate in aerospace and defense applications like satellites.⁵²

1.4.1. Physical processes in polymer:fullerene bulk heterojunction solar cells

The schematic structure of a typical polymer photovoltaic device is depicted in Figure 4. In these devices, the photoactive layer is sandwiched between two metal electrodes. One of the electrodes Indium-Tin-Oxide (ITO) is transparent. The photoactive layer typically has a thickness of only a few hundred nanometers.^{26,51,53}

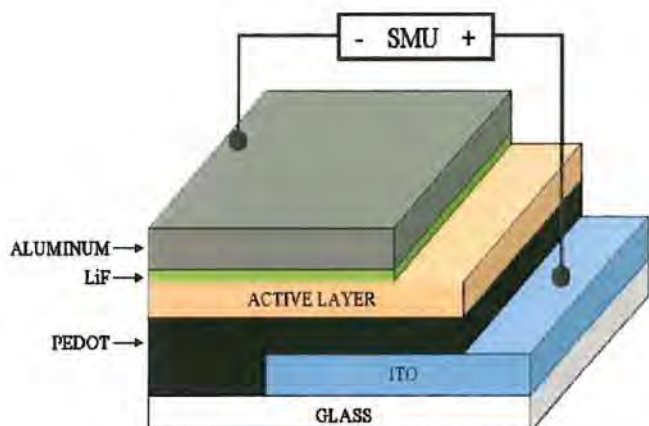


Figure 4. Schematic structure of a bulk heterojunction photovoltaic device.

In general, in a polymer:fullerene bulk heterojunction solar cell six processes occur in the conversion of solar energy into electricity (Figure 5).⁵⁴ When light is absorbed by the donor material (a) an electron is promoted from the highest occupied molecular orbital (HOMO) to the lowest unoccupied molecular orbital (LUMO) creating an exciton. This exciton diffuses towards a donor/acceptor interface (b) where the electron can be transferred to the acceptor material (c). Even though the hole and electron are on different materials, they are still strongly bound by Coulomb interactions and still need to be dissociated into free carriers (d) after which they are transported through the two respective phases and can be collected at the electrodes (f).

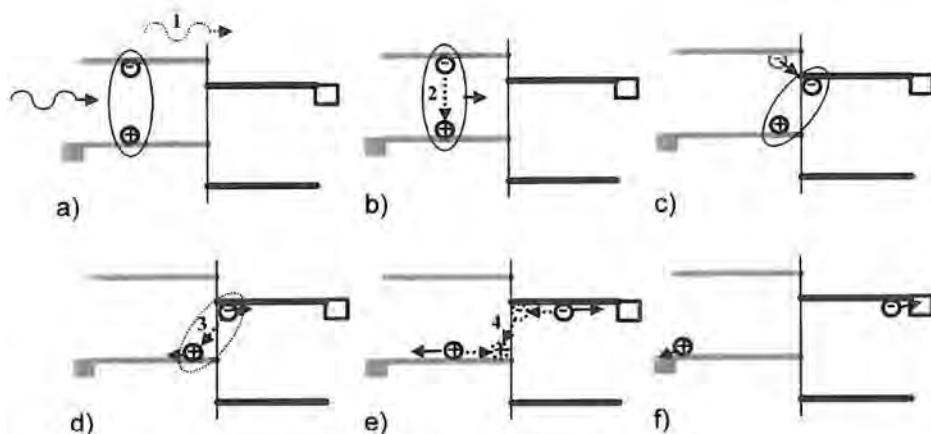


Figure 5. Charge generation in a polymer:fullerene bulk heterojunction solar cell: a) absorption of a photon creating an exciton, b) diffusion of the exciton towards the donor acceptor interface, c) electron transfer from donor to acceptor, d) dissociation of the bound electron hole pair into free carriers, e) transport of free carriers towards the electrodes, f) collection at the electrodes. Loss mechanisms are indicated by 1) non absorbed photons, 2) exciton decay, 3) geminate recombination of the bound pair, 4) bimolecular recombination.

Because of the high absorption coefficient (circa 10^5 cm^{-1}), a layer thickness of only a few hundred nanometer is required to absorb all the incoming light at the peak wavelength absorption. However, the performance of solar cells based on polymers is poor in comparison to inorganic solar cells as a result of the fact that the absorption bands of conjugated polymers are relatively narrow. In addition, when a photon is absorbed by the donor material, a strongly bound exciton (a bound electron-hole pair) is formed. Because of the low dielectric constant (high exciton binding energy) in conjugated polymers, the thermal energy at room temperature is

insufficient to dissociate this photogenerated exciton into free charge carriers. To dissociate the strongly bound exciton into free carriers an electron acceptor is used. Because of the limited exciton diffusion range (5-20 nm), the efficiency of a bilayer cell is limited. To solve this problem, the bulk heterojunction solar cell architecture has been developed by blending the polymer with a soluble electron acceptor. This results in an interpenetrating donor:acceptor network that allows an improved photon harvesting by a simple increase of the active layer thickness, while maintaining an efficient dissociation of excitons. At the donor/acceptor interface the electron is transferred to the acceptor material. Since the distance between hole and electron is very small, both charges are still bound by Coulomb attractions (0.5 eV binding energy). This means that charge transfer occurs, but that the free charge is not yet created. In order to achieve charge separation an electrical field is required, which is provided by the asymmetrical work functions of the two electrodes. Finally, the free electrons and holes must be transported *via* percolated PCBM and polymer pathways towards the electrodes to produce the photocurrent.

During each of the above-mentioned processes energy can be lost resulting in various loss mechanisms (Figure 5). First of all, not all photons are absorbed by the active layer, not only due to limitations of the band gap but also due to the often limited thickness of the active layer. Secondly, excitons will decay when created too far from the D-A interface. Finally after electron transfer, geminate recombination of the bound electron hole pair as well as bimolecular recombination of free charge carriers during transport to the electrodes can occur.

1.4.2. Basic description of a photovoltaic device

The basic parameters describing the performance of photovoltaic solar cells can be extracted from a current-voltage (IV) graph. Such a graph is obtained from a measurement in which the external electrical current is

measured as function of an externally applied voltage. A typical IV characteristic is given in Figure 6 for a PV cell under illumination. Figure 6a depicts the characteristic in semi-logarithmic representation, which is also commonly used. We will focus here on the linear representation to introduce some important photovoltaic parameters (Figure 6b). Upon illumination, the curve passes through the fourth quadrant, meaning that power $P = I \cdot V$ is extracted from device.

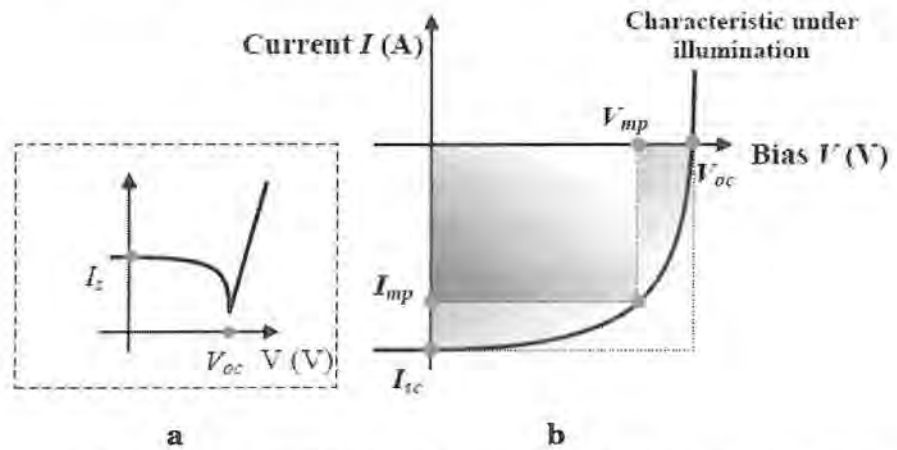


Figure 6. Typical IV curve for a solar cell under illumination with some important photovoltaic parameters indicated, a) shows a semi-logarithmic representation and b) a linear representation of the same data.

The point (V_{mp}, I_{mp}) where this power output is maximized is called the maximum power point P_{mp} and is given by:

$$\text{Equation 1} \quad P_{mp} = V_{mp} \cdot I_{mp}$$

This product corresponds also to the area of the smaller rectangle indicated in Figure 6. There are two other important parameters shown in this figure: the short-circuit current I_{sc} and the open-circuit voltage V_{oc} .

The short-circuit current I_{sc} is the electric current flowing through the device under illumination when no external voltage applied ($V = 0$ V). Since the actually measured short-circuit current depends on the active area of a photovoltaic device, it is often more common to list the short-circuit current density J_{sc} . It results from dividing the measured short-circuit current by active area A of the solar cell. The open-circuit voltage V_{oc} is the value of the external bias that has to be applied such that no external current is flowing through the illuminated device anymore ($I = 0$ A). The V_{oc} is ultimately limited by the energy difference between the HOMO of the donor and the LUMO of the acceptor. This means that the energy offset between donor HOMO and acceptor LUMO not only enables electron transfer but also generates a loss of V_{oc} . Analogous to the rectangle associated with the maximum power point, starting from I_{sc} and V_{oc} a second rectangle can be drawn, *i.e.* the larger rectangle in Figure 6. It can be seen from this figure that the two rectangles will resemble each other more if the IV curve has a more rectangular shape, which would be optimal for the power output. The ratio of the areas of the two rectangles can therefore be regarded as a measure of the quality of the shape of the IV characteristic; it is called the fill factor FF:

$$\text{Equation 2 } FF = V_{mp} \cdot I_{mp} / I_{sc} \cdot V_{oc}$$

It can also be stated that the product of I_{sc} and V_{oc} is the theoretical upper limit for the total power that can be delivered to an external load. The fill factor FF can in this way be defined as the ratio of the actual maximum power extracted and this theoretical upper limit. These parameters relate also to the energy-conversion efficiency η_e as follows:

Equation 3 $\eta_e = P_{mp}/P_{in} = I_{sc} \cdot V_{cc} \cdot FF / A \cdot 100 \text{ (mW/cm}^2\text{)}$

expressing how much of the total power P_{in} of the incident light on the photovoltaic cell is converted into electric power P_{mp} . This expression $P_{in} = A \cdot 100 \text{ (mW/cm}^2\text{)}$ shows that it is necessary to identify the characteristics of the incoming light carefully to have a fair comparison between the performances of different solar cells. A commonly used reference radiation distribution is the global air mass 1.5 spectrum (AM1.5G). The total intensity is scaled to a value of 1000 W/m^2 ($=100 \text{ mW/cm}^2$). It accords rather well to circumstances for Western European countries on a clear sunny day in the summer.

1.5. Aim and outline

Most of the research in the field of bulk heterojunction solar cells has been devoted to the optimization of cells based on poly(3-hexylthiophene) (P3HT) as the donor polymer combined with a soluble derivative of C_{60} , (6,6)-phenyl- C_{61} -butyric acid methyl ester (PCBM), as the electron acceptor.^{55,56}

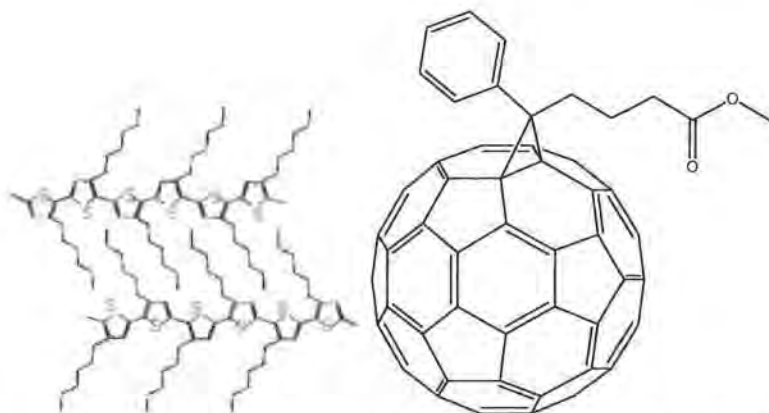


Figure 7. The structural formulae of commonly used compounds in the active layer of a bulk heterojunction solar cell: poly(3-hexylthiophene) (**P3HT**) and (6,6)-phenyl-C₆₁ butyric acid methyl ester (**PCBM**).

Improvements in device fabrication by thermal and solvent annealing have led to external quantum efficiencies surpassing 90% and power-conversion efficiencies around 4%. From this observation it is clear that there is not much room for improvement for this donor-acceptor combination and that there is a continuous need for new materials.⁵⁷ This quest for new materials mostly focuses on the synthesis of novel p-type materials, which can be explained by the fact that such donor materials are better synthetically accessible than n-type polymers. Until now the worldwide effort towards the development of n-type polymers has been quite limited. This is surprising since devices containing a blend of an electron donating and an accepting polymer may have several advantages over the polymer:fullerene bulk heterojunction.

First of all, an alternative for the currently used acceptor material, *i.e.* PCBM, may be of interest to facilitate the formation of an optimal and more stable morphology.⁹ It is well known that mixtures of polymers tend to phase separate as a result of the minimal entropy gains for mixing. Due to

this low entropy, the enthalpic term is dominant in the Gibbs free energy of mixing, and many polymers will tend to phase separate.⁵⁸⁻⁶⁰ This can be an advantage of polymers over lower molecular weight materials, where an optimal level of phase separation may be more complex to control. For efficient exciton dissociation, the photogenerated excitons should reach the donor/acceptor interface within their lifetime. Since the diffusion length of excitons in conjugated polymers is typically in the order of 5-10 nm, the phase separated blend should therefore possess a typical length scale of ~10 nm. Morphology studies on typical mixtures of two polymers show a strong intermixing of the two phases with the size of the polymer domains formed in the blend being of a similar order of magnitude as the exciton diffusion length. It can be shown that the molecular weight of the polymers influences the typical domain size from ~200 nm down to less than 5 nm in these polymer:polymer bulk heterojunction.⁶¹ For efficient charge collection, a continuous network of the donor and acceptor phases throughout the blend is required. The nature of phase-separation is highly dependant upon the relative viscosities, molecular weights, concentrations, interactions between the two polymers, and temperature of the substrate and solution.⁶²⁻⁶⁴

Furthermore, in polymer-fullerene solar cells a comparatively poor overlap exists between the solar spectrum and the optical absorption of the used materials (Figure 8).⁶⁵ Potentially, in all polymer devices both the donor and acceptor materials can contribute significantly to the overall light absorption. It is anticipated that the use of polymer-polymer solar cells will lead to a significant increase of the photon harvesting, which in turn will lead to an improved performance. Ideally both components could cover complementary parts of the solar spectrum. It should be relatively easy to tune both components individually to optimize optical properties, charge transfer and charge collection processes.^{59,60,64,66-71}

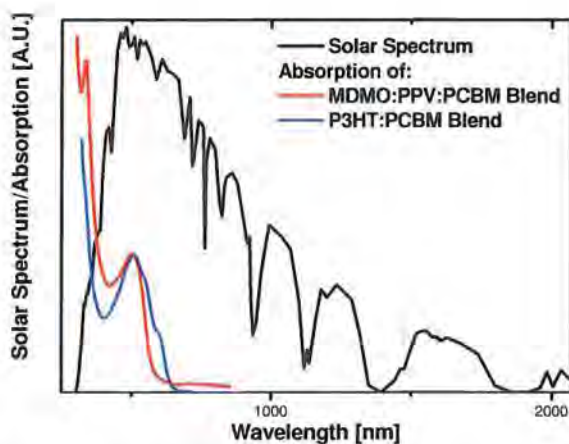


Figure 8. AM 1.5 spectrum, defined as the spectral photon flux on the earth's surface under illumination of 45° (black), compared to the absorption profile of a MDMO-PPV : PCBM (1 : 4) film (red) and the absorption profile of a P3HT : PCBM (1 : 1) film (blue).⁶⁵

When we analyze the HOMO and LUMO levels of the P3HT:PCBM system, a significant loss mechanism can be identified. For an efficient electron transfer from donor to acceptor to occur, it is generally found that the LUMO of the donor needs to be 0.3 eV to 0.5 eV higher than the LUMO of the acceptor. In the case of the reference system P3HT:PCBM, this difference is 1.1 eV. This results in a less than optimal V_{oc} and electron transfer.

There are two different strategies to optimize the solar cell performance, focusing on an adjustment of the energy levels either on the donor or on the acceptor side. By lowering the LUMO of the donor, and thus narrowing the polymer band gap, the absorption is shifted towards lower energy, while maintaining a constant open-circuit voltage (Figure 9a). In this way the photocurrent is improved, due to a better overlap between the donor absorption and the solar spectrum. Making use of a recently developed

device model for polymer:fullerene bulk heterojunction solar cells,⁷² it was calculated that a lowering of the LUMO of the donor ultimately leads to efficiencies in the order of 6.5%. On the other hand, raising the LUMO of the acceptor will directly result in a higher V_{OC} without affecting the absorption of the cell. It has been shown that this approach is more effective, and results in an estimated efficiency of 8.4% when the LUMO offset is reduced with 0.6 eV (Figure 9b). Summarizing, one can conclude that there is a quest for an n-type conjugated material of a polymeric nature with a higher LUMO than PCBM.

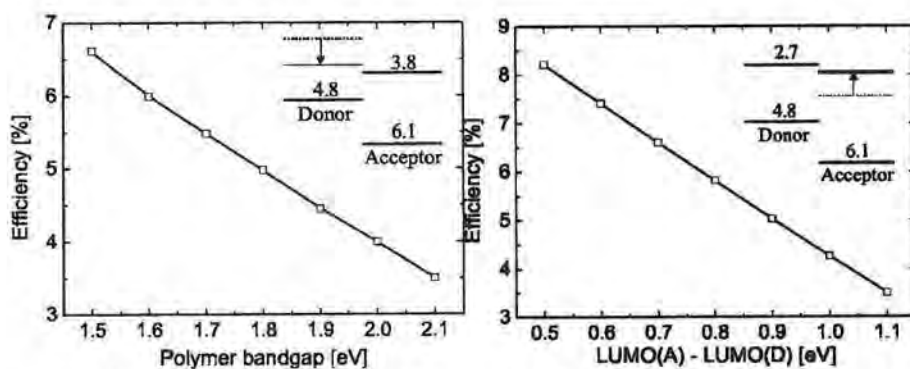


Figure 9. (left) The influence of the band gap of the polymer on device efficiency (symbols). The line is drawn as a guide to the eye. (right) The influence of the offset between the LUMO of the donor and the acceptor (symbols), the line is drawn as a guide to the eye.

1.6. Outline of this thesis

The aim of the research presented in this dissertation is the design and development of a new class of n-type conjugated polymers. This aim is motivated by the expectation that such a class of materials potentially can

offer significant improvements over currently utilized material systems. **Chapter 2** describes our search for and discovery of a novel class of n-type conjugated polymers. The synthesis and characterization of the first representative of this class of polymers, *i.e.* poly(fluoranthene vinylene) **PFV**, is presented. In **chapter 3**, side chains are attached to the fluoranthene groups present in the **PFV** backbone. The major objective for this functionalization with alkyl groups is to improve the solubility and processability. In **chapter 4**, in a special way it is proven that the non-alternant character of fluoranthene is responsible for the highly desirable n-type behavior. Finally, **chapters 5** and **6** focus on our efforts to develop and characterize also other material systems containing conjugated polymers. **Chapter 5** presents a fundamental study of the radical polymerization behavior of PPV and demonstrates the reality of copolymer architectures. Such architectures are expected to facilitate the formation of nano-structured morphologies in thin films. Finally, **chapter 6** focuses on the opto-electronic characterization of a selection of typical novel low band gap conjugated polymer systems. Finally towards the end of this thesis general conclusions, perspectives and summaries in Dutch and English will be presented.

1.7. References

- (1) Heeger, A. J. *Rev. Mod. Phys.* **2001**, 73, 681.
- (2) Friend, R. H.; Gymer, R. W.; Holmes, A. B.; Burroughes, J. H.; Marks, R. N.; Taliani, C.; Bradley, D. D. C.; Dos Santos, D. A.; Bredas, J. L.; Logdlund, M. and Salaneck, W. R. *Nature* **1999**, 397, 121.
- (3) Samuel, I. D. W. *Philos. Trans. R. Soc. Londen* **2000**, 358, 193.
- (4) Samuel, I. D. W. and Turnbull, G. A. *Materials Today*, **2004**, 7, (9), 28.

- (5) Munters, T.; Martens, T.; Goris, L.; Beelen Z.; Goris, L.; Manca, J.; D'Olieslaeger, M.; Vanderzande, D.; De Schepper, L. and Andriessen, R. *Thin Solid Films* **2002**, *403*, 243.
- (6) Irwin, M. D.; Buchholz, B.; Hains, A. W.; Chang, R. P. H.; Marks, T. J., *Proc. Natl. Acad. Sci. USA* **2008**, *105*, 2783-2787.
- (7) Soci, C.; Hwang, I. W.; Moses, D.; Zhu, Z.; Waller, D.; Gaudiana, R.; Brabec C. J.; Heeger, A. J., *Adv. Funct. Mater.* **2007**, *17*, 632-636.
- (8) Muhlbacher, D.; Scharber, M.; Morana, M.; Zhu, Z.; Waller, D.; Gaudiana, R.; Brabec, C. J., *Adv. Mater.* **2006**, *18*, 2931-2931.
- (9) Hoppe, H. and Sariciftci, N. S. *J. Mater. Res.* **2004**, *19*, (7), 1924.
- (10) Spanggaard, H. and Krebs, F. C. *Sol. Energy Mater. Sol. Cells* **2004**, *83*, (2-3), 125.
- (11) de Gans, B. J.; Duineveld, P. C. and Schubert, U. S. *Adv. Mater.* **2004**, *16*, (3), 203.
- (12) Sheats, J. R. *J. Mater. Res.* **2004**, *19*, (7), 1974.
- (13) Brabec, C. J. *Sol. Energy Mater. Sol. Cells* **2004**, *83*, (2-3), 273.
- (14) Thompson, B. C.; Fréchet, M. J. *Angew. Chem. Int. Ed.* **2008**, *47*, 58.
- (15) <http://www.basf-fb.de/en/projects/printed-electronics.html>
- (16) <http://www.polyic.com/en/technology.php>
- (17) http://www.konarka.com/img/homepage/home_page_catch3.jpg
- (18) Geffroy, B.; Le Roy, P. and Prat, C. *Polym.* **2006**, *55*, (6), 572.
- (19) Burroughes, J. H.; Bradley, D. D. C.; Brown A. R.; Marks, R. N.; Mackay, K.; Friend, R. H.; Burns, P. L. and Holmes, A. B. *Nature* **1990**, *347*, 539.
- (20) Burroughes, J. H.; Jones, C. A. and Friend, R. H. *Nature* **1988**, *335*, 137.
- (21) Bradley, D. D. C. *Synth. Met.* **1993**, *54*, (1-3), 401.
- (22) Brabec, C. J.; Sariciftci, N. S. and Hummelen, J. C. *Adv. Funct. Mater.* **2001**, *11*, (1), 15.

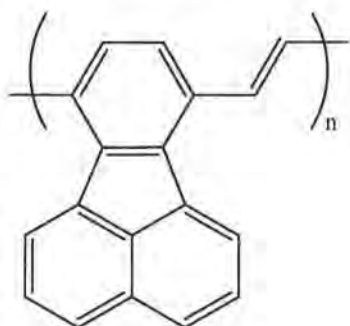
- (23) Nelson, J. *Materials Today* **2002**, 5, (5), 20.
- (24) Dennler, G. and Sariciftci, N. S. *Proc. IEEE* **2005**, 93, (8), 1429.
- (25) Coakley, K. M. and McGehee, M. D. *Chem. Mat.* **2004**, 16, (23), 4533.
- (26) Brabec, C. J.; Dyakonov, V. and Parisi, J. *Organic Photovoltaics, concepts and realization*, **2003**.
- (27) Chua, L. L.; Zaumseil, J.; Chang, J. F.; Ou, E. C. W.; Ho, P. K. H.; Sirringhaus, H. and Friend, R. H. *Nature* **2005**, 434, 194.
- (28) Horowitz, G. *Adv. Mater.* **1998**, 10, (5), 365.
- (29) Newman, C. R.; Frisbie, C. D.; da Silva, D. A.; Bredas, J. L.; Ewbank, P. C. and Mann, K. R. *Chem. Mat.* **2004**, 16, (23), 4436.
- (30) Davis, J.; Vaughan, D. H. and Cardosi, M. F. *Enzyme Microb. Technol.* **1995**, 17, (12), 1030.
- (31) Gerard, M.; Chaubey, A. and Malhotra, B. D. *Biosens. Bioelectron.* **2002**, 17, (5), 345.
- (32) Heeger, P. S. and Heeger, A. J. *Proc. Natl. Acad. Sci. U. S. A.* **1999**, 96, (22), 12219.
- (33) Argun, A. A.; Aubert, P. H.; Thompson, B. C.; Schwendeman, I; Gaupp, C. L.; Hwang, J.; Pinto, N. J.; Tanner, D. B.; MacDiarmid, A. G. and Reynolds, J. R. *Chem. Mat.* **2004**, 16, (23), 4401.
- (34) Gustafsson-Carlberg, J. C.; Inganas, O. and Andersson, M. R. *Electrochim. Acta* **1995**, 40, (13-14), 2233.
- (35) McGehee, M. D. and Heeger, A. J. *Adv. Mater.* **2000**, 12, (22), 1655.
- (36) Hide, F.; DiazGarcia, M. A.; Schwartz, B. J.; Andersson, M. R.; Pei, Q. B. and Heeger, A. J. *Science* **1996**, 273, (5283), 1833.
- (37) Liu, M. S.; Niu, Y. H. and Luo, J. D. *Polym. Rev.* **2006**, 46, (1), 7.
- (38) <http://www.philips.com/>
- (39) <http://gizmodo.com/342912/samsungs-31+inch-oled-is-biggest-thinnest-yet>
- (40) <http://www.polymervision.com/>
- (41) Kranzelbinder, G. and Leising, G. *Rep. Prog. Phys.* **2000**, 358, 193.

- (42) Scherf, U.; Riechel, S.; Lemmer, U. and Mahrt, R. F. *Curr. Opin. Solid State Mater. Sci.* **2001**, 5, (2-3), 143.
- (43) Tessler, N. *Adv. Mater.* **1999**, 11, (5), 363.
- (44) Chabinye, M. L. and Salleo, A. *Chem. Mat.* **2004**, 16, (23), 4509.
- (45) Clemens, W.; Fix, I. and Ficker J. *J. Mater. Res.* 19, (7), **2004**, 19, (7), 1963.
- (46) Naber, R. C. G.; Tanase, C.; Blom, P. W. M.; Gelinck, G. H.; Marsman, A. W.; Touwslager, F. J.; Setayesh, S. and de Leeuw, D. M. *Nature Mater.* **2005**, 4, 243.
- (47) Naber, R. C. G.; Mulder, M.; de Boer, B.; Blom, P. W. M.; de Leeuw, D. M.; *Org. Electr.* **2006**, 7, 132.
- (48) Naber, R. C. G.; de Boer, B.; Blom, P. W. M. and de Leeuw, D. M. *Appl. Phys. Lett.* **2005**, 87, 203509-1.
- (49) Ong, B. S.; Wu, Y. L. and Liu, P. *J. Am. Chem. Soc.* **2004**, 126, (11), 3378.
- (50) Simms, A. *New Scientist* **2004**, 183, (2454), 18.
- (51) Green, M. A.; Emery K.; Hishikawa Y.; Warta W. *Prog. Photovolt: Res. Appl.* **2008**, 16, 61.
- (52) Zweibel, K. and Green, M. A. *Prog. Photovolt. Res. Appl.* **2000**, 8, 1.
- (53) Sariciftci, N. S. *Materials Today*, **2004**, 7, (9), 36.
- (54) Blom, P. W. M.; Mihhailetschi, V. D.; Koster, L. J. A. and Markov, D. E. *Adv. Mater.* **2007**, 19, (12), 1551.
- (55) Reyes-Reyes, M.; Kim, K. and Carroll, D. L. *Appl. Phys. Lett.* **2005**, 87, (8), 083506.
- (56) Koppe, M.; Scharber, M.; Brabec, C.; Duffy, W.; Heeney, M. and McCulloch, I. *Adv. Func. Mater.* **2007**, 17, 1371.
- (57) Lenes, M.; Wetzelaer, G. A. H.; Kooistra, F. B.; Veenstra, S. C.; Hummelen, K. J. and Blom, P. W. M. *Adv. Mater.* **2008**, 20, (11), 2116.
- (58) Casarino, P.; Lavaggi, P. and Pedemonte, E. *J. Thermal. Anal.* **1996**, 47, 165.

- (59) Yu, G. and Heeger, A. J. *J. Appl. Phys.* **1995**, 78, (7), 4510.
- (60) Halls, J. J. M.; Walch, C. A.; Greenham, N. C.; Marseglia, E. A.; Friend, R. H.; Moratti, S. C. and Holmes, A. B. *Nature* **1995**, 376, 498.
- (61) Veenstra, S. C.; Loos, J. and Kroon, J. M. *Prog. Photovolt: Res. Appl.* **2007**, 15, 727.
- (62) Snaith, H. J.; Arias, A. C.; Morteani, A. C.; Siva, C. and Friend, R. *Nano Lett.* **2002**, 2, (12), 1353.
- (63) Breeze, A. J.; Schlesinger, Z.; Carter, S. A.; Tillmann, H. and Hörhold H.-H. *Sol. Energy Mater. Sol. Cells* **2004**, 83, (2-3), 263.
- (64) Veenstra, S. C.; Loos, J. and Kroon, J. M. *Prog. Photovolt: Res. Appl.* **2007**, 15, 727.
- (65) Winder, C. and Sariciftci, N. S. *J. Mater. Chem.* **2004**, 14, 1077.
- (66) Zhang, F.; Jonforsen, M.; Johansson, D. M.; Andersson, M. R. and Inganäs, O. *Synthetic Metals* **2003**, 138, 555.
- (67) Quist, P. A. C.; Savenije, T. J.; Koetse, M. M.; Veenstra, S. C., Kroon, J. M. and Siebbeles, L. D. A. *Adv. Func. Mater.* **2005**, 15, (3), 469.
- (68) Veenstra, S. C.; Verhees, W. J. H.; Kroon, J. M.; Koetse, M. M.; Sweelssen, J.; Bastiaansen, J. J. A. M.; Schoo, H. F. M.; Yang, X.; Alexeev, A.; Loos, J. and Wienk, M. M. *Chem. Mater.* **2004**, 16, 2503.
- (69) Koetse, M. M.; Sweelssen, J.; Hoekerd, K. T.; Schoo, H. F. M.; Veenstra, S. C.; Kroon, J. M.; Yang, X. and Loos, J. *Appl. Phys. Lett.* **2006**, 88, (083504), 1.
- (70) McNeill, C. R.; Abrusci, A.; Zaumseil, J.; Wilson, R.; McKiernan, M. J.; Burroughes, J. H.; Halls, J. J. M.; Greenham, N. C. and Friend, R. *Appl. Phys. Lett.* **2007**, 90, (193506), 1.
- (71) Mandoc, M. M.; Veurman, W.; Koster, L. J. A.; de Boer, B. and Blom, P. W. M. *Adv. Func. Mater.* **2007**, 17, 2167.
- (72) Koster, L. J. A.; Mihailetschi, V. D. and Blom, P. W. M. *Applied Physics Letters* **2006**, 88, 9, 093511.

Chapter 2

Synthesis of Poly(*p*-fluoranthene vinylene)

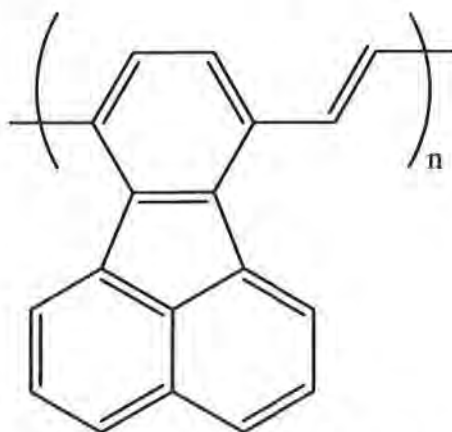


Abstract

Combining research efforts in the fields of conjugated polymers and non-alternant polycyclic aromatic hydrocarbons, has resulted in a novel conjugated polymeric material, poly(*p*-fluoranthene vinylene) **PFV**, with promising properties for application in organic optoelectronics. **PFV** is the first PPV-type polymer with non-alternant polycyclic aromatic hydrocarbon repeating units. **PFV** was prepared using the dithiocarbamate precursor route. While many properties of **PFV** are similar to those of its “parent” polymer PPV, **PFV** exhibits unusual *n*-type behavior, which is likely associated with the non-alternant character of its repeating units.

2.1. Introduction

Conjugated polymers continue to attract increasing attention as a result of their promising properties for optoelectronic applications such as light emitting diodes,¹ solar cells,² sensors³ and field effect transistors.⁴ Whereas for selected applications suitable conjugated polymers are available, the quest for materials with improved properties continues. One method to achieve this objective is the introduction of functional groups. A more radical approach focuses on the design of hitherto unknown polymer backbone architectures. We have combined both tactics and prepared the novel poly(*p*-fluoranthene vinylene) (PFV) (Scheme 1), with a new backbone architecture containing non-alternant polycyclic aromatic hydrocarbon repeating units, in which the base structure of poly(*p*-phenylene vinylene) PPV remains readily recognizable.



Scheme 1. The molecular structure of the goal structure poly(*p*-fluoranthene vinylene) (PFV).

2.2. N-type materials

2.2.1. Fullerenes

Fullerenes are a family of carbon allotropes, molecules composed entirely of carbon, in the form of a hollow sphere, ellipsoid, tube, or plane. Fullerenes were discovered in 1985 by Robert Curl, Harold Kroto and are named after Richard Buckminster Fuller. The most famous of all spherical fullerenes is the Buckminsterfullerene C_{60} .^{5,6} C_{60} is the smallest stable fullerene and consists of 12 pentagons which are completely surrounded by 20 hexagons (Figure 1).⁷⁻⁹

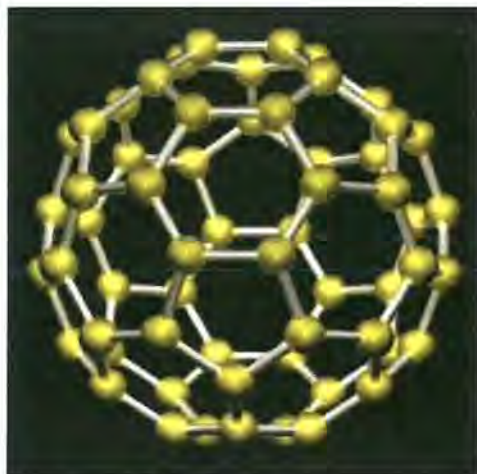


Figure 1. The chemical structure of C_{60} .

All double bonds in the molecule are situated in the hexagons and are not delocalized completely, as can be found in benzene.¹⁰ In theory C_{60} is not even an aromatic structure according to the rules for aromaticity.¹¹ After all it is not planar and the double bonds are not fully delocalized. This immediately implies that common reactions on aromatic systems like aromatic substitution reactions are not always possible.¹²

In the field of organic photovoltaics PCBM, a soluble derivative of C_{60} , is used as the electron acceptor. Until today, PCBM is used in every record

donor/acceptor bulk heterojunction solar cell. Under standard test conditions the highest reported polymer/fullerene solar cell efficiency is 5.15%.¹³ The advantages of using PCBM as an acceptor are the high electron mobility ($\mu_e = 2 \cdot 10^{-3} \text{ cm}^2/\text{Vs}$) and the ultrafast photo-induced charge separation ($\sim 45 \text{ fs}$).¹⁴

2.2.2. *N*-type polymers

The first reports of photovoltaic devices based on a blend of two different polymers as the donor and the acceptor were published in two separate reports in 1995.^{15,16} In both studies, poly(2-methoxy-5-(2'-ethylhexyloxy)-1,4-phenylenevinylene (MEH-PPV) was used as the electron donor, and the cyano-substituted analogue (CN-PPV) as the electron acceptor (Figure 2). Introducing the cyano group enhanced the electron affinity by about 0.5 eV, resulting in an efficient electron-accepting material. The photoluminescence and electroluminescence of both component polymers are quenched in the blend, indicative of rapid and efficient separation of photogenerated electron-hole pairs with electrons on the acceptor and holes on the donor.^{15,16,17}

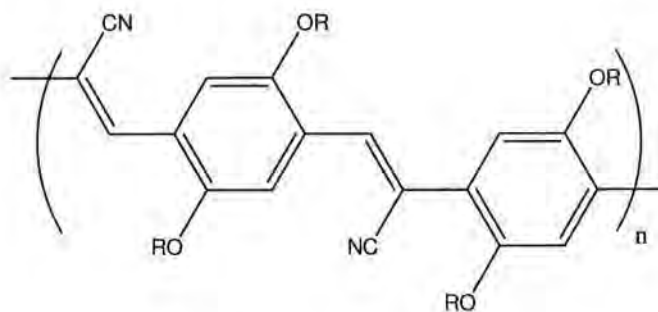


Figure 2. Chemical structure of CN-PPV.

In 1997, polymer diodes were made using MEH-PPV and poly-3,4-dicyanothiophene (PDCTh) (Figure 3).¹⁸ PDCTh has a high electron affinity due to the cyano groups attached directly to the thiophene ring. For this polymer the HOMO (6.7 eV) and LUMO (3.6 eV) levels are significantly lowered compared to poly(alkylthiophene) and it becomes insensitive to air.^{18,19}

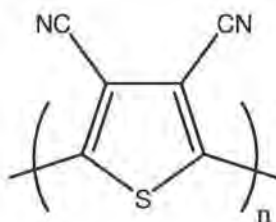


Figure 3. Chemical structure of PDCTh.

A few years later a photocell with a P3HT/ poly(*p*-pyridyl vinylene) (PPyV) (Figure 4) heterojunction was reported.²⁰ The enhanced electron affinity is related to the aromatic building blocks containing electron withdrawing entities, *e.g.* nitrogen. The photoluminescence of the both polymers was quenched. The I_{sc} of the heterojunction device was considerably improved from the P3HT single-layer device.

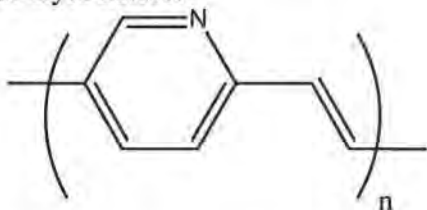


Figure 4. Chemical structure of PPyV.

In 2002 other reports described the blending of hole-accepting and electron-accepting polyfluorene related materials in photovoltaic devices, in which poly(9,9'-dioctylfluorene-co-benzene-thiadiazole) (F8BT) (Figure 5) was used as the acceptor polymer.²¹⁻²⁵

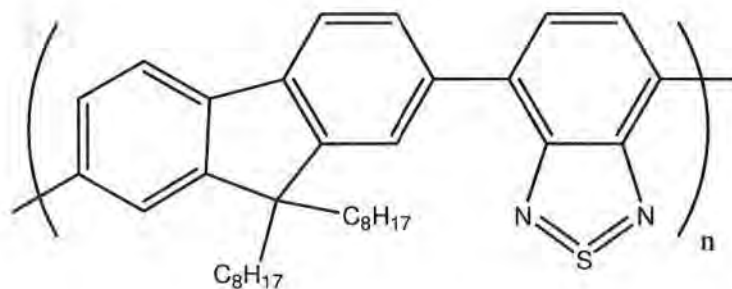


Figure 5. Chemical structure of F8BT.

In 2003, photodiodes and solarcells were made based on the n-type polymer poly(pyridopyrazine vinylene) (EHH-PPyPzV) as the electron acceptor (Figure 6) and MEH-PPV as donor.²⁶ The external quantum efficiency of these diodes can reach 7%. Under low-intensity monochromatic light, the open circuit voltage reached 900 mV.

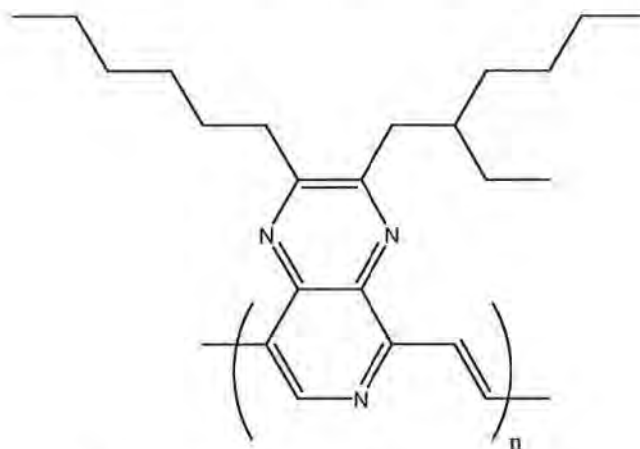


Figure 6. Chemical structure of EHH-PPyPzV.

Blend cells based on MDMO-PPV as the donor and poly(cyanoether phenylene vinylene) (PCNEPV), as the electron acceptor were reported in 2004 (Figure 7).²⁷ Using optical and electrochemical measurements, the

electron affinity of PCNEPV and the ionization potential of MDMO-PPV were determined and a driving force of more than 0.5 eV and 0.7 eV were found for electron and hole transfer, respectively. In addition, an almost complete luminescence quenching was found in combination with a moderate PV effect. Furthermore, it was shown that the PV performance improved by a thermal treatment, altering the morphology of the photoactive layer. Device optimization yielded solar cells with a power conversion efficiency of 0.75% under standard test conditions (AM 1.5, $1000\text{W}/\text{m}^2$).²⁷⁻³¹

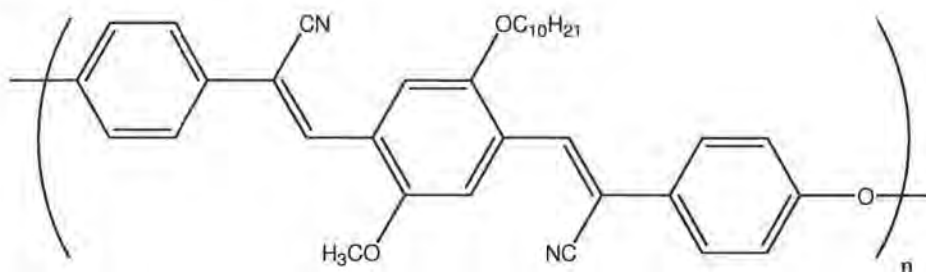


Figure 7. Chemical structure of PCNEPV.

The power efficiencies in the above listed first reports of all-polymer solar cells are below 1%. The 1% mark was reached in 2004 with devices based on M3EH-PPV:CN-ether-PPV (Figure 8). It was found that although the blends allow exciton dissociation to take place throughout the polymer layer, these devices are still limited by transport properties rather than by light absorption.^{32,33}

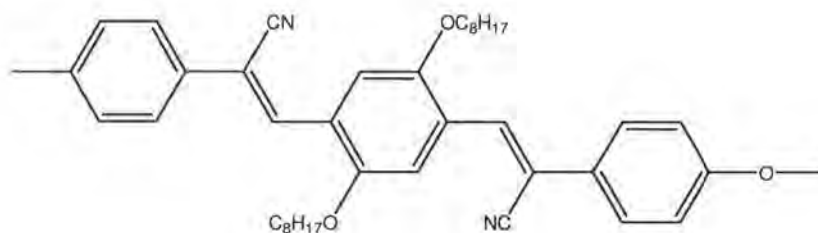


Figure 8. Chemical structure of CN-ether-PPV.

One of the critical challenges to improving electron injection and transport in organic electronic devices, particularly thin FETs, is the achievement of organic and polymer semiconductors with a high electron affinity. For facile electron injection and transport in n-channel polymer FETs, conjugated polymers with electron affinity values of about 4.0 eV or higher are needed in order to achieve ohmic contacts from aluminum electrodes. Even higher values are needed for ohmic contacts from gold electrodes. An example of such a polymer was reported in 2004 when the synthesis, photophysics and electrochemistry of poly(2,7-diphenylpyrazino(2,3-g)quinoxaline-3,8-diyl-1,4-phenylene) (PZQP) and poly(2,7-diphenylpyrazino(2,3-g)quinoxaline-3,8-diyl-2,5-thiophene) (PZQT) were described (Figure 9) PZQP and PZQT have optical bandgaps of 2.44 and 1.76 eV, respectively. Both polymers displayed a highly reversible electrochemical reduction, with an electron affinity of 3.6 eV for PZQP and 3.8 eV for PZQT, approaching the 4.0 eV mark.³⁴

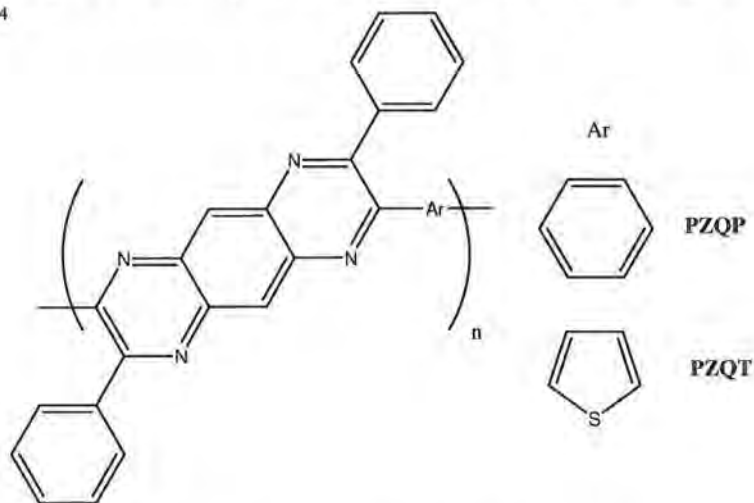


Figure 9. Chemical structure of PZQP and PZQT.

In 2006, a novel polymer:polymer bulk heterojunction solar cell was presented, which was based on a mixture of MDMO-PPV as the donor, and an alternating copolymer poly{9,9-dioctylfluorene-2,7-diyl-alt-1,4-bis[2-(5-

thienyl)-1-cyanovinyl]-2-methoxy-5-(3,7-dimethyl-octyloxy)benzene} (PF1CVTP) (Figure 10) as the acceptor. Measured under standard test conditions, a J_{sc} of 3.0 mA/cm², a V_{oc} of 1.40V and a FF of 0.37 were found, corresponding to a power conversion efficiency of 1.5%.³⁵

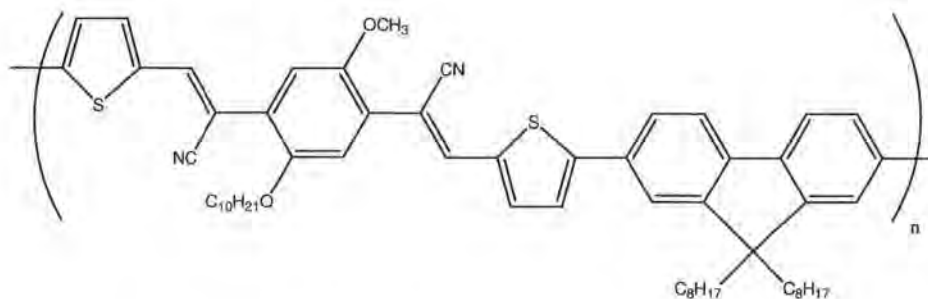


Figure 10. Chemical structure of PF1CVTP.

Recently an efficiency of 1.8% was achieved under standard test conditions. This efficiency was obtained for blends of poly((9,9-dioctylfluorene)-2,7-diyl-alt-[4,7-bis(3-hexylthien-5-yl)-2,1,3-benzothiadiazole]-2',2''-diyl) (F8TBT) (Figure 11) as the acceptor with P3HT as the donor.³⁶

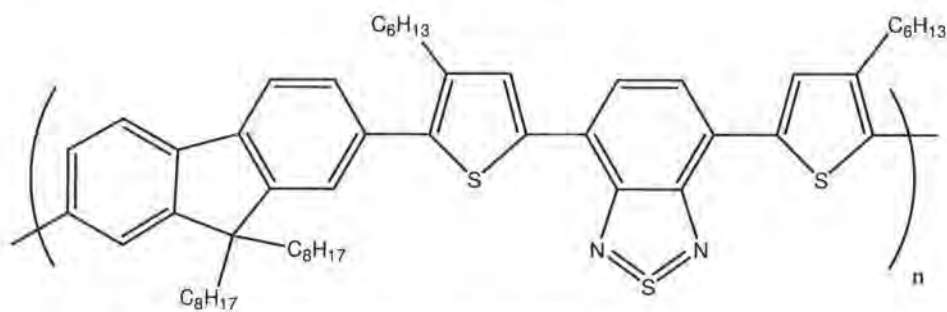


Figure 11. Chemical structure F8TBT.

However, one of the main reasons for the relatively low efficiencies for all-polymer solar cells as compared to their fullerene containing counterparts

is the fact that the fill factor (FF) is less than 25%, which is twice as low as found for typical MDMO-PPV:PCBM devices. Strongly unbalanced transport leads to the formation of a space charge in the solar cell. The resulting square-root dependence of the photocurrent on voltage also strongly reduces the FF of space-charge limited devices. The low FF and performance originates from low dissociation efficiency. This poor dissociation is a combined effect of low mobility, low dielectric constant, and the small separation distance between electrons and holes (related to the morphology). In a recent study, the charge-transport properties of MDMO-PPV:PCNEPV blends (1:1 wt %) were investigated. Hole transport in the MDMO-PPV phase is space-charge limited and the hole mobility is $5.0 \times 10^{-10} \text{ m}^2 \text{ V}^{-1} \text{ S}^{-1}$ at room temperature. Electron transport in the PCNEPV phase is strongly trap-limited and the electron mobility is $6.0 \times 10^{-10} \text{ m}^2 \text{ V}^{-1} \text{ S}^{-1}$. The presence of electron traps leads to highly unbalanced charge transport in this type of blend.³⁷

In general, the n-type polymers reported in literature can be divided into two different classes. In the first class the n-type behavior is introduced by electron accepting substituents attached to the polymer backbone. For example, introducing a cyano group enhances the electron affinity by about 0.5 eV, resulting in an efficient electron-accepting material. Examples of this type of electron acceptor polymers are CN-PPV (Figure 2), PDCTh (Figure 3), PCNEPV (Figure 7), CN-ether-PPV (Figure 8) and PF1CVTP (Figure 10). In the second class, the enhanced electron affinity is related to the aromatic building blocks containing electron withdrawing entities such as N or/and S. Examples are PPyV (Figure 4), F8BT (Figure 5), EHH-PPyPzV (Figure 6), PZQP/PZQT (Figure 9) and F8TBT (Figure 11).

2.2.3. Search for a new class of *n*-type conjugated polymers

Our search for a novel class of electron accepting polymers was inspired by the currently used acceptor PCBM in polymer:fullerene bulk heterojunction solar cells. An *n*-type polymeric alternative for PCBM is of interest to facilitate the formation of an optimal and stable morphology.³⁸ Moreover, the use of polymer-polymer solar cells will lead to a significant increase of the photon harvesting. Whereas it is possible to incorporate C₆₀ as the substituent in a polymer,³⁹ this approach is rather laborious and hence not necessarily cost effective for future applications. Fortunately, remarkable progress has been made in the synthesis of functionalized substructures of C₆₀ by researchers in the field of non-alternant hydrocarbons.⁴⁰ This prompted us to incorporate one of these substructures, *i.e.* fluoranthene, in the backbone of a conjugated polymer (Figure 12). The incorporation of such substructures can have a considerable impact on the electronic properties.⁴¹ The novel conjugated polymer **PFV** described in this chapter is of particular interest since it is the first PPV-type polymer with non-alternant repeating units. Non-alternant polycyclic aromatic hydrocarbon containing conjugated polymers can be regarded as a novel class of *n*-type polymers.

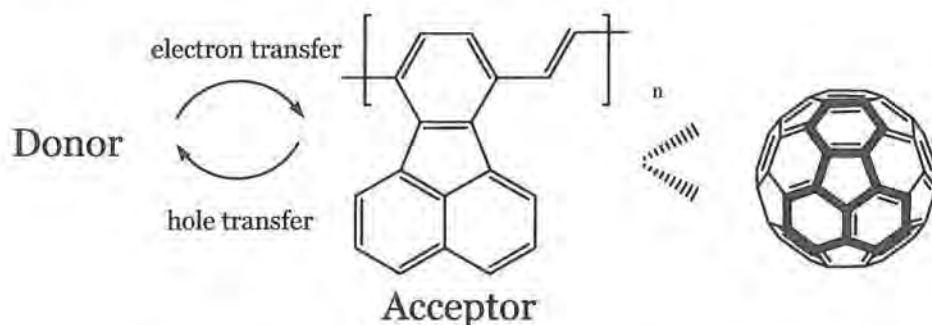
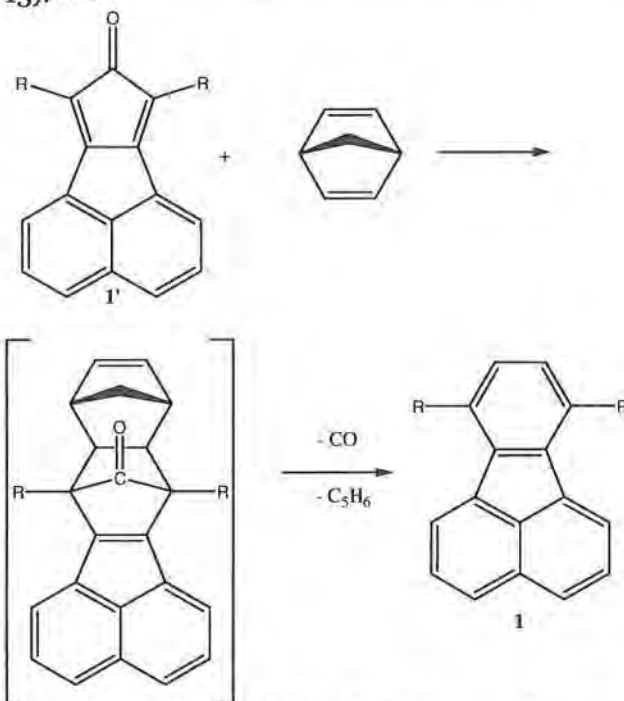


Figure 12. The visualization of our search to a novel *n*-type conjugated polymer.

2.3. Synthesis

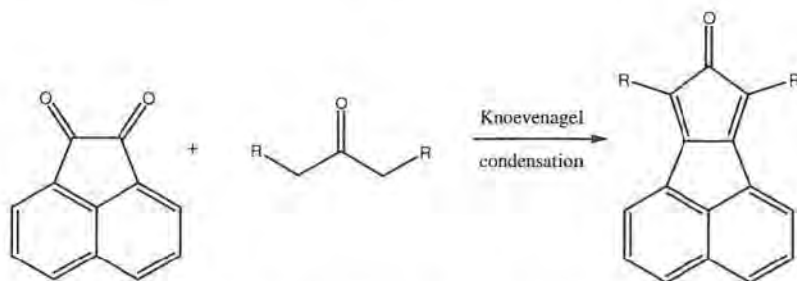
2.3.1. Synthesis of the fluoranthene containing monomer

The synthesis of PFV starts with the straightforward one-step synthesis of dimethyl fluoranthene-7,10-dicarboxylic ester **1** from acenaphthenequinone, acetone dicarboxylic ester and norbornadiene (Scheme 2). We were pleased to learn that earlier researchers had already discovered a versatile route to 7, 10-disubstituted fluoranthenes based on Diels-Alder additions of a masked acetylene to cyclopentadienones **1'**, norbornadiene is used as the dienophile in this reaction, carbon monoxide and cyclopentadiene are lost spontaneously under normal reaction conditions (toluene at reflux temperature), unveiling the final fluoranthene in an exceptionally direct way (Figure 13).^{42, 43}



Scheme 2. Diels-Alder addition to cyclopentadienone.

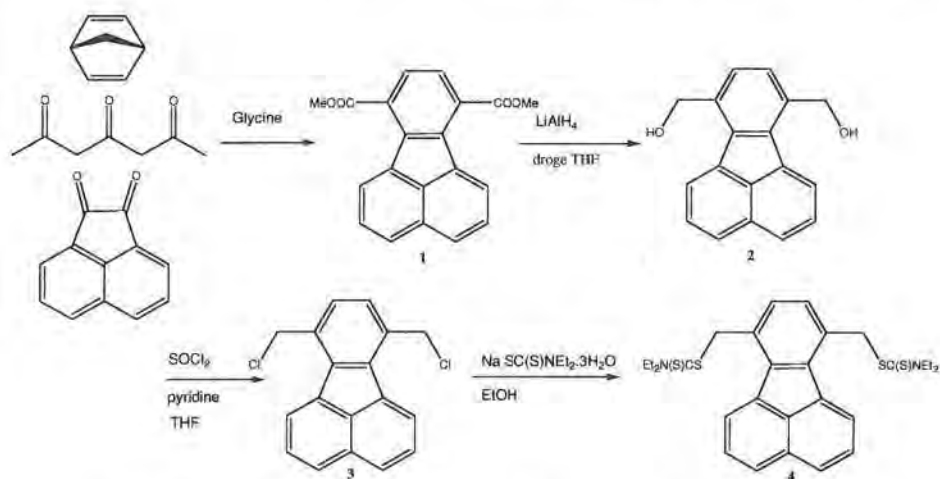
The requisite cyclopentadienones, in turn, are available in one step by the double Knoevenagel condensation of disubstituted acetones with acenaphthenequinone (Scheme 3).⁴⁴



Scheme 3. Double Knoevenagel condensation of disubstituted acetones with acenaphthenequinone.

By running the Knoevenagel condensation in the presence of norbornadiene at 100°C, rather than in pure toluene, these two powerful C-C bond-forming reactions can be compressed into a single operation, thus providing a remarkably straightforward one-step synthesis of dimethyl fluoranthene-7,10-dicarboxylic ester **1** from acenaphthenequinone, acetone dicarboxylic ester and norbornadiene.⁴⁰

The resulting dimethyl fluoranthene-7,10-dicarboxylic ester **1** can be readily converted into diol **2** by reduction with LiAlH₄ according to a literature procedure (Scheme 4).⁴⁰ Subsequently, 7,10-bis(chloromethyl)fluoranthene **3** was obtained by reaction with thionylchloride in THF solution. The rather limited solubility of **2** and **3** required the use of dilute solutions (*circa* 30 mM). After recrystallization from chloroform, pure **3** was obtained in 62% yield as light yellow crystals (melting point 232-234 °C).

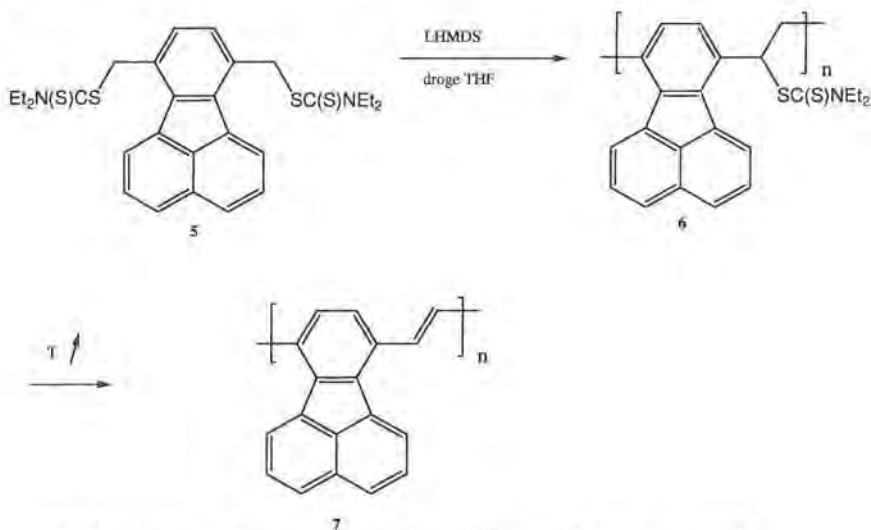


Scheme 4. Monomer synthesis of the fluoranthenone monomer.

2.3.2. Polymerization

For the polymerization, the dithiocarbamate (DTC) precursor route^{45,46} was chosen. The DTC precursor route has been previously developed at Hasselt University and offers not only a straightforward monomer synthesis, but also a precursor polymer of higher quality than most other available precursor routes.⁴⁶ The monomer for the DTC precursor route was synthesized from **3** by reaction with sodium diethyldithiocarbamate trihydrate, giving the monomer 7,10-bis((*N,N*-diethyl dithiocarbamate)methyl)fluoranthenone **4** in a yield of 94%. The introduction of the dithiocarbamate groups substantially increases the solubility of the fluoranthenone monomers. Hence, a polymerization can be accomplished in a straightforward manner. Polymerization of **4** was carried out with lithium bis(trimethylsilyl) amide (LHMDS) as the base in dry THF under inert atmosphere (Scheme 5). After polymerization for 3 hours at ambient temperature, the reaction was terminated by the addition of ice water followed by neutralization with hydrochloric acid. After extraction precursor polymer **5** was isolated by preparative SEC. In this way low molecular weight contaminants can be removed in an uncomplicated

manner. After purification, precursor polymer **5** was obtained in 82% yield as a yellow solid.



Scheme 5. Polymerization reaction of poly(*p*-fluoranthene vinylene) (PFV).

The observed molecular-weight distribution is monomodal, with $M_w = 5.9 \times 10^4$ and $PD = M_w/M_n = 1.6$ (Analytical SEC, solvent DMF). This is in the same order of magnitude as previously found for typical polymerizations of dithiocarbamate monomers.⁴⁶ However, it should be noted that since these molecular weights are referenced to polystyrene standards, the actual value for M_w may differ from the apparent M_w observed with analytical SEC.

2.4. Determination of the electrochemical and optical properties of poly(*p*-fluoranthene vinylene)

2.4.1. In situ UV-Vis spectroscopy and in situ FT-IR spectroscopy

DTC precursor polymers can be readily transformed into the corresponding conjugated polymers by thermal treatment either in solution or in a thin

film.^{45,46} During this treatment the dithiocarbamate group is eliminated from the precursor polymer. Since it appeared that the conjugated PFV was insoluble in all common organic solvents tested, the thermal conversion of **5** into PFV was only performed in a thin film. Otherwise an intractable solid would have been obtained. For the conversion, precursor polymer **5** was spin-coated from a CHCl₃ solution (10 mg/mL) onto NaCl or quartz disks. Subsequently, the disks were placed in a controlled temperature cell. A dynamic heating rate of 1 °C/min from ambient temperatures up to a temperature sufficiently high to have full conversion (*vide infra*) under a continuous flow of N₂ was used for the conversion process.

It is noteworthy that in the thin film processes the thermal elimination reaction can be followed by means of *in situ* UV-Vis and FT-IR spectroscopy. Indeed upon heating a thin film of **5** the formation of the conjugated structure of PFV is readily observed (Figure 13). In the precursor polymer, the long wavelength side of the UV-Vis absorption spectrum is dominated by the typical HOMO-LUMO absorption bands of the substituted fluoranthene at 359 and 380 nm, which are also present in monomer **4**. Upon heating, these “monomeric” bands disappear and two new absorption bands develop ($\lambda_{\text{max}} = 320 \text{ nm}$ and 420 nm at 25 °C), which originate from the conjugated structure. This is in contrast to unsubstituted PPV, which exhibits at ambient temperatures only a single band at *circa* 420 nm in the UV-Vis absorption spectrum.⁴⁶ The additional band at 320 nm is a result of the more extended conjugated system in PFV. As a result of the occurrence of multiple bands in the UV-Vis absorption spectrum, the π - π^* transition is not as distinct as usually found for (substituted) PPV derivatives. However, the occurrence of multiple bands in extended PPV-type conjugated systems is not uncommon.⁴⁷

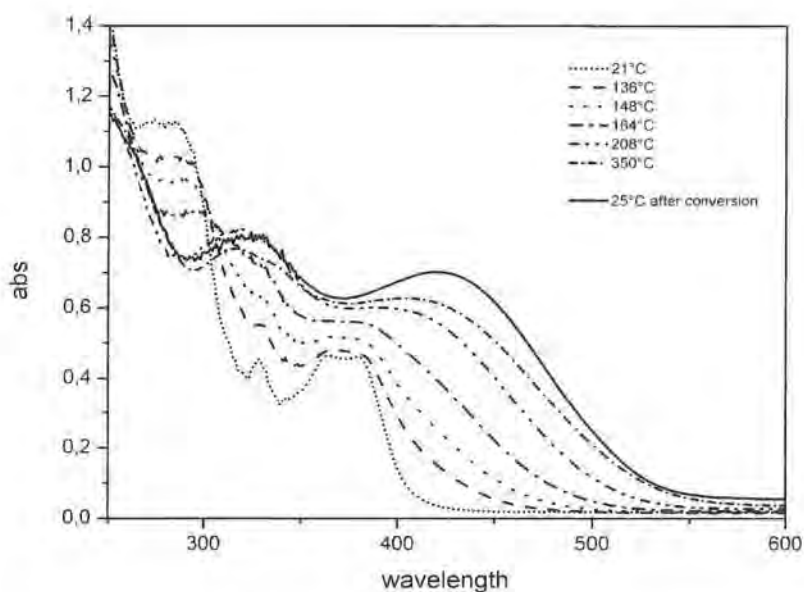


Figure 13. Temperature-dependent UV-Vis spectra of the conversion of precursor polymer **5** to **PFV**.

The optical band gap can be derived from the low energy side tangent to the π - π^* transition. A value for the bandgap of 2.34 eV is obtained, which is only slightly smaller than the reported band gap of PPV (circa 2.4 eV).^{46,48} From the absorption profile at 420 nm it is evident that conversion of **5** to **PFV** starts around 100 °C and is virtually complete at 200 °C (Figure 14). The apparent minor decrease in absorption at temperatures above 200 °C is a result of a reversible thermochromic effect. Furthermore, the UV-Vis analysis indicates that no substantial degradation of the conjugated structure is observed in the entire temperature range up to 300 °C. It has been previously observed that unsubstituted PPV is stable until 350 °C,⁴⁶ which indicates that the extension of the conjugated structure does not impact the thermal stability of the conjugated system to a significant extent.

For comparison, the thermal stability of PFV was also measured with TGA, although this does not directly give information about the thermal stability of the conjugated backbone.⁴⁹ From these measurements it is evident that the complete degradation of PFV as observed with TGA does not commence until 325 °C.

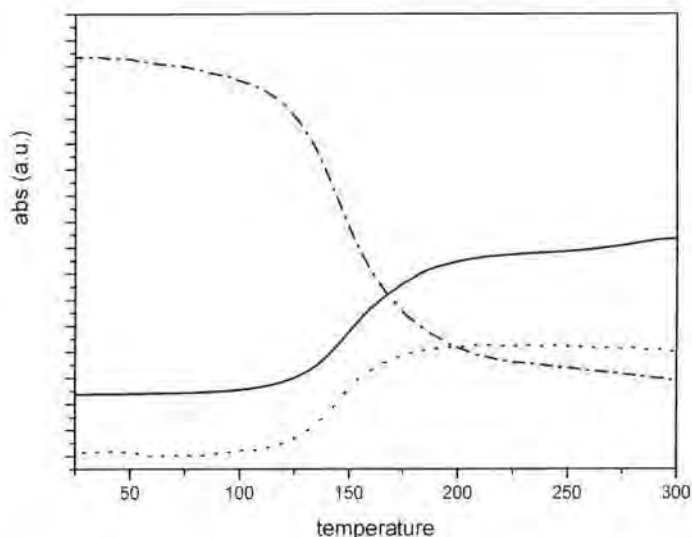


Figure 14. UV-Vis profile at 420 nm (dotted) and FT-IR profiles at 954 cm^{-1} (solid) and 1266 cm^{-1} (dashed-dotted) as a function of temperature during the conversion process of precursor polymer 5 to PFV.

Fluorescence measurements further confirm the successful formation of the conjugated structure. Whereas precursor polymer 5 has a fluorescence emission at $\lambda = 475$ nm (excitation at $\lambda = 380$ nm), this fluorescence is no longer present in the conjugated structure. Instead for PFV a distinct emission is found at $\lambda = 545$ nm (excitation at $\lambda = 412$ nm), which originates from the conjugated structure. The photoluminescence excitation (PLE)

spectrum of precursor polymer **5** has a maximum at $\lambda = 360$ nm (for emission at $\lambda = 475$ nm). The photoluminescence excitation (PLE) spectrum of PFV has a maximum at $\lambda = 440$ nm (for emission at $\lambda = 540$ nm).

The conversion process is also readily observed using temperature dependent FT-IR spectroscopy (Figure 15). Upon heating, the vibrations at 1485, 1415, 1266, 1204 cm^{-1} , which are associated with the dithiocarbamate group, decrease in intensity. At the same time, a new vibration develops at 954 cm^{-1} , which arises from the double bonds in the conjugated backbone. The FT-IR measurements confirm that the formation of double bonds starts at 100 °C and is virtually complete around 180 °C (Figure 15), with only minimal intensities of the dithiocarbamate groups remaining.

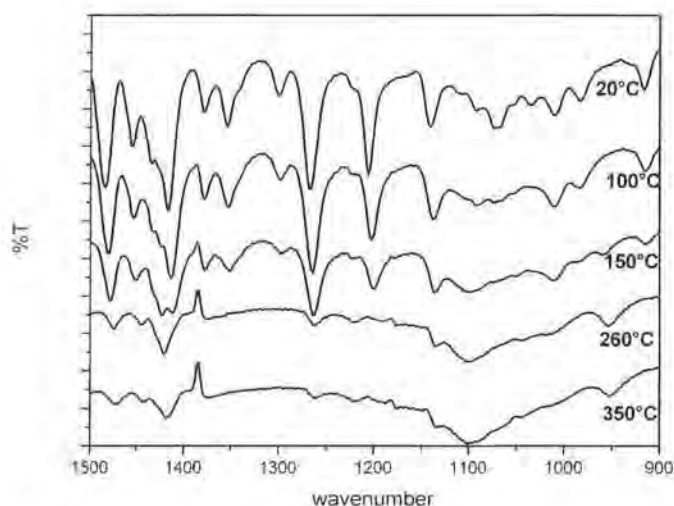


Figure 15. Temperature-dependent FT-IR spectra of the conversion of precursor polymer **5** to PFV.

2.4.2. cyclic voltammetry

Thin film cyclic voltammetry (CV) was employed to investigate the electrochemical behavior of PFV and to estimate the position of its lowest

occupied molecular orbital (LUMO) energy level. The cyclic voltammogram of **PFV** displays a distinct reduction process (Figure 16), *i.e.* n-doping. In contrast, the current density associated with the p-doping, *viz.* the oxidation process, is very small. This suggests that this new polymer under the applied electrochemical conditions acts as an n-type conjugated polymer. Such polymers are quite rare and highly desired for applications.⁵⁰ The observed unusual n-type behavior most likely originates from the non-alternant polycyclic aromatic hydrocarbon units in the backbone. The conduction band edge energy level is accurately determined from the onset of reduction at -1.82 V vs. Ag/AgNO₃. It should be noted that for the conversion to eV, all electrochemical potentials have been referenced to a known standard, ferrocene/ferrocinium, which is estimated to have an oxidation potential of -4.98 V *vs.* Vacuum. In this way the LUMO energy level of **PFV** can be estimated at -3.10 eV. This is significantly lower than the LUMO energy level observed for PPV (-2.7 eV) reported in literature.⁵¹ However, this apparent difference is a result of differences in the electrochemical procedures and reference system and in reality no significant difference between the LUMO values of **PFV** and PPV exists. We have measured thin films of unsubstituted PPV with the same electrochemical measurement setup and reference system as employed for **PFV**. In this way a LUMO energy level of -3.11 eV has been found for PPV, which is virtually identical to the LUMO of **PFV** (-3.10 eV). Furthermore, we estimate that the electrochemical band gap of PPV is 2.47 eV. Although the HOMO energy level of **PFV** is more difficult to estimate, based on the electrochemical measurements a value of -5.6 eV can be derived, which indicates that the electrochemical band gap of **PFV** is circa 2.5 eV. This is in the same order of magnitude as PPV.

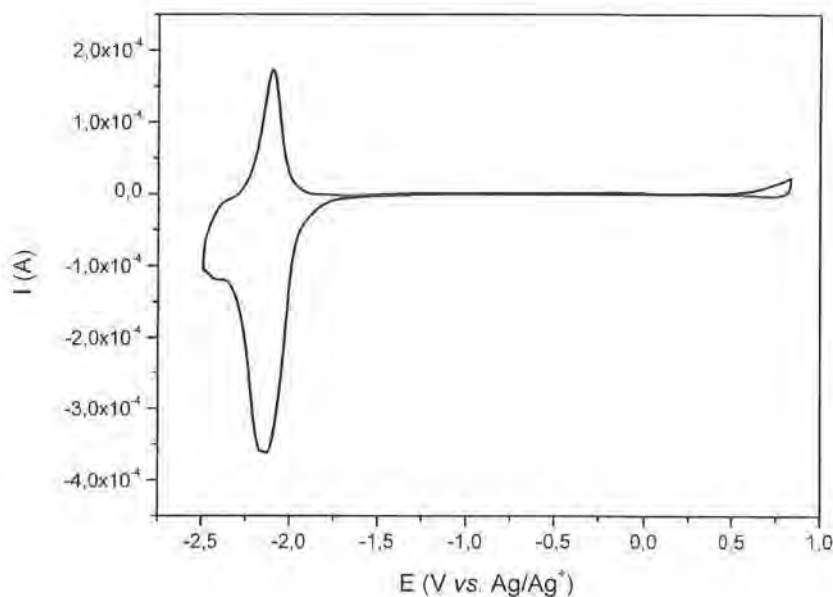


Figure 16. Cyclic voltammogram of the oxidation and reduction behavior of a thin film of **PFV** on ITO.

2.5. Conclusion

In conclusion, recent progress in the synthesis of substructures of C_{60} has provided us with an opportunity to create a new conjugated polymer with a hitherto unknown backbone structure containing non-alternant polycyclic aromatic hydrocarbon repeating units. While many properties of **PFV** are similar to those of its “parent” polymer PPV, **PFV** exhibits unusual n-type behavior, which is likely associated with the non-alternant character of its backbone. The straightforward synthesis towards this novel polymer as developed in our laboratory provides the opportunity to use **PFV** as a

platform for further functionalization, thus allowing for a further adjustment of the optoelectronic properties.

2.6. Experimental section

2.6.1. Reagents and methods

Unless stated otherwise, all reagents and chemicals were obtained from commercial sources and used without further purification. Tetrahydrofuran (THF) was purified by distillation from sodium/benzophenone.

^1H NMR spectra were obtained in CDCl_3 at 300 MHz. Chemical shifts (δ) in ppm were determined relative to the residual non-deuterated solvent absorption (7.24 ppm). The ^{13}C NMR experiments were recorded at 75 MHz on the same spectrometer. Chemical shifts were defined relative to the ^{13}C resonance shift of CHCl_3 (77.0 ppm). The molecular weight distributions were determined relative to polystyrene standards by Size Exclusion Chromatography (SEC). Chromatograms were recorded on a Spectra series P100 pump equipped with two Mixed-B columns (10 μm , 2 x 30 cm, Polymer Labs) and a refractive index (RI) detector (Shodex) at 70 °C. A DMF solution of oxalic acid ($1.1 \cdot 10^{-3}$ M) was used as the eluent at a flow rate of 1.0 mL/min. Toluene was used as a flow-rate marker. Fourier transform-infrared (FT-IR) spectroscopy was performed on a Perkin Elmer Spectrum One FT-IR spectrometer (nominal resolution 4 cm^{-1} , summation of 16 scans). Samples for the FT-IR characterisation of the conversion process were prepared by spin-coating the precursor polymer from a chloroform solution (10 mg/mL) onto NaCl disks at 500 rpm. The NaCl disks were heated in a Harrick oven high temperature cell, which was positioned in the beam of the FT-IR to allow *in-situ* measurements. The temperature of the sample and the heating source were controlled by a Watlow temperature controller. The heating source was in direct contact with the NaCl disk.

Spectra were taken continuously and the heating rate was 1 °C/min. All measurements were performed under a continuous flow of nitrogen. Ultraviolet visible (UV-Vis) spectroscopy was performed on a VARIAN CARY 500 UV-Vis-NIR spectrophotometer (interval: 1 nm, scan rate: 600 nm/min, continuous run from 200 to 800 nm). The precursor polymer was spin-coated from a chloroform solution (10 mg/mL) onto quartz glass at 700 rpm. The quartz glass was heated in the same Harrick oven high temperature cell as was used in the FT-IR measurements. The cell was placed in the beam of the UV-Vis spectrophotometer and spectra were taken continuously. The heating rate was 1 °C/min. All measurements were performed under a continuous flow of nitrogen. Fluorescence spectra were obtained with a Perkin Elmer LS-5B luminescence spectrometer. Electrochemical properties were measured with an Eco Chemie Autolab PGSTAT 20 Potentiostat/Galvanostat using a conventional three-electrode cell (electrolyte: 0.1 mol/L TBAPF₆ in anhydrous CH₃CN) with an Ag/AgNO₃ reference electrode (0.01 mol/L AgNO₃, 0.10 mol/L TBAPF₆ and CH₃CN), a platinum counter electrode and an Indium-Tin Oxide (ITO) coated glass substrate as working electrode. Cyclic voltammograms were recorded at 50 mV/s under N₂ atmosphere. All electrochemical potentials have been referenced to a known standard, ferrocene/ferrocinium, which is estimated to have an oxidation potential of -4.98 V *vs.* Vacuum.

2.6.2. Synthesis

Dimethyl Fluoranthene-7,10-dicarboxylate (1)

A mixture of acenaphthenequinone (10.00 g, 54.90 mmol), dimethyl 1,3-acetone dicarboxylate (18.0 mL, 130 mmol), and glycine (9.0 g, 120 mmol) in 150 mL of 2,5-norbornadiene was stirred at reflux for 3.5 days. The reaction flask was equipped with a Dean-Stark trap to remove the water generated from the reaction. Excess solvent was removed at the end of the reaction by simple distillation to give a brown solid, which was purified on

silica gel with 2:2:1 benzene/ hexane/ ethyl acetate as eluent. The product was further purified by crystallization from methanol to give 5.51 g (32% yield) of light brown colored crystals: mp 144-145°C. ¹H-NMR (300 MHz, CDCl₃) δ: 8.62 (d, 2H), 7.93 (d, 2H), 7.83 (s, 2H), 7.66 (t, 2H), 4.07 (s, 6H).

7,10-Bis(hydroxymethyl) fluoranthene (2)

A solution of diester **1** (6.84g, 21.51 mmol) in 200 mL of dry THF was added drop wise with stirring to a solution of lithium aluminum hydride (8.16 g, 0.215 mol) in 200 mL of dry THF at 0°C. The reaction mixture was stirred at room temperature for 6 h and then hydrolyzed with 100 mL of water, 100 mL of 10% aqueous sodium hydroxide and again with 100 mL of water. The mixture was subsequently extracted with 3 x 300 mL of 1:1 ether/THF. The combined organic layers were washed with 400 mL water and dried over magnesium sulfate. Removal of the solvents under reduced pressure gave 5.29 g (94% yield) of a light yellow solid. The product was used without further purification.

7,10-Bis(chloromethyl)fluoranthene (3).

To a solution of the diol **2** (7.64 g, 29.16 mmol) and pyridine (9.21 g, 116.64 mmol) in THF (1 L) at 0 °C, thionylchloride (7.64 g, 64.15 mmol) was added dropwise over a period of 5 minutes. After addition, the mixture was stirred at reflux temperature for 24 hours. After dilution with water (500 mL), an extraction with CHCl₃ (3 x 500 mL), the combined organic layers were dried over MgSO₄ and the solvent was evaporated. The product was further purified by crystallization from chloroform to give 5.42 g (62% yield) of light yellow crystals: mp 232-234 °C. ¹H NMR: 8.18 (d, 2H), 7.92 (d, 2H), 7.65 (dd, 2H), 7.36 (s, 2H), 5.08 (s, 4H), 4.07 (q, 4H), 3.67 (q, 4H), 1.32 (t, 6H), 1.20 (t, 6H). ¹³C NMR: 138.4, 135.1, 133.4, 132.5, 129.9, 129.3, 128.2, 127.6, 124.3, 44.6. GC-MS (EI, m/e): 298 (M⁺), 263 (M⁺-Cl), 228 (M⁺- 2 x Cl). FT-IR (NaCl, cm⁻¹): 1438, 1426, 1198, 823, 771, 700, 626.

7,10-Bis((N,N-diethyl dithiocarbamate)methyl)fluoranthene (4)

A mixture of dichloride **3** (1.06 g, 3.55 mmol), sodium diethyldithiocarbamate trihydrate (1.84 g, 8.15 mmol) in 350 mL ethanol was stirred at room temperature for 24 hours. Then, water was added and the desired monomer was extracted with chloroform (3 x 300 mL) and dried over MgSO₄. Evaporation of the solvent gave 1.76 g (94% yield) of the pure product as a light yellow solid: mp 154-155 °C. ¹H NMR: 8.08 (d, 2H), 7.86 (d, 2H), 7.71 (t, 2H), 7.35 (s, 2H), 4.96 (s, 4H). ¹³C NMR: 194.9, 138.4, 135.5, 132.3, 130.3, 130.1, 129.6, 128.0, 126.9, 123.9, 49.2, 46.7, 41.1, 12.3, 11.5. GC-MS (EI, m/e): 524 (M⁺), 376 (M⁺-SC(S)NEt₂), 228 (M⁺- 2 x SC(S)NEt₂), 148 (SC(S)NEt₂), 116 (C(S)NEt₂), 72 (NEt₂). FT-IR (NaCl, cm⁻¹): 2975, 1486, 1416, 1378, 1354, 1300, 1268, 1205, 1142, 1069, 1007, 983, 917, 826, 773.

Precursor polymer (5)

A solution of monomer **4** (500 mg, 0.954 mmol) in dry THF (9.54mL) at ambient temperature was degassed for 1 hour by passing through a continuous nitrogen flow. A 1.6 equivalent LHMDS solution (1.53 mL of a 1 M solution in THF) was added in one go to the stirred monomer solution. The mixture was kept at room temperature for 3 hours and the passing of nitrogen was continued, after which the polymer was precipitated in ice water (100 mL) and extracted with chloroform (3 x 200 mL). The solvent of the combined organic layers was evaporated under reduced pressure. The high molecular weight polymer fraction was subsequently isolated by preparative SEC (Biobeads SX-1, eluent THF). The polymer fractions were collected and dried *in vacuo*. A yellow solid was obtained (250 mg, 82% yield). Calcd. For C₂₃H₂₁NS₂: C 73.6, H 5.6, N 3.7, S 17.1; Found C 74.5, H 6.0, N 3.5, S 16.0. ¹H NMR: 8.7-6.1 (b, 8H), 4.4-3.0 (b, 7H), 1.4-0.4 (b, 6H). ¹³C NMR: 193.9, 136.6, 135.6, 134.3, 132.2, 129.3, 127.3, 126.3, 124.4, 123.3,

50.6, 48.9, 46.5, 42.0, 12.3, 11.3. FT-IR (NaCl, cm^{-1}): 3051, 2975, 1484, 1417, 1267, 1206, 1140, 1074, 825, 773, 754. TGA: 100 °C (100%) – 330 °C (65.2%) (elimination of DTC groups), 330 °C (65.2%) – 600 °C (34.8%) (degradation).

Polymer PFV

The precursor polymer **5** was spin-coated from a CHCl_3 solution (10 mg/mL) onto a NaCl disk at 500 rpm or quartz disk at 700 rpm, respectively. Subsequently, the disks were placed in the controlled temperature cell. A dynamic heating rate of 1 °C/min up to 350 °C under a continuous flow of N_2 was used for the conversion process. FT-IR (NaCl, cm^{-1}): 3045, 1102, 954, 820, 766.

2.7. References

- (1) Akcelrud, L. *Prog. Polym. Sci.* **2003**, 28, 875.
- (2) Dennler, G. and Sariciftci, N. S. *Proc. IEEE* **2005**, 93, 1429.
- (3) Mauthner, G.; Wenzl, F. P.; Collen, M.; Bouguettaya, M.; Reynolds, J. R.; Leising, G. and List, E.J.W. *Synth. Met.* **2003**, 139, 613.
- (4) Porzio, W.; Destri, S.; Giovanella, U.; Pasini, M.; Motta, T.; Natali, D.; Sampietro, M. and Campione, M. *Thin Solid Films* **2005**, 492, 212.
- (5) Kroto, H. W.; Heath, J. R.; O'Brien, S. C.; Curl, R. F. and Smalley, R. E. *Nature* **1985**, 318, 162.
- (6) Krätschmer, W.; Lamb, L. D.; Fostiropoulos, K. and Huffman, D. R. *Nature* **1990**, 347, 354.
- (7) Liu, S.; Lu, Y.; Kappes, M. M. and Ibers, J. A. *Science* **1991**, 254, 408.
- (8) Hedberg, K.; Hedberg, I.; Bethune, D. S.; Brown, C. A.; Dorn, H. C.; Johnson, R. D. and De Vries, M. *Science* **1991**, 254, 410.

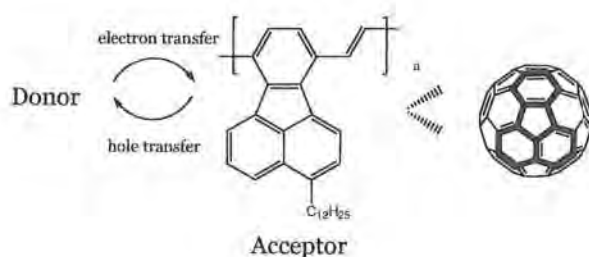
- (9) David, W. I. F.; Ibberson, R. M.; Matthewman, J. C.; Prassides, K.; Dennis, T. J. S.; Hare, J. P.; Kroto, H. W.; Taylor, R. and Walton, D. R. M. *Nature* **1991**, 353, 147.
- (10) Yannoni, C. S.; Bernier, P. P.; Bethune, D. S.; Meijer, G. and Salem, J. R. *J. Am. Chem. Soc.* **1991**, 113, 3190.
- (11) Buhl, M. and Hirsch, A. *Chem. Rev.* **2001**, 101, 1153.
- (12) Haddon, R. C. *Science* **1993**, 261, 1545.
- (13) Green, M. A.; Emery K.; Hishikawa Y. and Warta W. *Prog. Photovolt: Res. Appl.* **2008**, 16, 61.
- (14) Hummelen, J. C.; Mihailetschi, V. D.; Duren, K. J.; Blom, P. W. M.; Janssen, R. A. J.; Kroon, J. M.; Rispens, M. T. and Verhees, W. J. H. *Adv. Func. Mater* **2003**, 13, 43.
- (15) Yu, G. and Heeger, A. J. *J. Appl. Phys.* **1995**, 78, (7), 4510.
- (16) Halls, J. J. M.; Walch, C. A.; Greenham, N. C.; Marseglia, E. A., Friend, R. H.; Moratti, S. C. and Holmes, A. B. *Nature* **1995**, 376, 498.
- (17) Granström, M.; Petritsch, K.; Arias, A. C.; Lux, A.; Andersson, M. R.; and Friend, R. H. *Nature* **1998**, 395, 257.
- (18) Hide, F.; Greenwald, Y.; Wudl, F. and Heeger, A. J. *Synthetic Metals* **1997**, 85, 1255.
- (19) Greenwald, Y.; Xu, X.; Fourmigué M.; Srdanov, G.; Koss, C.; Wudl, F. and Heeger, A. J. *J. Pol. Science* **1998**, 36, 3115.
- (20) Tada, K.; Onada, M.; Nakayama, H. and Yoshino, K. *Synthetic Metals* **1999**, 102, 982.
- (21) Snaith, H. J.; Arias, A. C.; Morteani, A. C.; Siva, C. and Friend, R. *Nano Lett.* **2002**, 2, (12), 1353.
- (22) Kim, Y.; Cook, S.; Choulis, S. A.; Nelson, J.; Durrant, J. R. and Bradley, D. D. C. *Chem. Mater.* **2004**, 16, 4812.
- (23) Kim, J-S.; Ho, P. K.; Murphy, C. E. and Friend, R. H. *Macromolecules* **2004**, 37, 2861.

- (24) Arias, A. C.; MacKenzie, J. D.; Stevenson, R.; Halls, R. R. M.; Inbasekaran, M.; Woo, E. P., Richards, D. and Friend, R. H. *Macromolecules* **2001**, 34, 6005.
- (25) McNeill, C. R.; Frohne, H.; Holdsworth, J. L. and Dastoor, P. C. *Nano Lett.* **2004**, 4, 2503.
- (26) Zhang, F.; Jonforsen, M.; Johansson, D. M.; Andersson, M. R. and Inganäs, O. *Synthetic Metals* **2003**, 138, 555.
- (27) Veenstra, S. C.; Verhees, W. J. H.; Kroon, J. M.; Koetse, M. M.; Sweelssen, J.; Bastiaansen, J. J. A. M.; Schoo, H. F. M.; Yang, X., Alexeev, A., Loos, J. and Wienk, M. M. *Chem. Mater.* **2004**, 16, 2503.
- (28) Veenstra, S. C.; Loos, J. and Kroon, J. M. *Prog. Photovolt: Res. Appl.* **2007**, 15, 727.
- (29) Quist, P. A. C.; Savenije, T. J.; Koetse, M. M.; Veenstra, S. C., Kroon, J. M. and Siebbeles, L. D. A. *Adv. Func. Mater.* **2005**, 15, (3), 469.
- (30) Offermans, T.; van Hal, P. A.; Meskers, S. C. J.; Koetse, M. M. and Janssen, R. A. J. *Phys. Review* **2005**, 72, (045213), 1.
- (31) Morteani, A. C.; Sreearunothai, P.; Herz, L. M.; Friend, R. H. and Silva, C. *Phys. Review Lett.* **2004**, 92, (045213), 1.
- (32) Breeze, A. J.; Schlesinger, Z.; Carter, S. A.; Tillmann, H. and Hörhold H.-H. *Sol. Energy Mater. Sol. Cells* **2004**, 83, (2-3), 263.
- (33) Kietzke, T.; Hörhold, H-H. and Neher, D. *Chem. Mat.* **2005**, 17, 6532.
- (34) Zhu, Y.; Yen, C-T.; Jenekhe, S. A. and Chen, W-C. *Macromol. Rapid Commun.* **2004**, 25, 1829.
- (35) Koetse, M. M.; Sweelssen, J.; Hoekerd, K. T.; Schoo, H. F. M.; Veenstra, S. C.; Kroon, J. M.; Yang, X. and Loos, J. *Appl. Phys. Lett.* **2006**, 88, (083504), 1.
- (36) McNeill, C. R.; Abrusci, A.; Zaumseil, J.; Wilson, R.; McKiernan, M. J.; Burroughes, J. H.; Halls, J. J. M.; Greenham, N. C. and Friend, R. *Appl. Phys. Lett.* **2007**, 90, (193506), 1.

- (37) Mandoc, M. M.; Veurman, W.; Koster, L. J. A.; de Boer, B. and Blom, P. W. M. *Adv. Func. Mater.* **2007**, 17, 2167.
- (38) Hoppe H. and Sariciftci, N. S. *J. Mater. Res.* **2004**, 19, 1924.
- (39) Ramas, A. M.; Rispens, M. T.; van Duren, J. K. J.; Hummelen, J. C. and Janssen, R. A. J. *J. Am. Chem. Soc.* **2001**, 123, 6714.
- (40) Scott, L. T.; Cheng, P.; Hashemi, M. M.; Bratcher, M. S.; Meyer, D. T. and Warren, H. B. *J. Am. Chem. Soc.* **1997**, 119, 10963.
- (41) Quinto, M. and Bard, A. J. *J. Electronanal. Chem.* **2001**, 498, 67.
- (42) Craig, J. T. and Robins, M. D. W. *Aust. J. Chem.* **1968**, 21, 2237.
- (43) Harana, K.; Yasuda, M. and Kanematsu, K. *J. Org. Chem.* **1982**, 47, 4736.
- (44) Allen, C. F. H. and Van Allen, J. A. *J. Org. Chem.* **1952**, 17, 845.
- (45) Henckens, A.; Colladet, K.; Fourier, S.; Cleij, T. J.; Lutsen, L.; Gelan, J. and Vanderzande, D. *Macromolecules* **2005**, 38, 19.
- (46) Henckens, A.; Duyssens, I.; Lutsen, L.; Vanderzande, D. and Cleij, T. J. *Polymer* **2006**, 47, 123.
- (47) Behnisch, B.; Martinez-Ruiz, P.; Schweikart, K. and Hanack, M. *Eur. J. Org. Chem.* **2000**, 2541.
- (48) Eckhardt, H.; Shacklette, L.W.; Jen, K.Y. and Elsenbaumer, R. L. *J. Chem. Phys.* **1989**, 91, 1303.
- (49) Kesters, E.; Vanderzande, D.; Lutsen, L.; Penxten, H. and Carleer, R. *Macromolecules* **2005**, 38, 1141.
- (50) Babel, A. and Jenekhe, S. A. *J. Am. Chem. Soc.* **2003**, 125, 13656.
- (51) Alam, M. M. and Jenekhe, S. A. *Chem. Mater.* **2004**, 16, 4647.

Chapter 3

Synthesis of Alkyl-Poly(*p*-fluoranthene vinylene)



Abstract

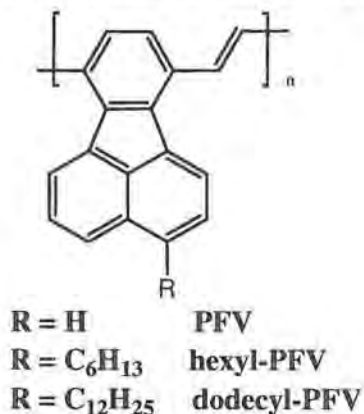
Considerable interest exists in the use of conjugated polymers for organic photovoltaics. Although most of the research has focused on using PCBM as the electron acceptor, a polymeric alternative is desirable for a variety of reasons. To this end a new polymer, **PFV**, has been developed (cf. Chapter 2). In the current chapter, a universal synthesis route is presented towards alkyl derivatives of **PFV**, which display enhanced solubility. The introduction of solubilizing alkyl side chains, leads to a significantly enhanced purity and processability as compared to unsubstituted **PFV**. Additional CELIV mobility measurements on **dodecyl-PFV**, a typical representative of this novel class of polymers with a high purity, reveal an excellent electron mobility, $\mu_e = 1.4 \cdot 10^{-8} \text{ m}^2/\text{Vs}$.

3.1. Introduction

In the second chapter, the synthesis of a PPV-type polymer with a new backbone architecture, *i.e.* poly(*p*-fluoranthene vinylene) **PFV** has been described. The design and synthesis of this **PFV** have been inspired by the progress, which has been made in the synthesis of substructures of C₆₀ by researchers in the field of non-alternant hydrocarbons.¹ In the backbone of this conjugated polymer a small substructure of C₆₀, *i.e.* fluoranthene, is incorporated.² As demonstrated by electrochemical measurements, the resulting **PFV** exhibits the desired n-type behavior, although many of its other properties remain similar to those of its “parent” polymer PPV. The n-type character is assumed to be associated with the non-alternant character of the repeating units. Unfortunately, the solubility of **PFV** as well as its precursors is rather low, complicating synthesis and purification procedures. As a result, incorporation into actual devices has proven troublesome. Hence, the development of more soluble derivatives of **PFV** is of paramount importance.

In this chapter, a universal synthesis route is presented towards derivatives of **PFV**. This route is illustrated for two conjugated polymers with alkyl side chains, *i.e.* functionalized hexyl-poly(*p*-fluoranthene vinylene) **hexyl-PFV** and dodecyl poly(*p*-fluoranthene vinylene) **dodecyl-PFV** (Scheme 1). Furthermore, the results are compared with those found for unsubstituted **PFV**. It is demonstrated that as a result of the alkyl side chains the solubility is considerably improved, leading to enhanced purity and physical properties. All polymers were synthesized *via* the dithiocarbamate (DTC) precursor route.^{2,3} The optical and electronic properties of these polymers were compared using UV-Vis absorption spectroscopy and cyclic voltammetry. As a result of the enhanced purity, especially **dodecyl-PFV** is a promising material for optical and electronic applications. Therefore, a first evaluation of charge carrier mobility by CELIV-measurement of

dodecyl-PFV will be presented, which demonstrates the suitability of this novel material as an n-type material in optoelectronic applications.



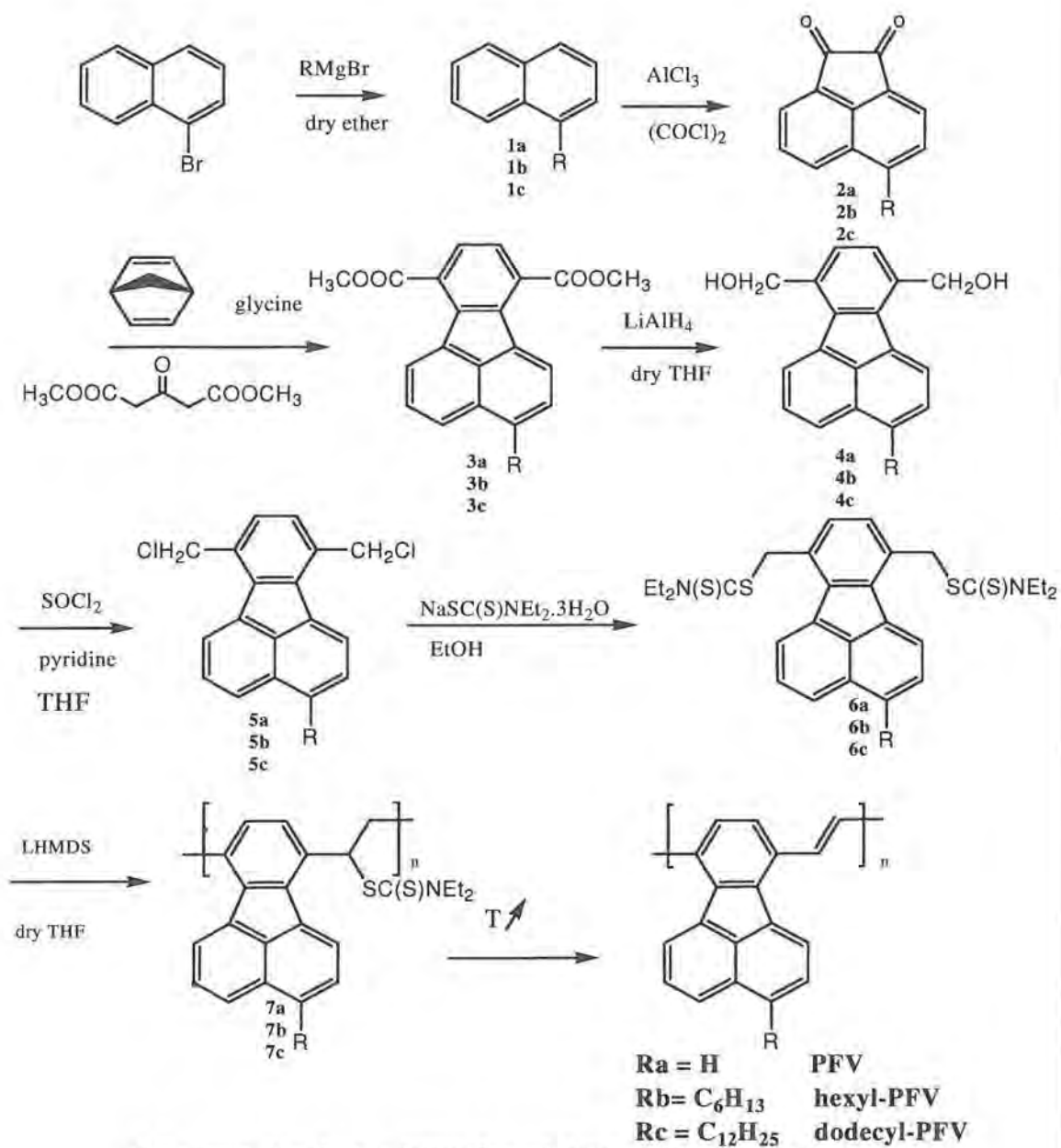
Scheme 1. Chemical structure of the conjugated polymer **PFV** and its substituted derivatives **hexyl-PFV** and **dodecyl-PFV**.

3.2. Synthesis

3.2.1. Monomer Synthesis (Scheme 2)

Since for production of optoelectronic devices soluble polymers are needed, various strategies have been explored to achieve this. One possibility to overcome the solubility issue is the use of a precursor route for the polymerization.^{3,4} With such a route a soluble non-conjugated precursor polymer is obtained, which subsequently can be converted into its conjugated form *in situ*. This approach has been utilized to obtain thin films of the unsubstituted **PFV**. However, unfortunately the solubility of the precursor polymer of **PFV** is insufficient to obtain thin films of sufficient quality for device applications. Therefore as an alternative, long flexible solubilizing side chains have been introduced giving the functionalized **hexyl-PFV** and **dodecyl-PFV**. The synthesis of these alkyl-PFV derivatives starts with the virtually quantitative Grignard reaction between

magnesium alkyl bromide and bromonaphthalene. Subsequently, these alkyl naphthalenes **1b** and **1c** have been converted into the acenaphthenequinone derivatives **2b** and **2c** using a double Friedel-Crafts acylation. The further steps of the monomer synthesis are similar as described in Chapter 2 for the monomer of PFV.² It is comprised of a straightforward one-step synthesis of the dimethyl fluoranthene-7,10-dicarboxylic esters **3b** and **3c** from the corresponding acenaphthenequinone derivatives, acetone dicarboxylic ester and norbornadiene, followed by the reduction with LiAlH_4 of the ester groups giving the diols **4b** and **4c** according to a literature procedure.¹ Subsequently, the 7,10-bis(chloromethyl)fluoranthene derivatives **5b** and **5c** were obtained by reaction with thionylchloride in THF solution. Whereas the rather limited solubility of the unsubstituted **4a** and **5a** required the use of dilute solutions, this is not the case for the alkyl substituted derivatives. Finally, the monomers for the DTC precursor route were synthesized by reaction with sodium diethyldithiocarbamate trihydrate, giving the monomers **6b** and **6c** as light yellow crystalline solids in an excellent yield of *circa* 75%.



Scheme 2. Synthesis of PFV, hexyl-PFV and dodecyl-PFV.

3.2.2. Polymerization

For the polymerization, the dithiocarbamate (DTC) precursor route^{3,4} was chosen, which was previously developed in our laboratory. As mentioned in Chapter 2, this route offers not only a straightforward monomer synthesis, but also precursor polymers of higher quality than many other available precursor routes.⁴ Hence, a polymerization can be accomplished in a straightforward manner. Polymerization of **6b** and **6c** was carried out with lithium bis(trimethylsilyl) amide (LHMDS) as the base in dry THF under inert atmosphere (Scheme 2). After extraction the precursor polymers **7b** and **7c** were isolated in excellent yield by precipitation in MeOH. Further purifications by soxhlet extractions in MeOH, hexane and acetone have been utilized to remove low molecular weight contaminants and/or oligomers.

Selected polymerization results are presented in Table 1. The weight-average molecular weights (M_w) of the precursor polymers have been determined by analytical SEC in THF (**7b** and **7c**) using polystyrene standards. In view of the differences in solubility, molecular weights of **7b** and **7c** were measured in a different solvent as compared to **7a**, which was measured in DMF (*cf.* Chapter 2). It should be noted that since all molecular weights are referenced to polystyrene standards, the actual value for M_w will likely somewhat differ from the apparent M_w observed with analytical SEC. The polymerization results clearly demonstrate the significantly enhanced molecular weights of **7b** and **7c**, as compared to **7a**. This is a result of the enhanced purity of the monomers used for the polymerization of **7b** and **7c**, which can be explained by their improved solubility as a result of the alkyl side chains.

Polymer	M _w (x 10 ⁻³)	PD	Yield (%)
7a	59	1.6	82
7b	272	2.8	62
7c	230	2.1	58

Table 1. Selected polymerization results for the synthesis of the precursor polymers **7a**, **7b** and **7c**. Molecular weights are given as determined by analytical SEC in DMF (**7a**) and THF (**7b** and **7c**) using polystyrene standards.

The employed synthetic methodology can be regarded as a universal scheme towards a wide variety of substituted **PFV** derivatives. This is a result of the fact that the first two steps in this scheme, which involve the introduction of the actual substituent, are compatible with a variety of side chains. One can envisage many different types and even numbers of side chains being introduced in this manner, with the **hexyl-PFV** and **dodecyl-PFV** presented here being only a proof-of-principle.

3.3. Determination of the electrochemical and optical properties of the poly(*p*-fluoranthene vinylene) derivatives

3.3.1. Optical Properties

Thin films of the conjugated polymers **hexyl-PFV** and **dodecyl-PFV** have been obtained by a thermal treatment under N₂ atmosphere of the corresponding precursor polymers **7b** and **7c** in a similar fashion as was done for **7a** (*cf.* Chapter 2). It was observed that for the polymers the conversion to the conjugated structure started at *circa* 100 °C and was completed at *circa* 150 °C under the thermal conditions used. The converted polymers have an orange color as a result of their π -conjugation.

The thin film conversion process can readily be followed by means of *in situ* UV-Vis spectroscopy and FT-IR spectroscopy. For example, upon heating a thin film of **7c** the formation of the conjugated structure of **dodecyl-PFV** is readily observed (Figure 1).

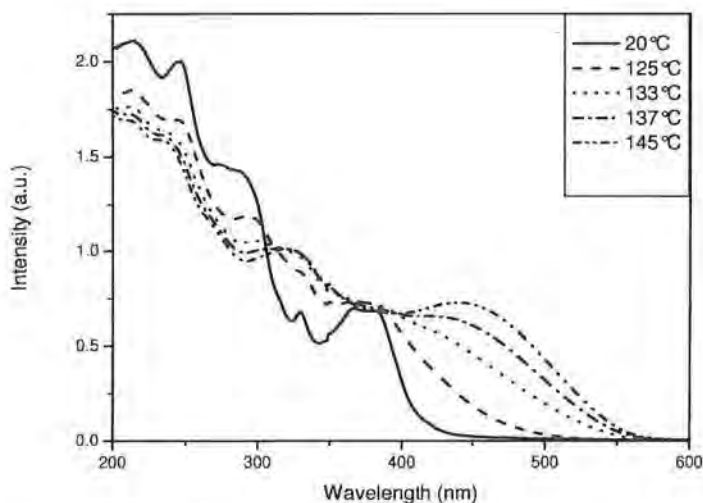


Figure 1. Temperature-dependent UV-Vis spectra of the conversion of precursor polymer **7c** to **dodecyl-PFV** at selected temperatures.

At low temperatures, in the precursor polymer the long wavelength side of the UV-Vis absorption spectrum is dominated by the typical HOMO-LUMO absorption bands of the substituted fluoranthene at 359 and 380 nm (Figure 2), which are also present in monomers **6b** and **6c**. Upon heating, these bands disappear and two new absorption bands develop, which originate from the conjugated structure. The new band at 320 nm is a result of the more extended conjugated system in this type of polymers.⁵ The broad band around 450 nm can be associated with the π - π^* transition ($\lambda_{\text{max}} = 448$ nm for **hexyl-PFV** and 453 nm for **dodecyl-PFV**). These values are

in the same order of magnitude and are significantly red shifted as compared to **PFV** ($\lambda_{\text{max}} = 420 \text{ nm}$). This is a result of the presence of the alkyl side chains in **hexyl-PFV** and **dodecyl-PFV**. The increased solubility of all intermediates during the synthesis, including the monomer and the precursor polymer, as a result of these solubilizing side chains, results in the formation of a better defined precursor polymer. Ultimately, this apparently leads after thermal treatment to a conjugated polymer with a considerably longer effective conjugation length. From the above considerations, it can be concluded that **dodecyl-PFV** is the PFV derivative with the highest purity. In this context, it should be noted that the actual solubility of the substituted conjugated **PFV-derivatives** remains not optimal and the polymers remain insufficiently soluble to perform, for example, analytical SEC or to make thin layers using spincoating. Whereas an improved solubility is observed because of the introduced side chains, further optimizations of these chains will be required to obtain full solubility in a wide range of solvents. One can imagine that for example branched side chains may induce additional solubility.

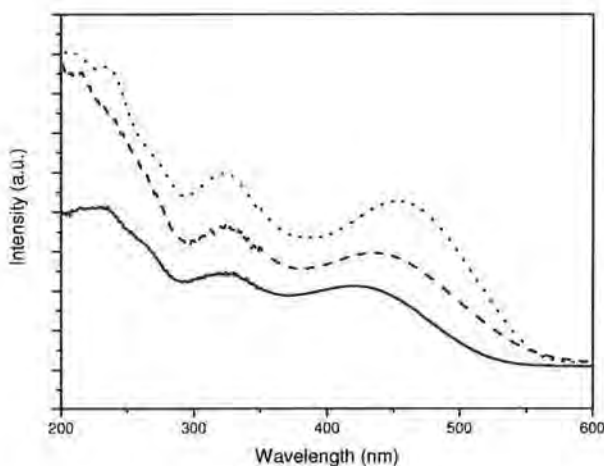


Figure 2. Comparison of the room temperature UV-Vis absorption spectra of thin films of the conjugated polymers **PFV** (solid line), **hexyl-PFV** (dashed line) and **dodecyl-PFV** (dotted line). The intensities of the individual spectra are adjusted to allow for a clear comparison of λ_{max} of the polymers.

The optical band gap can be derived from the low energy side tangent to the π - π^* transition. In this manner, values for the band gap of circa 2.2 eV for **hexyl-PFV** and **dodecyl-PFV** are obtained, which is somewhat smaller than the bandgap of unsubstituted PFV of 2.34 eV (*cf.* Chapter 2). This small decrease is probably also the result of the increased purity of the conjugated system. Notwithstanding, all these values are only slightly smaller than the reported band gap of PPV (circa 2.4 eV).^{4,6} Apparently both the extension of the conjugated system and the functionalization with alkyl side chains, have only a minimal impact on the optical band gap.

To gain a better understanding of the conversion process, the formation of **dodecyl-PFV**, the PFV derivative with the highest purity, was studied in more detail. From the absorption profile at 453 nm it is evident that

conversion of **7c** to its conjugated form starts around 100 °C and is virtually complete at 150 °C (Figure 3). The minor decrease in absorption at temperatures above 200 °C is a result of a reversible thermochromic effect. Furthermore, the UV-Vis analysis indicates that no degradation of the conjugated structure of **dodecyl-PFV** is observed in the entire temperature range up to 250 °C. A similar observation was already made in Chapter 2 for unsubstituted PFV. Apparently, the introduction of side chains has, as expected, no impact on the thermal stability. Temperature dependent UV-Vis is the analytical method of choice to assess the thermal stability of conjugated polymers.⁴ Although the thermal stability of our PFV-derivatives is better than many conjugated polymer systems, this is not unexpected since the base structure, *i.e.* PPV, also has a thermal stability well above 300 °C.⁴ Notwithstanding, this confirms that this new class of materials will not exhibit any form of thermal degradation during standard device operations.

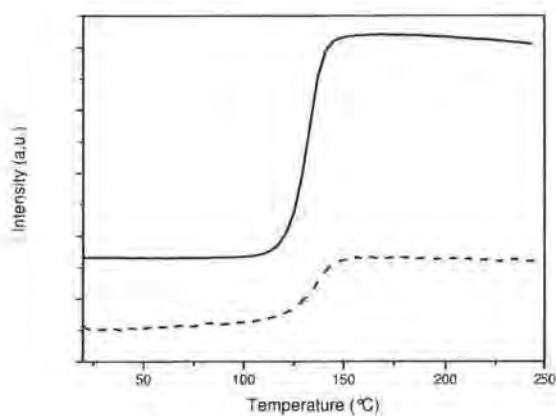


Figure 3. UV-Vis intensity profile at 453 nm (solid) and FT-IR intensity profile at 958 cm^{-1} (dashed) as a function of temperature during the conversion process of precursor polymer **7c** to **dodecyl-PFV**.

The thermal conversion process of **7c** into **dodecyl-PFV** has also been followed using temperature dependant FT-IR spectroscopy (Figures 3 and 4). Upon heating, the vibrations at 1485, 1417, 1266, 1206 cm^{-1} , which are associated with the dithiocarbamate groups, decrease in intensity. At the same time a new vibration develops at 958 cm^{-1} , which arises from the double bonds in the conjugated backbone. The FT-IR measurements confirm that the formation of double bonds starts at 100 °C and is virtually complete around 180 °C with only minimal intensities of the dithiocarbamate groups remaining.

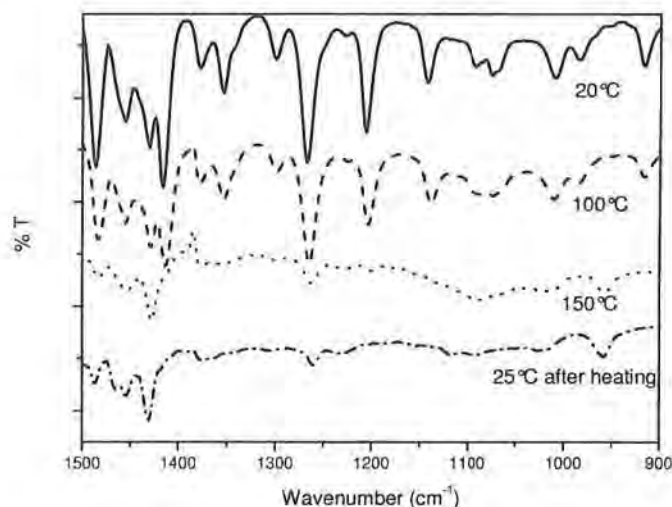


Figure 4. Temperature-dependent FT-IR spectra of the conversion of precursor polymer **7c** to **dodecyl-PFV**.

Fluorescence measurements further confirm the successful formation of the conjugated structure. Whereas precursor polymer **7c** has a fluorescence emission at $\lambda = 475$ nm (excitation at $\lambda = 380$ nm), which is typical for fluoranthene, this fluorescence is no longer present in the corresponding conjugated polymer. Instead for **dodecyl-PFV** a distinct emission is found

at $\lambda = 576$ nm (excitation at $\lambda = 453$ nm), which originates from the conjugated structure. The emission maximum of dodecyl-PFV is significantly red-shifted as compared to unsubstituted PFV (emission at $\lambda = 545$ nm; cf. Chapter 2), further confirming the enhanced purity and effective conjugation of the alkyl substituted polymers.

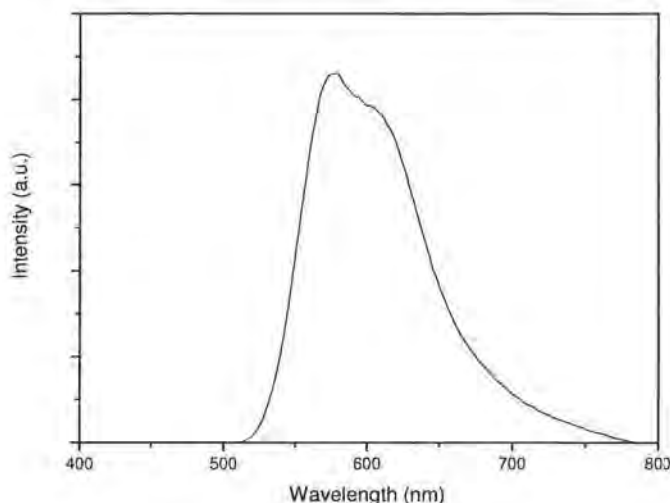


Figure 5. Fluorescence emission spectrum of **dodecyl-PFV** (excitation at 453 nm).

3.3.2. Electronic Properties

Thin film cyclic voltammetry (CV) was employed to investigate the electrochemical behavior of the obtained conjugated polymers and to estimate the position of their lowest occupied molecular orbital, *viz.* the LUMO energy level or conduction band edge. The latter is possible, since the cyclic voltammograms of the polymers display discernable reduction processes, *i.e.* n-doping. In marked contrast, the current density associated with the p-doping, *viz.* the oxidation processes, is very small. This n-type behavior is associated with the non-alternant polycyclic aromatic

hydrocarbon units in the backbone. The conduction band edge energy levels of **hexyl-PFV** and **dodecyl-PFV**, which are determined from the onset of reduction, are located around -1.90 V *vs.* Ag/AgNO₃, which correspond to a LUMO energy level of *circa* -3.0 eV. It should be noted that for the conversion to eV, all electrochemical potentials have been referenced to a known standard, ferrocene/ferrocinium, which is estimated to have an oxidation potential of -4.98 V *vs.* Vacuum.

Although the HOMO energy levels are more difficult to estimate, based on the optical band gap the HOMO of the PFV-type polymers can be anticipated around -5.2 eV. The LUMO energy level is in the same order of magnitude as found for unsubstituted PFV, for which the LUMO could be more accurately determined, since the alkyl side groups in **hexyl-PFV** and **dodecyl-PFV** interfere with the cyclic voltammetry by somewhat blocking the flow of electrolyte ions. From the electrochemical measurements it is clear that the introduction of an alkyl side chain has only minimal impact on the energy levels of the obtained conjugated polymers. Especially for the construction of organic solar cells, the position of the HOMO and LUMO energy levels is of interest. Currently PCBM (LUMO -3.96 eV and HOMO -5.53 eV) is the n-type material of choice for organic photovoltaic applications. The position of the energy levels in **dodecyl-PPV** are, although far from identical to PCBM, possibly sufficiently close to replace PCBM as the electron accepting material in solar cell applications, although further tuning of the band gap energy levels may be required.

3.3.3. Mobility Measurements

For an optimal performance of conjugated polymers in optoelectronic devices, sufficient charge carrier mobility is essential. More specifically, in order for the novel PFV derivatives to be suitable n-type electron accepting materials in organic photovoltaics, sufficient electron mobility is needed. Whereas the limited solubility and poor film forming properties of the

precursor polymer of unsubstituted **PFV** hampers the application of this material in thin film electronic applications, our novel alkyl substituted materials can be successfully incorporated. Hence, to verify the n-type character of the materials, the charge carrier mobility in the representative with the highest purity, **dodecyl-PFV**, was measured.

Charge Carrier Extraction by Linearly Increasing Voltage (CELIV) is a rather novel technique used to measure the carrier mobility in semiconductors with a broad range of conductivities.⁷ The advantage of this technique is that the carrier mobility can be directly measured from the experimentally recorded current transients and no data fitting procedures are required. An additional advantage of CELIV is the possibility to estimate the mobility even when rather dispersive charge carrier transport prevails. Given the experimental conditions, the charge carrier mobility can be directly estimated from the extraction maximum of the current transient.⁸ Even though the carrier mobility and conductivity of the semiconducting materials can be measured in the dark, in case of pure undoped organic semiconducting films in which the sample conductivity is low, the charge carriers can also be generated using a laser pulse. The essence of this technique is that a triangular-shaped voltage pulse is applied to the sample. The initial current step (displacement current) is caused by the geometrical capacity of the film between the two electrodes. The following increasing extraction current is caused by the photoconductivity of the sample due to the generated charge carriers. As the triangular voltage pulse continues to increase, the electric field redistribution takes place inside the sample and carrier mobility values μ can be calculated directly from the current transients.

In Figure 6 the experimental CELIV current transients of **dodecyl-PFV** are shown. The capacitive current response (solid lower transient) shows rather low conductivity of the film under the given experimental conditions, which is typical for high quality undoped materials, in which the equilibrium

charge carrier concentration is low. In order to photo-generate additional charge carriers, a laser pulse was applied. The extraction current transient (upper dashed transient in Figure 6) shows rather dispersive extraction with an unpronounced extraction maximum, from which the electron mobility can directly be derived $\mu_e = 1.4 \cdot 10^{-4} \text{ cm}^2/\text{Vs}$. To prevent the extraction of photo-generated charge carriers prior to the application of the triangular voltage pulse, an offset voltage $U_{\text{offset}} = -0.6 \text{ V}$ was used. The electron mobility is measured at an electric field approximately equal to 30 kV/cm. In this context it is noteworthy that the electron mobility reported in literature for PCBM is $\mu_e = 2 \cdot 10^{-3} \text{ cm}^2/\text{Vs}$.⁹ This demonstrates the surprisingly high electron mobility for unoptimized thin films of **dodecyl-PFV**, which are currently only one order of magnitude smaller than those of the most commonly applied material PCBM.

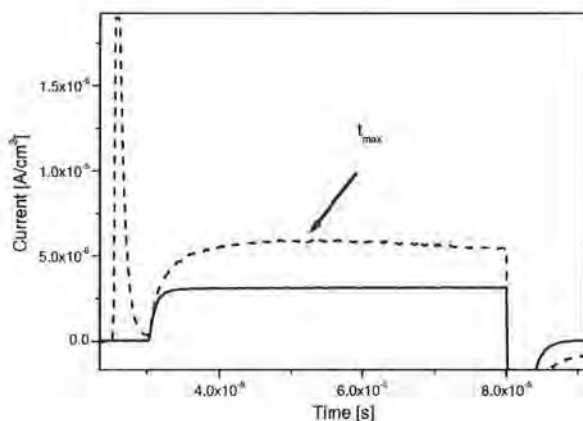


Figure 6. Charge Carrier Extraction by Linearly Increasing Voltage (CELIV) current transients in **dodecyl-PFV**: bottom transient (solid line) is the capacitive response to the applied triangle-shaped voltage pulse in the dark and the top transient (dashed line) demonstrates extraction of photogenerated charge carriers.

To validate the above observation and in order to determine which charge carriers, electrons or holes, are faster, an additional Hecht dependence resembling experiment was performed. To this end, the ITO electrode was illuminated under positive and negative bias. To measure the electron conduction through the film (solid transient in Figure 7), negative bias was applied to the ITO electrode, whereas to measure the hole conduction (dashed transient in Figure 7), positive bias was applied. As can be seen from Figure 7, the extraction transient as well as the total extracted charge for the electrons is larger than those for the holes. Since the same amounts of electrons and holes are photo-generated for both biases, the larger current would correspond to the larger carrier mobility. Therefore, it can be concluded that the electron mobility is indeed faster than the hole mobility.

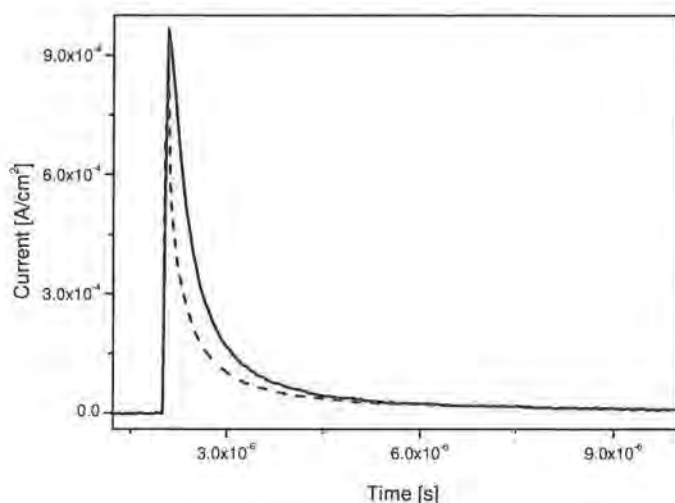


Figure 7. Time-of-Flight photocurrent transients for electrons (solid line) and for holes (dashed line) upon illumination of the ITO contact.

The high electron mobility confirms that this novel class of polymers holds significant promise for the application in solar cells. A first attempt was made to construct bulk heterojunction solar cells with **dodecyl-PFV** as an acceptor and MDMO-PPV as a donor in a 1:1 ratio. Since **dodecyl-PFV** is only to a limited degree soluble in dichlorobenzene, MDMO-PPV was mixed with the precursor polymer for the spincoating procedure. Subsequently the precursor polymer was converted into the conjugated polymer *in situ*. Dark and illuminated IV-characteristics were measured under AM1.5 conditions. Preliminary solar cell characteristics for this cell containing **dodecyl-PFV** obtained under these measurement conditions are: $I_{sc} = 3.98 \cdot 10^{-3} \text{ mA/cm}^2$, $V_{oc} = 0.70 \text{ V}$, $FF = 24\%$, $\eta_e = 0.01 \%$. These experiments indicate that indeed organic solar cells can be obtained using **dodecyl-PFV** as the n-type material. For electron transfer from donor to acceptor to occur, the LUMO of the donor needs to be 0.3 eV to 0.5 eV higher than the LUMO of the acceptor. In the case of the MDMO-PPV:**dodecyl-PFV**, this difference is lower, namely 0.17 eV. Apparently, this difference is too small to have an efficient electron transfer from donor to acceptor. Hence, further tuning of the energy levels of the PFV-type polymers, using for example functional groups, is needed.

3.4. Conclusion

A novel class of PPV-type polymers with a backbone structure containing fluorene repeating units has been developed. The presented synthetic methodology, which allows for the introduction of a variety of substituents, can be regarded as a universal synthesis route towards this class of conjugated polymers. This is exemplified by the synthesis of two substituted PFV derivatives, *i.e.* **hexyl-PFV** and **dodecyl-PFV**. It is confirmed that PFV and its derivatives exhibit unusual n-type behavior, which is likely associated with the non-alternant character of the repeating units. The

introduction of alkyl side chains, leads to conjugated polymers with a significantly enhanced purity as compared to unsubstituted **PFV**. This is a result of the fact that all synthetic intermediates, including the precursor polymers, display an improved solubility. As a result, a polymer such as **dodecyl-PFV** is excellently suitable for device applications. The electronic properties of **dodecyl-PFV** indicate that this polymer may provide a substitute for PCBM, a soluble C₆₀ derivative currently used in organic solar cells as the n-type material. A polymeric alternative for PCBM could facilitate the formation of a more favorable morphology. It is demonstrated using CELIV mobility measurements that **dodecyl-PFV** indeed has sufficiently high electron mobility for use in optical and electronic applications as an n-type material. Notwithstanding, the position of the energy levels is not optimal to facilitate charge transfer in a typical bulk-heterojunction solar cell. Hence, further tuning of the energy levels will be required.

3.5. Experimental

3.5.1. General

NMR spectra were recorded with a Varian Inova Spectrometer (¹H-NMR 300 MHz, ¹³C-NMR 75 MHz). Analytical Size Exclusion Chromatography (SEC) was performed using a Spectra series P100 (Spectra Physics) pump equipped with two mixed-B columns (10 μm, 2 x 30 cm, Polymer Labs) and a Refractive Index detector (Shodex) at 40 °C or 70 °C. THF or a DMF solution of oxalic acid (1.1x10⁻³ M) was used as the eluent at a flow rate of 1.0 mL/min. Molecular weight distributions are given relative to polystyrene standards.

Gas chromatography/mass spectrometry (GC/MS) analyses were carried out on TSQ-70 and Voyager mass spectrometers (Thermoquest); the capillary column was a Chrompack Cpsil5CB or Cpsil8CB. DIP-MS

measurements were performed at a heating rate of 10 °C/min up to 600 °C. In this technique the material is brought directly on the heating element of the probe as a thin film and this enables to study the products that are liberated in the high vacuum ($4 \cdot 10^{-4}$ Pa) inside the spectrometer. Liberated products were ionized by electron impact. FT-IR spectra were collected with a Perkin Elmer Spectrum One spectrometer (nominal resolution 4 cm^{-1} , summation of 16 scans). UV-Vis measurements were performed on a Cary 500 UV-Vis-NIR spectrophotometer (scan rate 600 nm/min, continuous run from 200 to 600 nm). The conversions of the precursor polymers into the corresponding conjugated structures were followed *in situ* with FT-IR and UV-Vis spectroscopy. The *in-situ* FT-IR elimination reactions in the solid state were performed in a Harrick variable temperature cell (Safir), positioned in the beam of the FT-IR spectrometer. The temperature of the sample was controlled by a Watlow (serial number 999, dual channel) temperature controller. The precursor polymer was drop-casted from a CHCl_3 solution on a KBr pellet (diameter 25 mm, thickness 1 mm). Afterwards, the KBr-pellet was brought into the cell, which was continuously flushed with nitrogen (open system). The spincoated KBr pellet was in direct contact with the heating element. "Timebase software" (Perkin Elmer) was used to follow the processes. The *in-situ* UV-Vis measurements in the solid state were performed in a similar Harrick variable temperature cell as was used for the FT-IR measurements, which was for the UV-Vis measurements positioned in the beam of the UV-Vis-NIR spectrometer. The precursor polymer was drop-casted from a CHCl_3 solution on a quartz glass (diameter 25 mm, thickness 3 mm). The experiments were performed in the same manner as the *in-situ* FT-IR measurements. All measurements were performed under a continuous flow of nitrogen (open system). "Scanning Kinetics software" (Varian) was used to follow the processes. Electrochemical properties were measured with an Eco Chemie Autolab PGSTAT 20 Potentiostat/Galvanostat using a

conventional three-electrode cell (electrolyte: 0.1 M TBAPF₆ in anhydrous CH₃CN) with an Ag/AgNO₃ reference electrode (0.01 M AgNO₃, 0.10 M TBAPF₆ and CH₃CN), a platinum counter electrode and a platinum or Indium-Tin Oxide (ITO) coated glass substrate as working electrode. Cyclic voltammograms were recorded at 50 mV/s under N₂ atmosphere. All electrochemical potentials have been referenced to a known standard, ferrocene/ferrocinium, which is estimated to have an oxidation potential of -4.98 V *vs.* Vacuum.

3.5.2. Synthesis (Scheme 2)

Unless stated otherwise, all reagents and chemicals were obtained from commercial sources and used without further purification. Tetrahydrofuran (THF) was purified by distillation from sodium/benzophenone. Compounds **3a**, **4a**, **5a**, **6a** as well as PFV were prepared as described in Chapter 2.¹³

1-Hexylnaphthalene (1b). 100 mL of a 2 M solution of hexylmagnesiumbromide in diethyl ether was added dropwise to a stirred mixture of 1-bromonaphthalene (29.6 g, 0.143 mol) and Ni(dppp)Cl₂ (0.77g, 0.00143 mol) in diethyl ether (150 mL) while maintaining the temperature below 30 °C. After stirring overnight at room temperature, 2M aqueous HCl (572 mL) was slowly added after which the resulting layers were separated. The water layer was extracted with diethyl ether (3x 300 mL). The combined organic layers were washed with a saturated NaHCO₃ solution (3x 200 mL) and dried over anhydrous MgSO₄. The solvent was evaporated under reduced pressure and the mixture was further purified by kugelrohr distillation to give 29.5 g of a white solid product (97% yield). ¹H-NMR (CDCl₃): δ = 8.12 (d, 1H), 7.91 (dd, 1H), 7.77 (d, 1H), 7.55 (m, 2H), 7.46 (t, 1H), 7.38(d, 1H), 3.13 (t, 2H), 1.79 (m, 2H), 1.54-1.34 (br m, 6H), 0.99 (t, 3H); ¹³C-NMR (CDCl₃): δ = 138.9, 133.8, 131.8, 128.6, 126.3, 125.7, 125.5, 125.4, 125.2, 123.8, 33.0, 31.7, 30.8, 29.5, 22.6, 14.0.

1-Dodecyl-naphthalene (1c). Starting from 600 mL of a 1 M solution of dodecylmagnesiumbromide in diethyl ether, 1-bromonaphthalene (105g, 0.507 mol) and Ni(dppp)Cl₂ (2.74g, 0.00507 mol) dissolved in 600 mL of diethyl ether and 2M aqueous HCl (2 L) using a similar procedure as described for **1b**, compound **1c** was obtained as a white solid. (144 g, 96% yield). ¹H-NMR (CDCl₃): δ = 8.08 (d, 1H), 7.88 (dd, 1H), 7.73 (d, 1H), 7.51 (m, 2H), 7.42 (t, 1H), 7.35 (d, 1H), 3.10 (t, 2H), 1.79 (m, 2H), 1.62-1.21 (br m, 18 H), 0.94 (t, 3H); ¹³C-NMR (CDCl₃): δ = 138.9, 133.8, 131.8, 128.6, 126.3, 125.7, 125.5, 125.4, 125.2, 123.8, 33.1, 31.9, 30.9, 29.8, 29.7, 29.7, 29.6, 29.6, 29.5, 29.3, 22.7, 14.1.

5-Hexylacenaphthylene-1,2-dione (2b). Oxalyl chloride (8.98 g, 0.0708 mol) was added to a stirred suspension of AlCl₃ (28 g, 0.212 mol) in 1,2-dichloroethane (300 mL) at 0°C. After the drop wise addition of **1b** (15 g, 0.0708 mol) in 1,2-dichloroethane (50 mL) the stirring was continued for 6 hours at the same temperature. The reaction mixture was quenched with water (200 mL) and the resulting layers were separated. Subsequently the organic layer was washed with an aqueous 2 M solution of sodium carbonate (1x 200 mL) and water (1x 300 mL) after which it was dried over anhydrous MgSO₄. After removal of the solvent at reduced pressure, the crude product was further purified by column chromatography (silica, CH₂Cl₂) to give 4.15 g **2b** as yellow crystals (22% yield). ¹H-NMR (CDCl₃): δ = 8.33 (d, 1H), 8.01 (t, 2H), 7.80 (t, 1H), 7.61 (d, 1H), 3.16 (t, 2H), 1.77 (m, 2H), 1.46-1.23 (br m, 6H), 0.87 (t, 3H); ¹³C-NMR (CDCl₃): δ = 188.8, 187.6, 147.4, 146.1, 129.7, 129.5, 128.7, 127.8, 127.8, 126.8, 122.1, 121.4, 32.9, 31.5, 30.4, 29.2, 22.4, 13.9.

5-Dodecyl-acenaphthylene-1,2-dione (2c). Starting from oxalyl chloride (6.43 g, 0.0507 mol), AlCl₃ (20.27 g, 0.152 mol) and **1c** (15 g, 0.0507 mol), using a similar procedure as described for **2b**, compound **2c** was obtained as yellow crystals (4.01 g, 22% yield). ¹H-NMR (CDCl₃) δ: 8.35

(d, 1H), 8.06 (d, 1H), 8.03 (d, 1H), 7.82 (dd, 1H), 7.64 (d, 1H), 3.18 (t, 2H), 1.78 (p, 2H), 1.49-1.28 (br m, 18H), 0.85 (t, 3H); $^{13}\text{C-NMR}$ (CDCl_3): δ = 188.6, 187.4, 147.4, 146.0, 129.6, 129.5, 128.6, 127.7, 127.7, 126.7, 122.0, 121.3, 32.8, 31.7, 30.4, 29.5, 29.4, 29.4, 29.4, 29.4, 29.3, 29.1, 22.5, 13.9.

3-Hexylfluoranthene-7,10-dicarboxylic acid dimethyl ester (3b).

A mixture of **2b** (3.0 g, 11.28 mmol), dimethyl 1,3-acetone dicarboxylate (4.7 g, 26.99 mmol) and glycine (1.86 g, 24.78 mmol) in 2,5-norbornadiene (70 mL) was stirred at reflux temperature for 3.5 days. The reaction flask was equipped with a Dean-Stark trap to remove the water generated from the reaction. Excess solvent was removed at the end of the reaction by simple distillation to give a red-brown solid. The resulting solid was dissolved in CHCl_2 (200 mL) and washed with H_2O (200 mL). After evaporation the product was further purified by column chromatography (silica, CH_2Cl_2) to give 3.72 g of **3b** as yellow crystals (82% yield). $^1\text{H-NMR}$ (CDCl_3): δ = 8.59 (d, 1H), 8.52 (d, 1H), 8.10 (d, 1H), 7.80 (dd, 2H), 7.67 (t, 1H), 7.45 (d, 1H), 4.06 (s, 6H), 3.15 (t, 2H), 1.77 (m, 2H), 1.42-1.19 (br m, 6H), 0.87 (t, 3H); $^{13}\text{C-NMR}$ (CDCl_3): δ = 168.0, 167.9, 142.2, 139.5, 139.3, 133.8, 133.4, 131.6, 129.5, 129.0, 128.8, 128.1, 127.5, 127.4, 127.2, 126.4, 125.8, 125.2, 52.5, 52.4, 32.3, 31.9, 31.7, 29.3, 22.6, 14.1.

3-Dodecylfluoranthene-7,10-dicarboxylic acid dimethyl ester

(3c). Starting from a mixture of **2c** (3.73 g, 10.53 mmol), dimethyl 1,3-acetone dicarboxylate (4.4 g, 25.27 mmol) and glycine (1.73 g, 23.05 mmol) in 2,5-norbornadiene (70 mL), using a similar procedure as described for **3b**, compound **3c** was obtained as yellow crystals (4.15 g, 81% yield). $^1\text{H-NMR}$ (CDCl_3): δ = 8.59 (d, 1H), 8.53 (d, 1H), 8.09 (d, 1H), 7.79 (dd, 2H), 7.66 (t, 1H), 7.45 (d, 1H), 4.06 (s, 6H), 3.14 (t, 2H), 1.77 (m, 2H), 1.49-1.16 (br m, 6H), 0.87 (t, 3H); $^{13}\text{C-NMR}$ (CDCl_3): δ = 167.9, 167.8, 142.1, 139.4, 139.3, 133.7, 133.3, 131.4, 129.3, 128.8, 128.7, 128.0, 127.3, 127.3, 127.1,

126.3, 125.7, 125.2, 52.4, 52.3, 33.3, 31.3, 30.2, 29.4, 29.4, 29.3, 29.3, 29.3, 29.2, 29.0, 22.3, 13.7.

3-Hexyl-7,10-bis(hydroxymethyl) fluoranthene (4b). A solution of diester **3b** (1 g, 2.49 mmol) in dry THF (50 mL) was added drop wise with stirring to a dispersion of lithium aluminium hydride (0.24 g, 6.25 mmol) in THF (50 mL) at 0°C. The reaction mixture was allowed to warm to room temperature and stirred for 6 h. Subsequently, water (10 mL), 10% aqueous sodium hydroxide (10 mL) and water (10 mL) were added. After acidification of the water layer to pH = 6 with 1N HCL the layers were separated and the water layer was extracted with 1:1 ether/THF (3 x 200 mL). The combined organic layers were washed with water (300 mL), after which they were dried over anhydrous MgSO₄. Removal of the solvents under reduced pressure gave a yellow solid, which was further purified by crystallization from methanol to give 0.33 g of **4b** as yellow crystals (38% yield). ¹H-NMR (DMSO): δ = 8.07 (d, 1H), 8.05 (d, 1H), 7.94 (d, 1H), 7.71 (dd, 1H), 7.50 (d, 1H), 7.47 (s, 2H), 5.43 (m, 2H), 5.00 (t, 4H), 3.11 (t, 2H), 1.70 (m, 2H), 1.43-1.18 (br m, 6H), 0.84 (t, 3H); ¹³C-NMR (DMSO): δ = 139.8, 137.2, 136.9, 136.4, 135.3, 135.2, 134.1, 131.9, 128.5, 127.8, 127.6, 126.0, 125.7, 124.3, 124.0, 123.5, 61.4, 61.4 31.8, 31.4, 31.2, 28.7, 22.1, 14.0.

3-Dodecyl-7,10-bis(hydroxymethyl) fluoranthene (4c). Starting from **3c** (2 g, 4.15 mmol) and LiAlH₄ (0.38 g, 9.96 mmol), using a similar procedure as described for **4b**, compound **4c** was obtained as yellow crystals (0.92 g, 52% yield). ¹H-NMR (DMSO): δ = 8.07 (d, 1H), 8.05 (d, 1H), 7.95 (d, 1H), 7.72 (dd, 1H), 7.50 (d, 1H), 7.47 (s, 2H), 5.42 (m, 2H), 5.00 (t, 4H), 3.13 (t, 2H), 1.72 (m, 2H), 1.49-1.13 (br m, 18H), 0.84 (t, 3H). ¹³C-NMR (DMSO): δ = 139.8, 137.2, 136.9, 136.4, 135.3, 135.2, 134.1, 131.9, 128.5, 127.8, 127.6, 126.0, 125.7, 124.3, 124.0, 123.5, 61.4, 61.4, 31.8, 31.4, 31.3, 30.4, 29.0, 28.8, 28.7, 28.6, 28.5, 28.4, 22.1, 14.0.

3-Hexyl-7,10-bis(chloromethyl) fluoranthene (5b). Thionylchloride (0.38 g, 3.18 mmol) was added drop wise to a solution of the diol **4b** (0.5 g, 1.45 mmol) and pyridine (0.46 g, 5.78mmol) in THF (80 mL) at 0 °C. The mixture was stirred at reflux temperature for 24 hours. After dilution with water (150 mL) and extraction with CHCl₃ (3 x 200 mL), the combined organic layers were dried over MgSO₄ and the solvent was evaporated. The resulting product was further purified by crystallization from CH₂Cl₂ to give 0.35 g of **5b** as light yellow crystals (63% yield). ¹H NMR (CDCl₃): δ = 8.11 (d, 1H), 8.03 (t, 2H), 7.68 (t, 1H), 7.46 (d, 1H), 7.28 (s, 2H), 5.02 (s, 2H), 5.01 (s, 2H), 3.13 (t, 2H), 1.78 (m, 2H), 1.44-1.23 (br m, 6H), 0.89 (t, 3H); ¹³C NMR (CDCl₃): δ = 141.3, 138.1, 138.0, 135.3, 133.0, 132.7, 128.9, 128.6, 127.6, 127.5, 124.4, 124.3, 123.9, 44.5, 44.5, 32.2, 31.9, 31.6, 29.2, 22.5, 14.0.

3-Dodecyl-7,10-bis(chloromethyl) fluoranthene (5c). Starting from **4c** (2.1 g, 4.88 mmol), thionylchloride (1.54g, 19.5 mmol) and pyridine (1.28 g, 10.7 mmol), using a similar procedure as described for **5b**, compound **5c** was obtained as light yellow crystals (1.52 g, 67% yield). ¹H NMR (CDCl₃): δ = 8.16 (d, 1H), 8.08 (d, 1H), 8.05 (d, 1H), 7.70 (dd, 1H), 7.48 (d, 1H), 7.32 (s, 1H), 7.32 (s, 1H), 5.07 (s, 2H), 5.06 (s, 2H), 3.15 (t, 2H), 1.78 (m, 2H), 1.52-1.17 (br m, 18H), 0.86 (t, 3H); ¹³C NMR: (CDCl₃): δ = 141.3, 138.2, 138.0, 135.4, 133.1, 132.7, 129.0, 128.6, 127.6, 127.5, 124.4, 124.3, 123.9, 44.5, 44.5, 32.2, 31.9, 31.7, 29.5, 29.5, 29.4, 29.4, 29.3, 29.3, 29.2, 22.5, 14.0.

3-Hexyl-7,10-bis((N,N-diethyl dithiocarbamate)methyl)

fluoranthene (6b). A mixture of dichloride **5b** 0.3 g, 0.78 mmol), sodium diethyldithiocarbamate trihydrate (0.53 g, 2.35 mmol) in ethanol (80 mL) was stirred at room temperature for 24 hours. Subsequently, water (50 mL) was added after which the desired monomer was extracted with chloroform (3 x 150 mL). The combined CHCl₃ layers were dried over MgSO₄ and after evaporation of the solvent the crude monomer was obtained. Further

crystallization from methanol yielded 0.34 g of pure **6b** as light yellow crystals (72% yield). ^1H NMR (CDCl_3): $\delta = 8.06$ (d, 1H), 7.98 (dd, 2H), 7.64 (dd, 1H), 7.43 (d, 1H), 7.31 (s, 2H), 4.94 (s, 2H), 4.93 (s, 2H), 4.07 (dd, 4H), 3.67 (dd, 4H), 3.12 (t, 2H), 1.76 (m, 2H), 1.44-1.23 (br m, 6H), 1.20 (t, 6H) 0.87 (t, 3H); ^{13}C NMR (CDCl_3) $\delta = 195.1, 195.1, 140.6, 138.4, 138.2, 135.9, 133.6, 132.8, 130.2, 130.0, 129.9, 129.6, 128.9, 127.6, 127.5, 124.1, 123.8, 123.7, 49.2, 49.2, 46.6, 46.6, 41.2, 41.2, 32.2, 31.9, 31.6, 29.2, 22.5, 13.4, 12.3, 12.3, 11.5, 11.5$; GC-MS (EI, m/e): 608 (M^+), 460 ($\text{M}^+ - \text{SC}(\text{S})\text{NEt}_2$), 312 ($\text{M}^+ - 2 \times \text{SC}(\text{S})\text{NEt}_2$), 242 ($\text{M}^+ - \text{SC}(\text{S})\text{NEt}_2 - \text{C}_5\text{H}_{13}$), 148 ($\text{SC}(\text{S})\text{NEt}_2$), 116 ($\text{C}(\text{S})\text{NEt}_2$), 72 (NEt_2); FT-IR (NaCl, cm^{-1}): 2959, 2924, 2853, 1486, 1457, 1415, 1318, 1354, 1305, 1269, 1204, 1141, 1068, 1009, 982, 918, 830, 759.

3-Dodecyl-7,10-bis((N,N-diethyldithiocarbamate)methyl)

fluoranthene (6c). Starting from **5c** (1.5 g, 3.21 mmol) and sodium diethyldithiocarbamate trihydrate (3.6 g, 16.0 mmol), using a similar procedure as described for **6b**, compound **6c** was obtained as light yellow crystals (1.48 g, 76% yield). ^1H NMR (CDCl_3): $\delta = 8.04$ (d, 1H), 7.97 (dd, 2H), 7.64 (dd, 1H), 7.42 (d, 1H), 7.30 (s, 2H), 4.93 (s, 4H), 4.07 (d, 4H), 3.65 (d, 4H), 3.11 (t, 2H), 1.76 (m, 2H), 1.51-1.16 (br m, 30H), 0.87 (t, 3H); ^{13}C NMR (CDCl_3): $\delta = 195.1, 195.1, 140.6, 138.4, 138.2, 135.9, 133.6, 132.8, 130.2, 130.0, 129.9, 129.6, 128.9, 127.6, 127.5, 124.1, 123.8, 123.7, 49.2, 49.2, 46.6, 46.6, 41.2, 41.2, 32.2, 31.9, 31.8, 29.5, 29.5, 29.5, 29.4, 29.4, 29.3, 29.2, 22.6, 14.0, 12.3, 12.3, 11.5, 11.5$; GC-MS (EI, m/e): 692 (M^+), 544 ($\text{M}^+ - \text{SC}(\text{S})\text{NEt}_2$), 396 ($\text{M}^+ - 2 \times \text{SC}(\text{S})\text{NEt}_2$), 242 ($\text{M}^+ - \text{SC}(\text{S})\text{NEt}_2 - \text{C}_{11}\text{H}_{25}$), 148 ($\text{SC}(\text{S})\text{NEt}_2$), 116 ($\text{C}(\text{S})\text{NEt}_2$), 72 (NEt_2); FT-IR (NaCl, cm^{-1}): 2960, 2925, 2852, 1593, 1485, 1455, 1430, 1415, 1378, 1354, 1300, 1268, 1205, 1142, 1068, 1008, 984, 917, 829, 762.

Precursor polymer for hexyl-poly(*p*-fluoranthene vinylene) (7b).

A solution of monomer **6b** (0.3 g, 0.49 mmol) in dry THF (2.47 mL) was degassed for 1 hour by passing through a continuous N_2 flow. Subsequently,

0.78 mL of a 1 M LHMDS solution in THF was added in one go to the stirred monomer solution. The mixture was stirred for an additional 3 hours under N₂ atmosphere after which the polymer was precipitated in ice water and subsequently extracted with chloroform (3 x 200 mL). The solvent of the combined organic layers was evaporated under reduced pressure. After dissolving the precursor polymer in a small amount of CHCl₃, **7b** was isolated by precipitation in methanol. After further purifications by soxhlet extractions with MeOH, hexane and acetone, respectively, to remove low molecular weight contaminants and/or oligomers, 143 mg of the pure precursor polymer **7b** was isolated as a light yellow solid (62% yield). ¹H NMR (CDCl₃): δ = 8.8-6.0 (b, 7H), 4.4-2.4 (b, 9H), 2.0-0.2 (b, 17H); SEC (THF) M_w = 2.7×10⁵ g/mol (PD = M_w/M_n = 2.8); FT-IR (NaCl, cm⁻¹): 2954, 2928, 2856, 1486, 1456, 1430, 1416, 1354, 1266, 1206, 1142, 1074, 1010, 916, 830.

Precursor polymer for dodecyl-poly(*p*-fluoranthene vinylene) (7c). Starting from monomer **6c** (0.2 g, 0.29 mmol) and 0.46 mL of a 1 M LHMDS solution in THF, using a similar procedure as described for **7b**, precursor polymer **7c** was obtained as a light yellow solid (92 mg, 58% yield). ¹H NMR (CDCl₃): δ = 9.0-6.0 (b, 7H), 4.4-2.4 (b, 9H), 2.2-0.2 (b, 29H); SEC (THF) M_w = 2.3×10⁵ g/mol (PD = M_w/M_n = 2.1); FT-IR (NaCl, cm⁻¹): 2924, 2850, 1486, 1458, 1431, 1417, 1354, 1266, 1206, 1142, 1074, 1010, 916, 830.

Thermal Conversion of 7b and 7c into the corresponding conjugated form (hexyl-PFV and dodecyl-PFV). Thin films of precursor polymers **7b** and **7c** have been converted into the conjugated polymers **hexyl-PFV** and **dodecyl-PFV** by a thermal treatment under N₂ atmosphere. During this treatment the dithiocarbamate group is eliminated from the precursor polymers. For the thermal treatment, the precursor polymers **7b** and **7c** were spin-coated from CHCl₃ solutions onto a suitable

substrate. Subsequently, these coated substrates were placed in a controlled temperature cell and were heated to a suitable conversion temperature (*e.g.* 165 °C). **Hexyl-PFV** and **dodecyl-PFV** were obtained as yellow-orange solids. **Hexyl-PFV**: FT-IR (NaCl, cm⁻¹): 2956, 2928, 2856, 1430, 960, 822, 808, 750. **Dodecyl-PFV**: FT-IR (NaCl, cm⁻¹): 2924, 2852, 1430, 958, 822, 808, 750.

3.5.3. Mobility Measurements

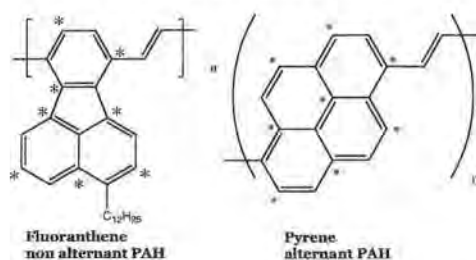
Sandwich-type samples were prepared for charge carrier mobility measurements of **dodecyl-PFV**. To this end, the precursor polymer **7c** was dissolved in chloroform (40 mg/mL). The solution was filtered through a 0.45 μm filter before deposition by spin coating on top of prepatterned ITO-covered glass substrates. Subsequently, the precursor polymer was converted to the conjugated **dodecyl-PFV** (*vide supra*) and 100 nm aluminum top contacts were evaporated on top of the polymer (vacuum 10⁻⁶ mbar). Samples were prepared under inert atmosphere and the films were measured *in vacuo* using an optical cryostat (Oxford Optistat DNV). For the CELIV experiments a variable pulse generator (Agilent 33250A) and oscilloscope (Tektronix TDS 754C) were used to record the current transients. For triggering purposes to ensure the proper delay time between voltage and light pulse, a pulse and the delay function generator (Stanford DG535) was used. A Nd:YAG laser (Coherent Infinity 40-100) was employed to photogenerate the charge carriers using a 5 ns laser pulse at a wavelength of 355nm and an intensity of less than 1 mJ/pulse per standard laser beam output area. The films were illuminated through the ITO side when forward and reverse voltage was applied to the sample.

3.6. References

- (1) Scott, L. T.; Cheng, P.; Hashemi, M. M.; Bratcher, M. S.; Meyer, D. T. and Warren, H. B. *J. Am. Chem. Soc.* **1997**, 119, 10963.
- (2) Palmaerts, A.; Haren, M. van; Lutsen, L.; Cleij, T. J. and Vanderzande, D. *Macromolecules* **2006**, 39, 2438.
- (3) Henckens, A.; Colladet, K.; Fourier, S.; Cleij, T. J.; Lutsen, L.; Gelan, J. and Vanderzande, D. *Macromolecules* **2005**, 38, 19.
- (4) Henckens, A.; Duysens, I.; Lutsen, L.; Vanderzande, D. and Cleij, T. J. *Polymer* **2006**, 47, 123.
- (5) Behnisch, B.; Martinez-Ruiz, P.; Schweikart, K. and Hanack, M. *Eur. J. Org. Chem.* **2000**, 2541.
- (6) Eckhardt, H.; Shacklette, L.W.; Jen, K.Y. and Elsenbaumer, R. L. *J. Chem. Phys.* **1989**, 91, 1303.
- (7) Juska, G.; Arlauskas, K.; Viliunas, M. and Kocka, J. *Phys. Rev. Lett.* **2000**, 84, 4946.
- (8) Österbacka, R.; Pivrikasa, A.; Juska, G.; Genevicius, K.; Arlauskas, K. and Stubb, H. *Current Applied Physics* **2004**, 4, 534.
- (9) Hummelen, J. C.; Mihailetschi, V. D.; Duren, K. J.; Blom, P. W. M.; Janssen, R. A. J.; Kroon, J. M.; Rispen, M. T. and Verhees, W. J. H. *Adv. Func. Mater* **2003**, 13, 43.

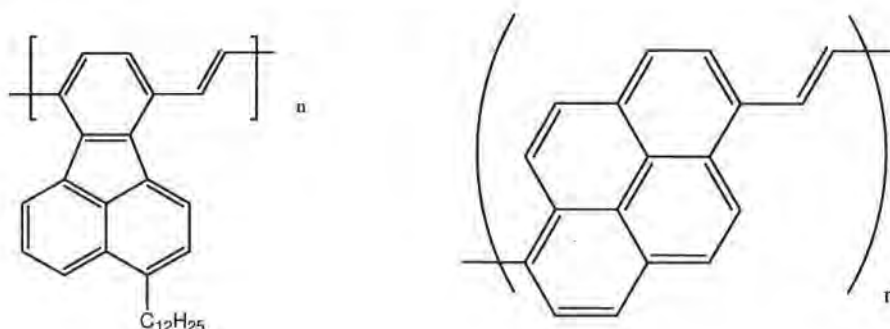
Chapter 4

Comparing the transport properties of two conjugated polymers with Polycyclic Aromatic Hydrocarbons substructures in the backbone



Abstract

In the domain of organic electronics mostly materials are used, which show relatively efficient hole transport. Notwithstanding, there is a need for polymeric materials, which show also a capability toward *n*-type transport. We have designed a novel class of *n*-type polymers containing a non-alternant polycyclic aromatic hydrocarbon, i.e. fluoranthene, in the backbone of the conjugated polymer. Fluoranthene ($C_{16}H_{10}$) is a substructure of C_{60} . To prove that the non-alternant character is indeed responsible for the *n*-type behavior, also a conjugated polymer (**PPyV**) containing an alternant PAH, i.e. pyrene ($C_{16}H_{10}$), has been synthesized. In this chapter the transport properties of both polymers in hole only and LED devices are compared.



Scheme 1. Dodecyl-Poly (Fluoranthene Vinylene) **dodecyl-PFV** and Poly(2,7-Pyrene Vinylene) **PPyV**.

4.1. Introduction

Extended conjugated systems like fluoranthene and pyrene are of interest in view of the fact that theoretical calculations indicate that the incorporation of such structures into a conjugated polymer chain will minimize the energy difference between the aromatic and the quinoid resonance structures when compared to the phenylene unit.^{2,3} This ultimately could lead to a narrowing of the band gap, which can be of interest for applications. Compared to the conjugated structure (benzene ring), the energetic state of the quinodimethane is less favorable because of the loss of aromaticity. When enlarging the conjugated system from a simple benzene ring into a fluoranthene or a pyrene ring system, part of the aromaticity is being preserved upon formation of a quinodimethane system in the polymer structure. As a result, the reorganization energy, which needs to be small for efficient electron hopping transport, potentially can minimize by using larger extended conjugated systems. This is also reflected in the bandgap. As an example, poly(2,7-pyrene vinylene) has a significantly lower bandgap, around 1.7 eV, compared with the 1-6 mode of connection, with a bandgap of 2.9 eV.¹

4.1.1. Polycyclic Aromatic Hydrocarbons PAH

Polycyclic Aromatic Hydrocarbons (PAH) consist of five-, six-, or seven membered rings and can be grouped in three classes. The way of linkage of these rings determines to which class they belong. For polyaryls two rings are connected by a single bond (*e.g.* biphenyl), for *ortho*-fused PAHs two rings share a common C-C bond (*e.g.* anthracene) and for *ortho*- and *peri*-fused PAHs three rings share a common C-C bond and a common central C-atom (*e.g.* pyrene and fluoranthene).

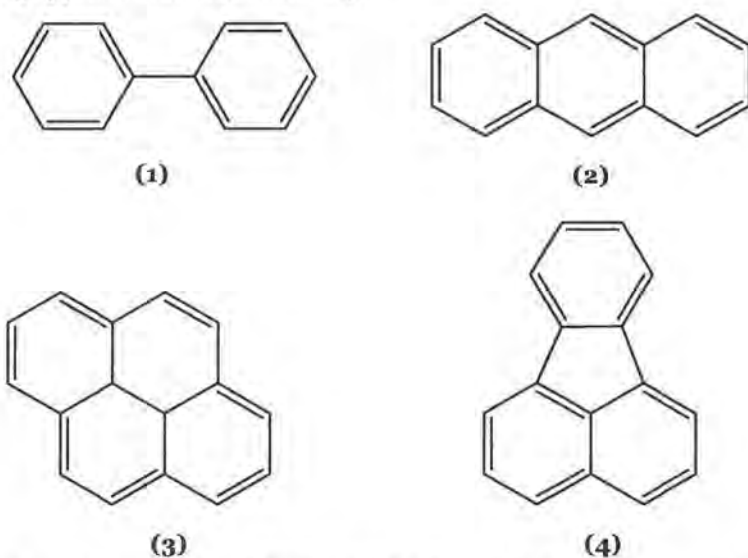


Fig. 1. Examples of PAHs: (1) biphenyl, (2) anthracene, (3) pyrene and (4) fluoranthene.

PAHs can be further classified into alternant and non-alternant PAHs. In alternant PAHs, the carbon atoms can be assigned as starred and unstarred with each starred carbon having only an unstarred neighbor and *vice versa* (Figure 2). In non-alternant PAHs either two adjacent starred carbons or unstarred carbons are present. This behavior is also reflected in the structure. Alternant PAHs constitute of only even-membered rings, whereas

in non-alternant PAHs at least one odd-membered ring is present. This difference in alternant and non-alternant character has a significant influence on the electronic properties of these molecules and their derivatives, as is reflected in the behavior of the conjugated polymers described in this chapter.

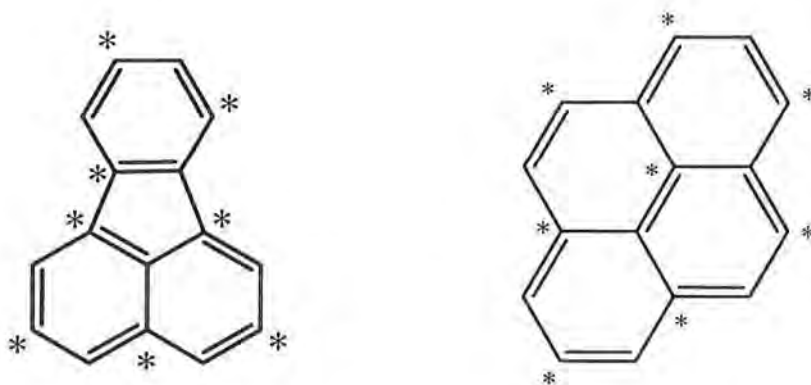


Figure 2. Example of a alternant PAH: pyrene (right) and a non-alternant PAH: fluoranthene (left)

Since the conjugated polymers in this chapter contain fluoranthene and pyrene in the backbone, a more detailed description of these two PAHs is of interest. Fluoranthene ($C_{16}H_{10}$) is a non-alternant cyclopenta-fused polycyclic aromatic hydrocarbon (CP-PAH) (Figure 2). It consists of a naphthalene and a phenylene unit, which are fused together by the 5-membered ring. On the other hand, pyrene ($C_{16}H_{10}$) is an alternant PAH (Figure 2) and a structural isomer of fluoranthene. If you compare the chemical structure of both it is clear that pyrene is better resonance stabilized than its isomer fluoranthene.

4.1.2. Charge transport

Due to the fact that a polymeric material generally consists of many chains of different lengths, with a substantial amount of defects, charge carriers can only move over larger distances by hopping between the conjugated parts of the polymer chains. This results in a spreading of the HOMO and LUMO levels, often approximated by a Gaussian density of states and consequently the charge transport in conjugated polymers cannot be described as simple band transport. Hopping transport is therefore more accurate and this type of transport has been described by many different theories, which are usually based on the theory of hopping from site to site.⁹ Since hopping transport is rather slow, the charge carrier mobility in conjugated polymers is generally quite low. When charges are injected into the polymer bulk, due to their low mobility they will accumulate at the injection interface and a space charge is formed. This space charge is generally referred to as the space, which is filled with a net positive or negative charge. This space charge will create an internal electric field that reduces the rate of charge carrier injection from the respective electrode. In cases where this injection barrier is low, the current depends only on the bulk properties of the material. In this case, the current is determined by the voltage (V) and the device thickness (L), leading to a square dependence on the voltage. This is called a space charge limited current. For a field-dependent mobility, Murgatroyd¹⁰ has demonstrated that the space charge limited current can be approximated by:

$$J = \frac{9}{8} \epsilon_0 \epsilon_r \mu_0 \exp\left(0.89 \gamma \sqrt{\frac{V}{L}}\right) \frac{V^2}{L^3}$$

with ϵ_0 the permittivity of vacuum, ϵ_r the dielectric constant of the polymer, and μ_0 the zero-field charge carrier mobility. The parameter γ describes the field-dependence.

4.1.3. Hole only devices

In order to assess the charge carrier mobility of the polymer a hole single carrier device can be made using a high work function metal, such as palladium, as an electron blocking top contact (Figure 3). By measuring the current through the hole-only device, the hole mobility can be determined by using the Murgatroyd equation.

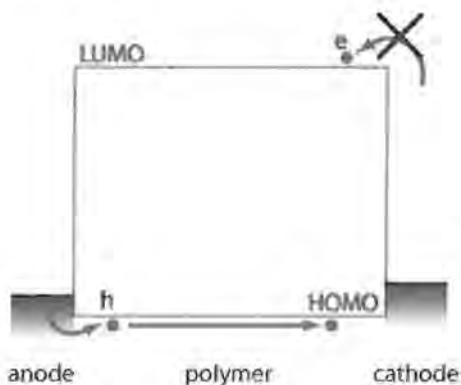


Figure 3. Energy band diagram of a hole-only diode, consisting of a polymer layer sandwiched between two high work function contacts

4.1.4. LED devices

In a polymer LED, a thin layer of light-emitting polymer is sandwiched between a high work function anode (such as ITO/ PEDOT:PSS) and a low work function cathode (such as Ba/Al). If the work function of the anode aligns with the HOMO of the polymer, holes can be injected from the anode

into the polymer. Electrons can be injected from the cathode, provided that its work function aligns with the LUMO of the polymer (Figure 4).

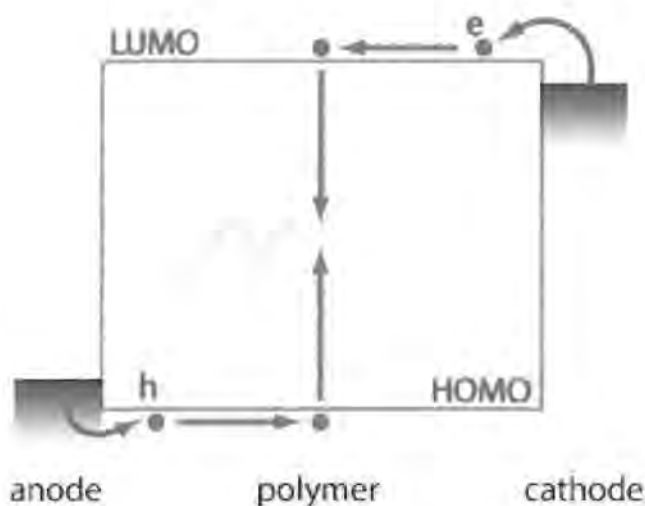


Figure 4. Energy band diagram of a polymer LED. Electrons are injected from a low work function material into the LUMO level of the polymer, holes are injected from a high work function material into the HOMO level.

Under forward bias, holes and electrons will be injected into the polymer. These charge carriers will travel across the device due to the applied field. If a hole and an electron come into each others vicinity, they can recombine to form a bound electron-hole pair, called an exciton. This exciton can decay in several ways.

One way of decay is by emission of a photon: an electron releases energy by making a transition from the LUMO to the HOMO, filling up the position of the hole. The released energy is emitted as light, of which the color depends on the energy gap between the HOMO and LUMO of the polymer (Figure 4).

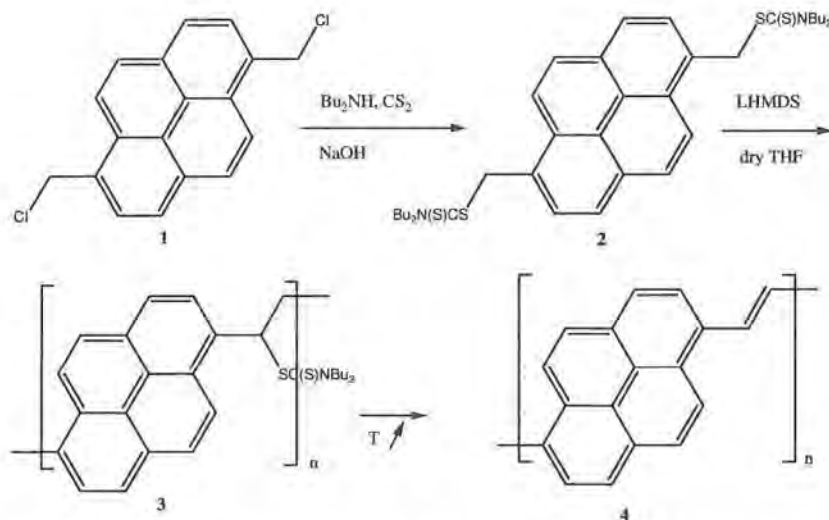
4.2. Synthesis

4.2.1. Dodecyl-PFV

In chapters 2 and 3, we have described the synthesis of poly(*p*-fluoranthene vinylene) PFV and its derivatives.

4.2.2. Poly (2,7-Pyrene Vinylene) PPyV

The synthesis of the 2,7-bis(chloromethyl) pyrene monomer was performed by Merck®. Addition of sodium dibutyldithiocarbamate trihydrate to the dichloride yielded the bisdithiocarbamate pyrene monomer. For the polymerization, the dithiocarbamate (DTC) precursor route^{4,5} was chosen, which was previously developed in our laboratory. This route was also utilized for the poly(*p*-fluoranthene vinylene) derivatives. Hence, a proper comparison of the transport properties between **dodecyl-PFV** and **PPyV** is possible and effects of the used precursor route can be neglected. Polymerization of the bis-dithiocarbamate pyrene monomer was carried out with lithium bis(trimethylsilyl) amide (LHMDS) as the base in dry THF under inert atmosphere (Scheme 2). After extraction the precursor polymer was isolated in excellent yield by precipitation in MeOH. Further purifications by soxhlet extractions in MeOH, hexane and acetone have been utilized to remove low molecular weight contaminants and/or oligomers. The weight-average molecular weights (M_w) of the precursor polymer has been determined by analytical SEC in DMF using polystyrene standards. The GPC analysis presents a monomodal molecular weight distribution and a molecular weight (M_w) of 20500 g/mol (DP= 3.45) were found. This is somewhat lower than the M_w of the studied C₁₂-PFV (230000 g/mol with a DP of 2.1), but still well within the range of a typical polymeric material.



Scheme 2. Polymerization reaction of Poly (2,7-pyrene vinylene) PPyV.

4.3. Evaluation of the conversion process of 3 into 4 using *in situ* UV-Vis and FT-IR spectroscopy

When studying the thermal conversion to the conjugated structure 4 by means of *in situ* UV-Vis spectroscopy, the absorption maxima of the 2,7-pyrene precursor polymer 3 are red-shifted to a maximum wavelength of 479 nm at room temperature (Figure 5). Under the utilized elimination conditions, the formation of the conjugated structure starts at 90 °C and is complete at 150 °C. After this temperature, a gradual decline in the intensity of the absorption at 479 nm is observed, which is caused by a thermochromic effect. A similar behavior was found for dodecyl-PFV. The value for the optical band gap of 2.0 eV is derived from the low energy side tangent to the π - π^* transition. This is in the same order of magnitude as

dodecyl-PFV (i.e. 2.2 eV, cf. Chapter 3), further indicating that these two polymers are reasonably comparable.

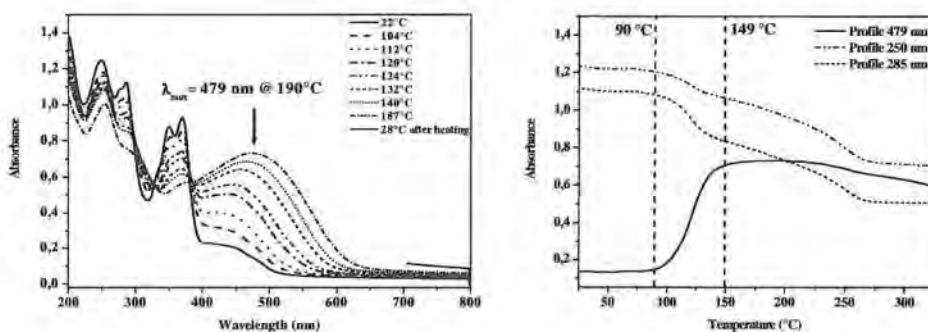


Figure 5. UV-Vis absorption spectra of the pyrene precursor polymer(left). UV-Vis profile of the precursor polymer ($\lambda = 250 \text{ nm}$ and 285 nm) and the conjugated polymer ($\lambda_{max} = 479 \text{ nm}$) as a function of temperature (right).

Additional *in situ* FT-IR spectroscopy measurements were carried out to acquire more information on the elimination process of the dithiocarbamate groups and thus the formation of the conjugated system. In the IR spectrum of the precursor polymer, the sharp vibrations at 1414 cm^{-1} and 1218 cm^{-1} are typical for the dithiocarbamate group (Figure 6). The vibrations of these groups decrease in intensity upon thermal elimination. Concomitantly, the formation of the vinylene double bond is visible at 950 cm^{-1} . The FT-IR data confirm that under the utilized experimental conditions the formation of the conjugated system around 90°C and is complete at about 150°C . The elimination characteristics are very similar as those found for the PFV derivatives (cf. chapters 2 and 3).

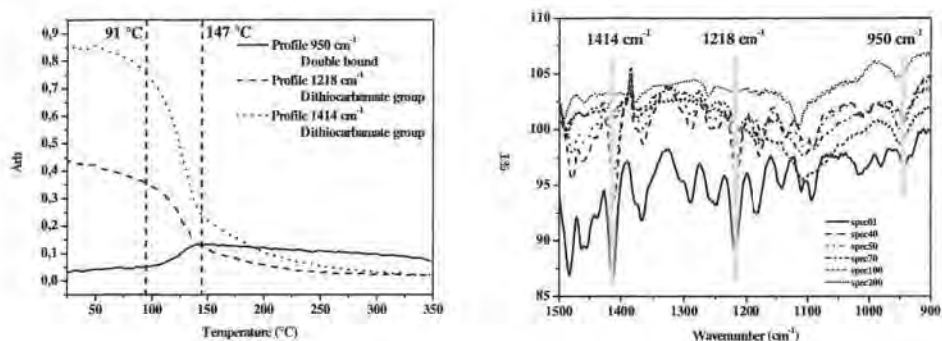


Figure 6. FT-IR spectra of the pyrene precursor polymer versus temperature (right) and the corresponding profiles (left) of the dithiocarbamate groups (1414 cm^{-1} and 1218 cm^{-1}) and the double bond (951 cm^{-1}).

4.4. Transport properties of PPyV and dodecyl-PFV

Subsequently, devices were made on pre-patterned ITO/Glass samples. After a cleaning procedure, a layer of PEDOT:PSS (Poly(3,4-ethylenedioxythiophene) doped with Poly(styrenesulfonate)) was spin coated on top of the ITO. The PEDOT:PSS has a better smoothness compared to the ITO and is applied in order to increase the wetting of the active polymer that is spin coated on top. Furthermore, it provides a more stable work function than ITO. Since the conjugated **PPyV** polymer was insoluble in all common organic solvents tested and only a limited solubility could be observed in dichlorobenzene for **dodecyl-PFV**, the thermal conversion of the precursors into the conjugated systems were performed in the thin film devices *in situ*. To this end, on top of the PEDOT:PSS, a layer of the respective precursor polymers was spin coated (precursor **PPyV 3** or precursor **dodecyl-PFV**, cf. Chapter 3). The spin coating conditions were optimized to obtain homogenous layers. Subsequently, the films were

subjected to a thermal treatment, during which the dithiocarbamate groups are eliminated from the precursor polymer. Finally, as a cathode, a metal top contact was evaporated.

Hole only devices were made by sandwiching the polymer in between a ITO/PEDOT:PSS anode and paladium/gold cathode. The red lines in Figure 7 represent the current density *versus* applied voltage characteristics of **dodecyl-PFV** (top) and **PPyV** (bottom) hole only devices with an active layer thickness around 100 nm. The **PPyV** hole only device shows good diode characteristics and high currents at forward bias indicating good hole carrier transport properties. In contrast, for the **dodecyl-PFV** hole only device virtually no device current is obtained indicating a low hole mobility. Furthermore, light emitting diodes were fabricated by sandwiching both polymers in between a ITO/PEDOT:PSS anode and barium/aluminum cathode. Figure 7 also shows the current density *versus* applied voltage characteristics of **dodecyl-PFV** (top) and **PPyV** (bottom) LEDs with an active layer thickness around 100 nm (black lines). Both LED devices exhibit good diode characteristics and high currents at forward bias indicating good charge carrier transport properties.

To determine which charge carriers (electrons or holes), are faster in both materials, the observed current of a LED has been compared to the current in a hole only device. The current to voltage characteristics of the LED of **PPyV**, corrected for the built in voltage, matches the current in the hole only device. This indicates that, perhaps not unexpectedly, holes are the dominant charge carriers in **PPyV**. In contrast, the current of the LED of **dodecyl-PFV** is several orders of magnitude higher than the current found for the hole only device, which only shows some leakage current. The absence of a significant current in the hole only device, in combination with the much higher current in the LED, indicates that electrons are the dominant charge carriers in **dodecyl-PFV** films.

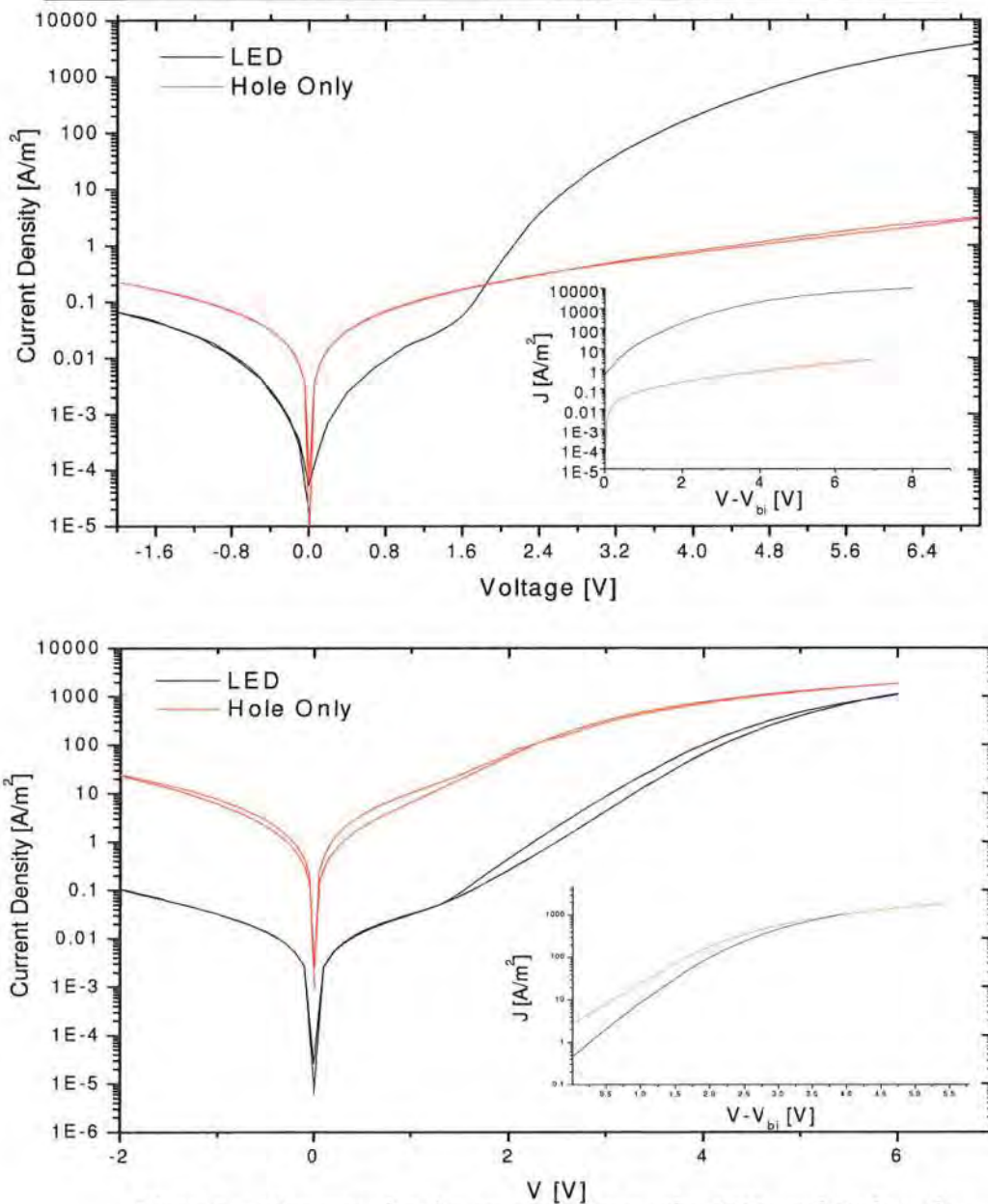


Figure 7. Current density versus voltage of a LED and Hole only device of **dodecyl-PFV** (top) and **PPyV** (bottom) showing **dodecyl-PFV** to be electron, and **PPyV** to be hole dominated. Inset: J - V plots corrected for built in voltage.

In spite of the fact that pyrene and fluoranthene are isomers of each other ($C_{16}H_{10}$), the transport properties of the corresponding conjugated polymers are markedly different. This difference most likely originates from the difference in the alternation between these structural units. **Dodecyl-PFV** exhibits the desired n-type behavior, which is associated with the non-alternant cyclo-penta fused character of the repeating units. **PPyV** is a typical p-type conjugated polymer, associated with the more commonly found alternant character of the PAH core. It is demonstrated in **chapter 3** using CELIV mobility measurements that **dodecyl-PFV** has a high electron mobility of $\mu_e = 1.4 \cdot 10^{-8} \text{ m}^2/\text{Vs}$. To determine the charge carrier mobility of **PPyV** hole single carrier devices were fabricated using palladium as an electron blocking top contact. The hole only device is fitted with a space charge limited current (see Figure 8) resulting in a zero field mobility of $1.5 \times 10^{-10} \text{ m}^2/\text{Vs}$. The CELIV hole mobility for **PPyV** is in the same order of magnitude at $3.0 \times 10^{-10} \text{ m}^2/\text{Vs}$, which confirms that the observed currents in hole only devices and CELIV measurements can be compared.

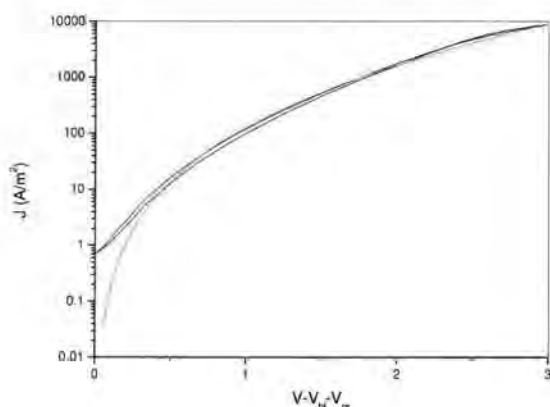


Figure 8. Current density versus voltage, corrected for built in voltage and series resistance of a **PPyV** hole only device. Data (black line) is fitted (red line) using a space charge limited current with a field dependent mobility.

4.5. Conclusion

In conclusion, two novel conjugated polymers with a PAH structure in the repeating unit have been synthesized. While **dodecyl-PFV** exhibits n-type behavior, which is associated with the non-alternant cyclo-penta fused character of its backbone. **PPyV** is a p-type conjugated polymer, as can be expected considering its alternant structural element pyrene. It is demonstrated that **PPyV** has a hole mobility of $\mu_h = 1.5 \cdot 10^{-10} \text{ m}^2/\text{Vs}$. The electronic properties of **dodecyl-PFV** indicate that this polymer has a sufficiently high electron mobility for use in optical and electronic applications as an n-type material. It can be concluded that non-alternant cyclo-penta fused polycyclic aromatic hydrocarbons are efficient structural elements to achieve n-type characteristics in conjugated polymers.

4.6. Experimental Section

4.6.1. Reagents and methods

Unless stated otherwise, all reagents and chemicals were obtained from commercial sources (Acros and Aldrich) and used without further purification. Tetrahydrofuran (THF) was refluxed under nitrogen with sodium metal and benzophenone until a blue-purple color persisted and then was distilled.

¹H-NMR spectra were obtained in CDCl₃ at 300 MHz on a Varian Inova Spectrometer using a 5 mm probe. Chemical shifts (δ) in ppm were determined relative to the residual CHCl₃ absorption (7.24 ppm). The ¹³C-NMR experiments were recorded at 75 MHz on the same spectrometer using a 5 mm broadband probe. Chemical shifts were defined relative to the ¹³C resonance shift of CHCl₃ (77.0 ppm).

Average Molecular weights and molecular weight distributions were determined relative to polystyrene standards (Polymer Labs) with a narrow polydispersity by Size Exclusion Chromatography (SEC). Separation to hydrodynamic volume was obtained using a Spectra series P100 (Spectra Physics) equipped with a pre-column (5 μ m, 50 mm, Polymer Labs) and two mixed-B columns (10 μ m, 2x300 mm, Polymer Labs) and a Refractive Index (RI) detector (Shodex) at 40°C. SEC samples are filtered through a 0.45 μ m filter. HPLC grade THF (p.a.) is used as the eluents at a constant flow rate of 1.0 mL/min. Toluene is used as flow rate marker.

Element Analysis was performed on a Flash EA 1112 CHNS-O analyzer from Thermo-Electro-Cooperation. C, H, N and S were determined under N₂-atmosphere and O was calculated under N₂-atmosphere. For elemental analysis, the precursor polymer was heated from room temperature to 900°C and the developed gasses were analyzed.

Gas chromatography/mass spectrometry (GC/MS) analyses were carried out with TSQ – 70 and Voyager mass spectrometers (Thermoquest); the capillary column was a Chrompack Cpsil5CB or Cpsil8CB. Melting points (uncorrected) were measured with a digital melting-point apparatus (Electrothermal IA 9000 series). Thin-layer chromatography (TLC) analyses were made on Merck aluminum sheets (20 x 20 cm) covered with silica gel 60.

Ultraviolet visible (UV-Vis) spectroscopy was performed on a VARIAN CARY 500 UV-Vis-NIR spectrophotometer (interval: 1 nm, scan rate: 600 nm/min, continuous run from 200 to 700 nm). The precursor polymer was spincoated from a chloroform solution (6 mg/mL) onto quartz substrates (diameter 25 mm and thickness 3 mm) at 700 rpm. The quartz glass was heated in a Harrick high temperature cell (purchased from Safir). The temperature of the sample and the heating source were controlled by a Watlow temperature controller (serial number 999, dual channel). The heating source was in direct contact with the quartz disc. The cell was placed in the beam of the UV-Vis spectrophotometer and spectra were taken continuously. The heating rate was 2°C/min. All measurements were performed under a continuous flow of nitrogen. Scanning kinetics software was used to investigate the regions of interest.

Fourier transform-infrared (FT-IR) spectroscopy was performed on a Perkin Elmer Spectrum One FT-IR spectrometer (nominal resolution 4 cm⁻¹, summation of 16 scans). Samples for the FT-IR characterization were prepared by spincoating the precursor polymer from a chloroform solution (6 mg/mL) onto NaCl discs (diameter 25 mm and thickness 1 mm) at 500 rpm. The NaCl discs were heated in the same Harrick high temperature cell with controller as was used in the UV-Vis measurements. The cell was positioned in the beam of the FT-IR to allow *in-situ* measurements. Spectra were taken continuously and the heating rate was 2°C/min up to 400°C. All

measurements were performed under a continuous flow of nitrogen. Timebase software was used to investigate regions of interest.

4.6.2. Synthesis

2,7-Bischloromethyl-pyrene (1)

This product was obtained from Merck ®. ^1H NMR (CDCl_3) δ : 8.40 (d, 2H), 8.19 (d, 2H), 8.18 (d, 2H), 8.04 (d, 2H), 5.32 (s, 4H) ppm; ^{13}C NMR (CDCl_3) δ : 131.3, 130.9, 129.1, 128.2, 127.9, 125.3, 124.9, 123.2, 44.2 ppm; FT-IR (NaCl , cm^{-1}): 2955, 2929, 2870, 1606, 1584, 1464, 1366, 1249, 1181, 1093, 1003, 982, 842, 780.

Dibutyldithiobarbamic-acid-7-dibutylthiocarbamoylsufanyl-pyrene-3-yl-ester (2)

A solution of dibutylamine (1.72 g, 13.37 mmol) in ethanol was cooled to 0°C . An aqueous NaOH (0.54 g, 13.37 mmol) solution was added in one portion and the reaction mixture was stirred for 30 minutes at 0°C . After addition of CS_2 (1.02 g, 13.37 mmol), the solution was stirred for another 90 minutes at 0°C and for 90 minutes at room temperature. Subsequently, a solution of the dichloride **1** (0.4 g, 1.337 mmol) in ethanol (400 mL) was added after which the total mixture was stirred at ambient temperature. After stirring for 2 days, 100 mL of water was added and the desired monomer was extracted with CHCl_3 (3 x 200 mL) and dried over MgSO_4 . After evaporation of the solvents the monomer was obtained as a light yellow solid (0.83 g; 98% yield); ^1H NMR (CDCl_3) δ : 8.31, (d, 2H), 8.13 (m, 6H), 5.20 (s, 4H), 4.01 (t, 4H), 3.60 (t, 4H), 1.78 (m, 12H), 1.20 (2t, 6H) ppm; ^{13}C NMR (CDCl_3) δ : 195.3, 130.7, 129.6, 129.1, 128.5, 127.8, 125.0,

124.8, 123.3, 54.8, 52.4, 41.0, 29.1, 28.3, 20.0, 19.8, 13.7, 13.5 ppm; FT-IR (NaCl, cm^{-1}): 2955, 2929, 2870, 1606, 1584, 1482, 1464, 1412, 1366, 1289, 1249, 1217, 1181, 1142, 1093, 1003, 982, 944, 842, 780, 709

Poly[*p*-pyrene(2,7-*N,N*-dibutyl-dithiocarbamate)methylene] (3)

A solution of LHMDS in THF (0.282 mL, 1.0 M) was added in one go to a mixture of dibutyldithiobarbamic acid 7-dibutylthiocarbamoylsufanylpyren-2-yl ester (**2**) (180 mg, 0.282 mmol) in dry THF (6.64 mL, 0.05 M). The reaction mixture was stirred for 90 minutes at room temperature under inert atmosphere (N_2). Subsequently, the pyrene precursor polymer was precipitated in ice water (100 mL) and solution was neutralized with a HCl-solution (37%). The polymer was extracted with chloroform (3 x 100 mL), the organic layers were dried with MgSO_4 and the solvent was evaporated under reduced pressure. After dissolving the precursor polymer in a small amount of CHCl_3 , **3** was isolated by precipitation in methanol. After further purifications by soxhlet extractions with MeOH, hexane and acetone, respectively, to remove low molecular weight contaminants and/or oligomers, 70 mg of the pure precursor polymer **3** was isolated as a yellow solid (54% yield). (300MHz, CDCl_3): 9.3-9.1 (b, 2H), 8.6-7.4 (b, 6H), 4.0-3.2 (b, 4H), 3.1-2.8 (b, 4H), 2.0-0.6 (b, 32 H) ppm; ^{13}C NMR (300MHz, CDCl_3): 195.3, 130.7, 129.6, 129.1, 128.5, 127.8, 125.0, 124.8, 123.3, 54.8, 52.4, 41.0, 29.1, 28.3, 20.0, 19.8, 13.7, 13.5 ppm; FT-IR (NaCl, cm^{-1}): 2955, 2929, 2870, 1606, 1584, 1482, 1464, 1412, 1366, 1289, 1249, 1217, 1181, 1142, 1093, 1003, 982, 944, 842, 780, 709. A typical polymerization at room temperature gave a polymer with an average molecular weight determined by Size Exclusion Chromatography (SEC) in THF of $M_w = 20500$ g/mol and a polydispersity PD of 3.45. Anal. Calcd for $\text{C}_{27}\text{H}_{28}\text{N}_1\text{S}_2$: C 73.60,; H, 5.60; N, 3.73; S, 17.07. Found: C, 70.46; H, 7.96; N, 4.08; S, 14.93.

4.6.3. Device preparation

All devices were made on pre-patterned ITO/Glass samples supplied by Philips. After a standardized cleaning procedure in a wet station, a layer of PEDOT:PSS (Poly(3,4-ethylenedioxythiophene) doped with Poly(styrenesulfonate)) was spin coated on top of the ITO. This layer has a thickness of 50 to 60 nm. The aqueous PEDOT:PSS solution (CLEVIOS P VP AI 4083 by H.C. Starck) was spin coated in exactly the same way for each substrate (10 seconds at 500 rpm followed by 50 seconds at 1500 rpm).

On top of the PEDOT:PSS, a layer of the respective precursor polymers was spin coated inside the glovebox (precursor PPyV **3** or precursor dodecyl-PFV, cf. Chapter 3). Table 1 shows the spin procedures and concentrations for both precursor polymers.

Polymer	Concentration (mg/ml)**	Speed* (rpm; 4 s lid closed)	Speed* (rpm; 60 s lid closed)	Speed* (rpm; 30 s lid open)
Precursor PPyV	10	500	800	800
Precursor dodecyl- PFV	20	500	800	800

* Acceleration: 500 rpm/s

** Precursor polymers dissolved in CHCl₃

Table 1. Utilized spin coating procedures and concentrations for both precursor polymers.

Subsequently, the thermal conversions of the precursors into the conjugated systems were performed in a thin film inside the glove box (185°C on a hotplate for 2 hours). Finally, as a cathode, a metal top contact was evaporated, consisting of 5 nm barium with 100 nm aluminum on top for LEDs and 20nm palladium with 80nm gold on top for hole only devices.

4.6.4. Device measurements

All measurements were performed in a glove box, under nitrogen atmosphere. Current *versus* voltage characteristics were determined using a Keithly 2400 Source meter. The device current was registered using a Labview program, while sweeping a voltage across the device, going up from 0 V to a positive voltage, then down to -2 V and up again to 0 V. Simultaneously, the photocurrent was determined using a photodiode connected to a Keithly 6514 electrometer.

4.7. References

- (1) Toussaint, J. M.; Wudl, F. and Brédas, J. L. *J. Chem. Phys.* **1989**, 91, (3), 1783.
- (2) Ohlemacher, A.; Schenk, R.; Weitzel, H.-P.; Tyutyulkov, N.; Tasseva, M. and Müllen, K. *Makromol. Chem.*, **1992**, 193, 81.
- (3) Onoda, M.; Ohmori, Y.; Kawai, T. and Yoshino, K. *Synth. Met.*, **1993**, 73, 2181.
- (4) Henckens, A.; Colladet, K.; Fourier, S.; Cleij, T. J.; Lutsen, L.; Gelan, J. and Vanderzande, D. *Macromolecules* **2005**, 38, 19.
- (5) Henckens, A.; Duyssens, I.; Lutsen, L.; Vanderzande, D. and Cleij, T. J. *Polymer* **2006**, 47, 123.
- (6) Harvey, R. G. *Cambridge Monographs on Cancer Research* **1991**, Cambridge Univ. Press.

- (7) Streitwieser, A. *Molecular Orbital Theory for Organic Chemists* **1961**, Wiley.
- (8) Fetzer, J. C. *The Chemistry and Analysis of the Large Polycyclic Aromatic Hydrocarbons* **2000**, Wiley.
- (9) Miller, A. and Abrahams, E. *Phys. Rev.* **1960**, *120*, 745.
- (10) Murgatroyd, P. N. *J. Phys.* **1970**, *3*, 151.

Chapter 5

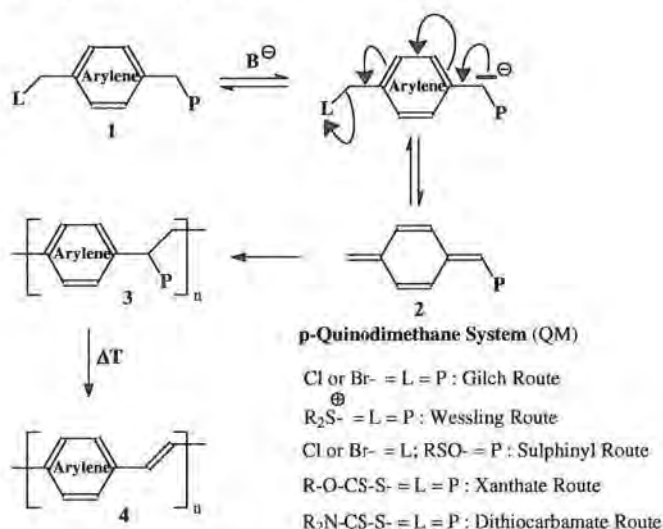
Towards complex architectures of PPV type polymers for device applications

Abstract

Poly(p-phenylene vinylene) derivatives are commonly synthesized from p-quinodimethane intermediates. Over the last forty years different synthetic routes have been developed and for all these routes mechanistic studies are rather scarce and the actual mechanism remains controversial. In general, it is believed that high molecular weight materials originate from a self-initiated radical chain polymerization and low molecular weight materials are obtained via an anionic mechanism. In this chapter, various aspects of the radical polymerization found for the sulfinyl precursor route, are studied in more detail and the question is addressed to what extent a living polymerization for this type of polymerization is realistic. In addition, the radical copolymerization of 1-(chloromethyl)-4-[(n-octylsulfinyl)methyl] benzene and n-butyl acrylate was investigated and the obtained PPV and PnBuA based copolymer was tested in devices. Green light emission and a turn-on voltage of 3.0 V were observed from a single-layer device. Furthermore, mobility measurements reveal that PPV-co-PnBuA has a sufficiently high hole mobility, $\mu_h = 4.10^{-9} \text{ m}^2/\text{Vs}$, for use in optoelectronic applications.

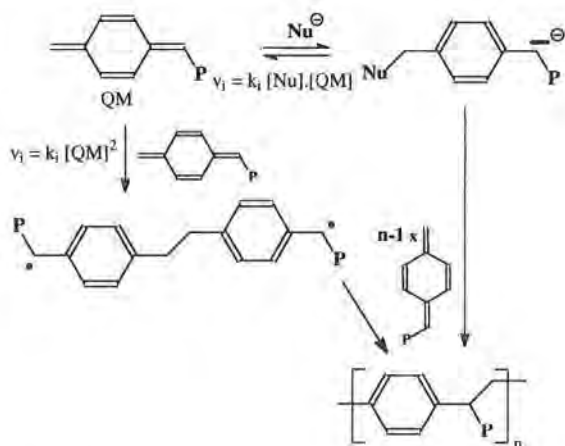
5.1. Introduction

Nowadays, conjugated polymers are well established organic semi-conductors that find their application in a wide range of electronic devices, *e.g.* OLEDs, FETs, OPVs and biosensors. Poly(arylene vinylene) derivatives constitute a very prominent class of such materials and the most important routes towards these structures make use of the polymerization behavior of *p*-Quinodimethane systems. Over the last 40 years a variety of routes have been developed making use of this type of chemistry. Chronologically, the Gilch¹ and Wessling² route were described first, later the Sulfinyl³ and the Xanthate route⁴ were developed and most recently the Dithiocarbamate route⁵ was introduced. The latter route has been used to prepare the polymers described in the previous chapters. All these routes have in common that they proceed *via* the *in situ* formation of a *p*-quinodimethane system, which is formed *via* a base induced elimination reaction in a pre-monomer as depicted in Scheme 1.



Scheme 1. General scheme for the polymerization of *p*-quinodimethane systems.

Typically, the pre-monomer structure contains at least two functionalities, a leaving group and a so-called polarizer group. In a typical reaction, a base abstracts the α -hydrogen next to the polarizer and *via* a 1,6-elimination the leaving group is expelled creating in this way the non-aromatic p-quinodimethane system. Subsequently, this very reactive system polymerizes yielding a precursor polymer with molecular weights typically above 100,000 Dalton and in some cases even in the range of a million Dalton. The precursor polymer obtained in this manner can be converted *in situ* or *ex situ* to the conjugated poly(arylene vinylene) derivative. It is generally agreed upon that these polymerization reactions behave as chain reactions, which start off as soon as an initiating species is formed. However, the exact nature of the initiating species is a long-standing issue of controversy. For every route initiation processes leading to anionic or radical polymerizations can be proposed side by side. For example, for the Wessling route the hypothesis of an anionic polymerization was first introduced by Latti *et al.*⁶ Previously, Wessling himself favored a self-initiated radical polymerization, analogous to the proposed polymerization behavior of the parent *p*-xylylene⁷ (Scheme 2). The “Amherst group” shifted later to the proposal of a radical mechanism,⁸ which was nicely elaborated by Cho *et al.*⁹ They demonstrated very convincingly that indeed rather radical and not anionic processes are responsible for the formation of the high molecular weight material observed in the Wessling route.



Scheme 2. Initiation reactions for anionic and radical (self-initiation) polymerization of *p*-quinodimethane systems.

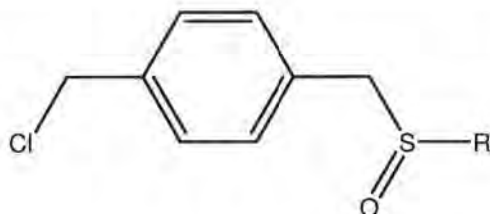
Also for the Sulfinyl route it was clearly proven that the high molecular weight polymer formed is originating from a self-initiating radical chain polymerization.¹⁰ It has been demonstrated this mechanism prevails for several solvent systems in which this polymerization can be performed.

In this chapter, various important aspects of precursor route chemistry will be highlighted, since the in depth knowledge of this chemistry is important for the successful application of these routes. After all, as has been demonstrated in the previous chapters, precursor routes are often essential to obtain novel conjugated materials, since they can be utilized to partially avoid solubility issues. This chapter focuses on a more in depth study of the polymerization behavior occurring in the sulfinyl route, one of the most promising precursor routes currently available. The ultimate goal is to develop a novel strategy towards more complex architectures, containing PPV-type polymers. To achieve this goal, it is important to have in depth knowledge of all aspects of the polymerization. To this end, three important polymerization variables of the sulfinyl precursor route will be evaluated

first. To begin with the effect of temperature will be investigated. Next, the influence of the actual addition sequence of the base and the pre-monomer will be studied. Finally the impact of changing either the pre-monomer or the base concentrations will be presented. In addition, the potential presence of a living species during the radical polymerization will be evaluated. In the domain of optoelectronics there is a strong interest in a living polymerization because it is the most convenient way to prepare block copolymers, *viz.* a complex architecture. Such block co-polymers are already reported for the Gilch polymerization.¹¹⁻¹⁴ Since the Sulfinyl route delivers conjugated polymers with a significantly enhanced purity, it is of fundamental interest to find an answer to the question whether it is possible to find also conditions where a termination process is excluded for the radical sulfinyl polymerization. In this way the sulfinyl route can be utilized to obtain such desirable block copolymers as well.

5.2. Radical polymerization

In order to reveal the specific characteristics of the above described radical polymerization process, the polymerization of 1-(chloromethyl)-4-[(*n*-alkylsulfinyl)methyl]benzene as the pre-monomer in *sec*-butanol as a solvent will be used as a representative example (Scheme 3). The full synthesis and characterization of the sulfinyl pre-monomer and precursor polymer are described elsewhere.¹⁵⁻²⁰ It is worth mentioning, that typically the base solution is added in one go to the pre-monomer solution, which is commonly referred to as a “normal” addition. Furthermore, previously it has been demonstrated that in alcohols the polymerization proceeds exclusively along a radical pathway.²⁰



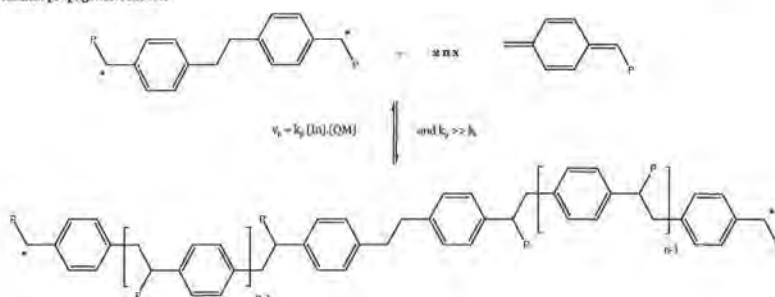
R = butyl

R = octyl

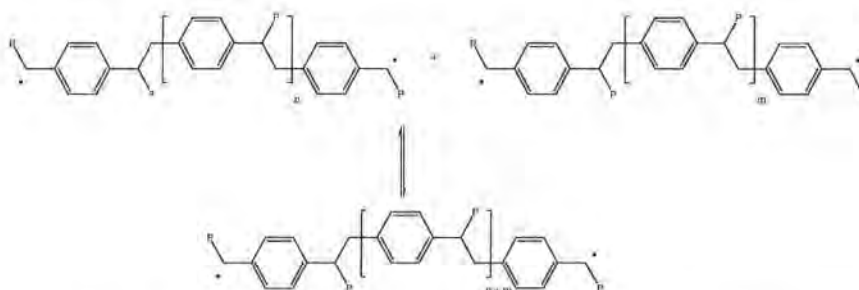
Scheme 3. Chemical structure of the sulfinyl pre-monomer.

In Scheme 4 both the propagation step and the envisaged pseudo-termination reaction are depicted. It is obvious that the proposed initiating species induces a particular propagation process, in the sense that chain growth occurs at both *termini* of the initiator. From the fact that high molecular weight material is obtained with a low defect level^{21,22} k_p has to be much larger than k_t . Furthermore, termination by recombination leads to a reduction of the total radical concentration, but at the same time results in a “living” polymer. Therefore, it can be referred to as a “pseudo”-termination reaction. Other termination reactions, such as cyclization, are unlikely to occur once the formation of high molecular weight material is reached. Termination by disproportionation is not possible for this precursor polymer as a result of the absence of a β -hydrogen. From a ¹³C labeling and sequential NMR study, potential end groups can be determined. It is observed that both for the Gilch and the Sulfinyl route similar groups can be identified, such as carboxylic and/or aldehyde functionalities. Hence, a termination reaction involving molecular oxygen is most probable. It is noteworthy that in these studies no indication was found for the solvent to be involved in a chain transfer process, which could have accounted for an alternative termination reaction.^{21,22}

Radical propagation reaction



Radical "pseudo"-termination reaction



Scheme 4. Radical propagation and termination reactions.

5.2.1. The effect of temperature in the radical polymerization

To investigate the effect of temperature on the polymerization a series of polymerizations was performed in duplicate at temperatures ranging from 0 °C to 75 °C (Table 1). For this study, a monomer with butyl side groups was utilized (Scheme 3). The obtained data demonstrate the good reproducibility of these polymerizations and show that the yield of the polymer seems to decrease slightly as the temperature is lowered. In contrast, the obtained molecular weights are significantly increasing from 150,000 to almost 700,000 Dalton upon going to lower temperature. This can be interpreted as the result of an increased initiation rate and possibly also an increased termination rate involving molecular oxygen at higher

temperatures. For two temperatures (30 °C and 0 °C) also the effect of a change in initial pre-monomer and base concentration at constant total volume of the solvent, was investigated (Procedure II, Table 1). The decrease of the ratio of initial base concentration over initial pre-monomer concentration ($[B]_i/[M]_i$) leads in a reproducible way to a slight increase (14%) in the molecular weight. This is believed to reflect the dependence of the polymerization on the initial concentration of the reagents. This may relate to the fast kinetics, which are typical for this type of polymerizations.

Temperature (°C)	Procedure I ^a			Procedure II ^b		
	Yield (%)	M _w (x 10 ⁻³ g/mol)	PD	Yield (%)	M _w (x 10 ⁻³ g/mol)	PD
75	90	150	1.80			
	89	145	1.95			
50	88	370	2.27			
	83	450	2.85			
30	78	535	2.98	83	620	2.80
	80	560	2.66	78	590	2.95
0	73	685	2.45	63	780	2.49
	65	680	2.96	65	810	2.47

^a Pre-monomer dissolved in 14 ml sec-butanol, initial pre-monomer concentration $[M]_i = 143$ mM; base (sodium tert.butoxide) dissolved in 6 ml sec-butanol; initial base concentration $[B]_i = 434$ mM; $[B]_i/[M]_i = 3.03$; base added to solution of pre-monomer

^b Pre-monomer dissolved in 10 ml sec-butanol, initial pre-monomer concentration $[M]_i = 200$ mM; base dissolved in 10 ml sec-butanol; initial base concentration $[B]_i = 260$ mM; $[B]_i/[M]_i = 1.3$; base added to solution of pre-monomer

Table 1. Effect of temperature on the polymerization of pre-monomer in sec-butanol.

5.2.2. The effect of concentration in the radical polymerization

To clarify this aspect unambiguously a series of experiments was performed in which the effect of the base and pre-monomer concentration on the molecular weight of the resulting polymer was studied. In this experiment the same amount of pre-monomer (2 mmol) was dissolved in an increasing amount of solvent. To this solution a fixed amount of base (2.1 mmol) dissolved in 10 ml of solvent was added in one go. For this study, a monomer with octyl side groups was utilized (Scheme 3). The results are presented in Table 2 and show a uniform decrease of molecular weight with decreasing pre-monomer concentration. From the graph in Figure 1 (squares) it is evident that a linear dependency is observed. Such a linear behavior is typically found for a radical chain polymerization and is therefore not unexpected. This can be explained by the fact that higher concentrations of the pre-monomer lead to higher concentrations of the intermediate *p*-quinodimethane system and thus more *p*-quinodimethane units can add to the growing chain before termination occurs. It should be noted that such an interpretation assumes the occurrence of a termination process.

Concentration pre-monomer (mmol/L) ^a	Initial volume solvent ^b (mL)	Yield (%)	M _w (x 10 ⁻³ g/mol)	PD
80	15	56	399	3.44
66.7	20	66	328	3.82
50	30	73	265	3.26
40	40	68	213	3.23
25	70	57	145	2.89
18.2	100	61	119	2.93

^a Concentration pre-monomer after addition of the base solution

^b Pre-monomer (2 mmol) dissolved in a variable amount of sec-butanol; base dissolved in 10 ml sec-butanol; initial base concentration [B]₀ = 210 mM; base added to solution of pre-monomer; T = 30°C; experiment performed in duplo, presented values are averages.

Table 2. Effect of pre-monomer concentration on the polymerization of pre-monomer in sec-butanol.

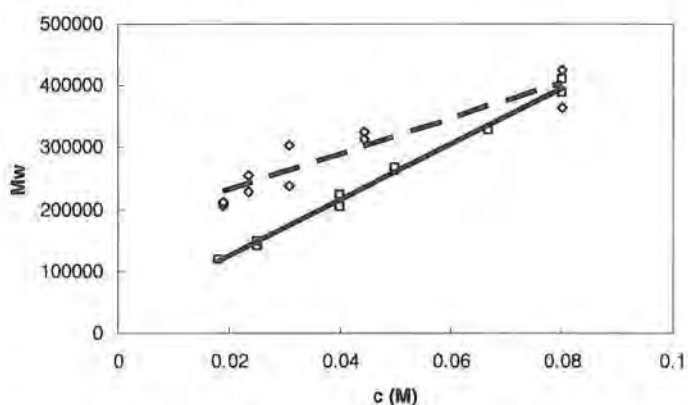


Figure 1. Radical propagation and termination reactions: (squares) dilution experiment, (diamonds) sequential polymerizations

Whether termination reactions effectively occur can be tested by using sequential polymerization reactions. Such an experiment would start with the same polymerization reaction as discussed previously, but after the reaction time of typically 40 minutes, instead of a work-up, a new batch of pre-monomer solution (2 mmol in 15 ml) is added to the reaction mixture. Prior to the addition of this new monomer batch, a sample of 5 ml reaction mixture is extracted and quenched in ice water. This sample is used for the GPC analysis. The second polymerization is started by adding the appropriate amount of base (2.1 mmol in 10 ml of solvent). After 40 minutes again a sample of the reaction mixture of 5 ml is extracted for GPC analysis. These two sequential steps can be repeated another two times taking care that the initial polymerization conditions are not disrupted by using degassed solutions, working under nitrogen atmosphere and utilizing syringes. After each addition step of the base and a reaction time of 40 minutes a sample is taken out of the vessel and prepared for GPC analysis. If no termination reaction occurs, active radical species remain in solution and the molecular weight should increase after each sequential polymerization step. However, what is observed for such an experiment (Table 3) is actually the same as for the study of the effect of dilution of the pre-monomer concentration, *i.e.* a decrease in M_w is observed. The slope (Figure 1) is less steep but similar compared to the graph of the dilution experiments. This difference originates from the fact that every time a sample is taken out of the reaction medium for GPC analysis, the GPC sample will also contain polymeric material obtained in the previous polymerization steps. These earlier polymerization steps yielded higher molecular weights and this will affect the slope of the curve, giving a smaller slope

Polymerization step	Concentration pre-monomer ^a (mmol/L)	Initial volume solvent ^b (mL)	M _w (x 10 ⁻³ g/mol)	PD
1	80	15	394	3.69
2	44.4	35	319	3.40
3	30.8	55	270	3.37
4	23.5	75	242	3.04
5	19.1	95	209	3.13

^a Concentration pre-monomer after addition of the base solution

^b Pre-monomer (2 mmol) dissolved in a variable amount of sec-butanol; base dissolved in 10 ml sec-butanol; initial base concentration [B]_i = 210 mM; base added to solution of pre-monomer; T = 30°C; experiment performed in duplo, presented values are averages.

Table 3. Effect of sequential polymerizations of pre-monomer in sec-butanol.

The results demonstrate unambiguously that under these conditions for the polymerization reactions a termination reaction is active, which can be identified as most probably related to traces of oxygen. Therefore, no living polymerization is found for this polymerization. A possible explanation can be the high reactivity and short lifetime of the active centre.

5.3. Green light emitting copolymer with both conjugated and non-conjugated segments

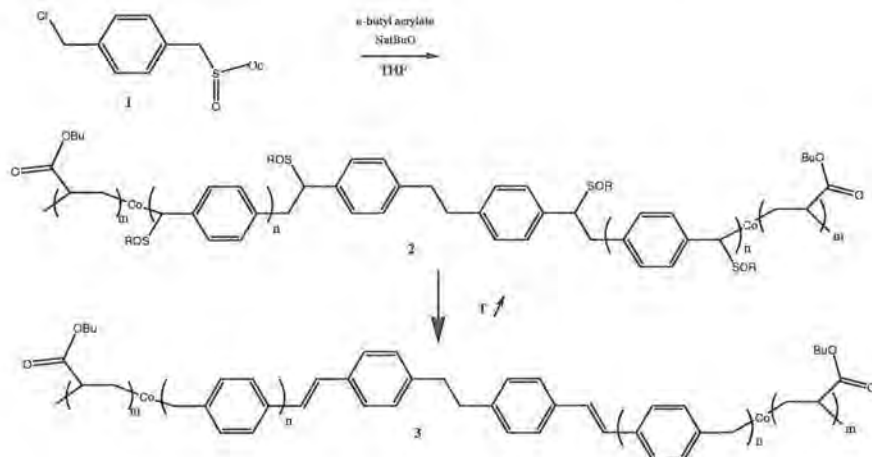
The results in the previous sections do not necessarily restrict the possibility to incorporate another monomer. However, this monomer would have to be present during polymerization. Its incorporation would lead to a copolymer. The choice of such a co-monomer has to be made, taking in

account the fast kinetics of the sulfinyl precursor polymerization. As a representative example the monomer *n*-butylacrylate (**nBuA**) has been chosen, which displays a very high reactivity.

In this section, we describe the synthesis of a new co-polymer consisting of nonconjugated Poly (Butyl Acrylate) (**PnBuA**) and conjugated Poly (Phenylene Vinylene) **PPV** segments.

5.3.1. Copolymerization

The copolymerization of the sulfinyl monomer **1** and *n*-butyl acrylate (**nBuA**) was carried out in typical conditions for a radical polymerization, *i.e.* under inert atmosphere in dry THF using **NatBuO** as the base, as depicted in Scheme 4.



Scheme 4. Copolymerization of sulfinyl monomer **1** and *n*-butyl acrylate (**nBuA**), followed by the conversion to the conjugated state.

In this experiment, a solution of NatBuO in THF and the undiluted *n*-butyl acrylate were successively added to a solution of the sulfinyl pre-monomer dissolved in THF. ([sulfinyl monomer]/[NatBuO]/[*n*-BuA]=1/1/88). A large amount of *n*-BuA was used in comparison to the sulfinyl pre-monomer in order to favor its incorporation into the copolymer. The reaction mixture was stirred under nitrogen flow for 2 h after which it was poured into water and neutralized with hydrochloric acid. After extraction, the formed polymeric material was isolated by precipitation from chloroform in a 50/50 mixture of hexane/ether. This purification step allowed the elimination of some of the homoPnBuA and to recover a sulfinyl rich copolymer as demonstrated below.

The recovered polymer was then analyzed by ¹H-NMR in CDCl₃. (Figure 2) Besides typical signals of the precursor polymer of PPV, resonances characteristic of PnBuA appear at 3.9 ppm (-CH₂-CH(CO₂CH₂-*n*Pr) and 2.6 ppm (-CH₂-CH(CO₂CH₂-*n*Pr). The detection of PnBuA in the material after several precipitations in hexane/diethyl ether mixture, a good solvent for the homoPnBuA, confirms the formation of a copolymer. Moreover, comparison of signal intensities of each segment allow the determination of the composition of copolymer **2**, *i.e.* PPV/PnBuA is 5/1.

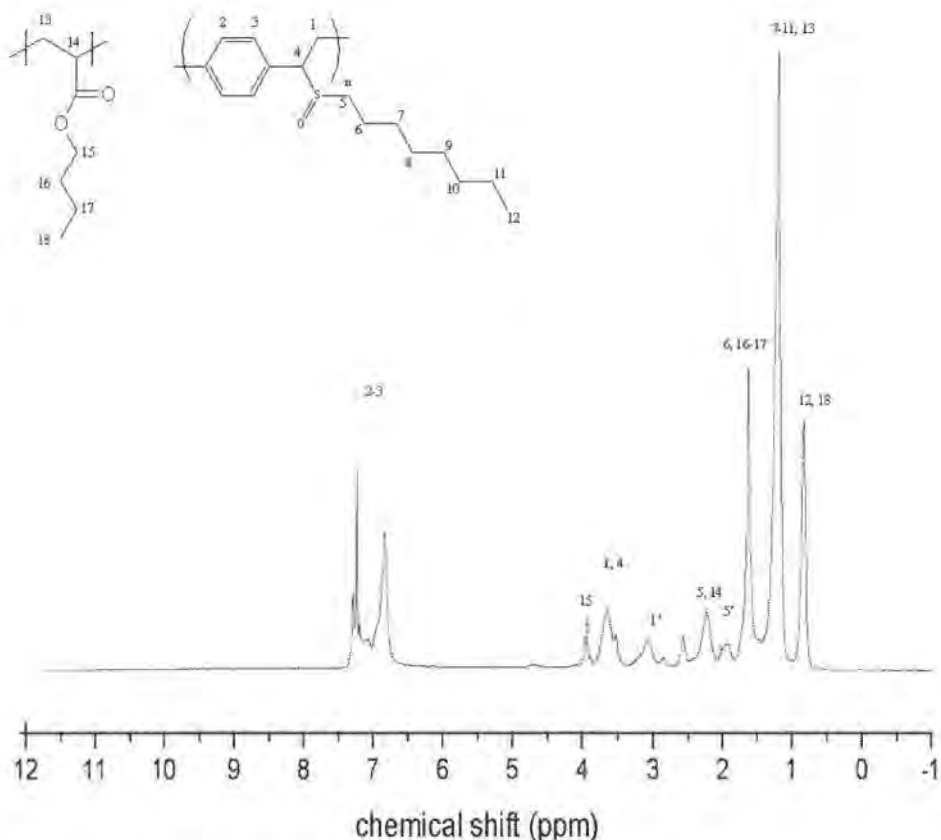


Figure 2. ^1H NMR spectrum of the copolymer.

Copolymer **2** was also analyzed by SEC using a dual detector (UV and RI). Typically, the observed molecular-weight distribution appeared monomodal with $M_w = 106,000$ and $PD = M_w/M_n = 3.3$ (Analytical SEC, solvent DMF/LiBr using PMMA as calibration). As is evident from Figure 3, there is a very good overlap between the UV and the RI curves after second precipitation of the copolymer in diethyl ether:hexane. With the RI detector both the copolymer and contaminations with homo-PnBuA and homo-PPV precursor polymer are potentially observable. In contrast, in the UV

response ($\lambda=256\text{nm}$) only the presence of homo-PPV precursor polymer can be detected. The good fit of the SEC traces in combination with the NMR-data suggests the presence of a copolymer and the absence of contamination of the copolymer by homo-PnBuA chains.

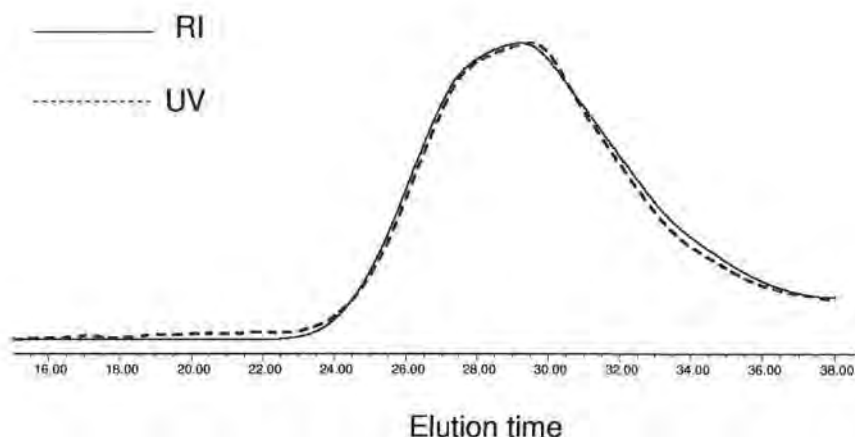


Figure 3. Size exclusion chromatogram in DMF of copolymer **2** after the second precipitation of the copolymer using a dual UV ($\lambda = 256 \text{ nm}$) and RI detector.

Finally, this sulfinyl precursor polymer **2** can be readily transformed into the corresponding conjugated polymer by thermal treatment either in solution or in a thin film. During this treatment the sulfinyl group is eliminated from the precursor polymer. Since it was found that the resulting conjugated block copolymer was insoluble in all common organic solvents tested, the thermal conversion of **2** into **3** was only performed in a thin film. Otherwise an intractable solid would have been obtained. For the conversion, precursor polymer **2** was spin-coated from a CHCl_3 solution onto a suitable substrate. After thermal conversion, the copolymer has a yellow color as a result of the formation of π -conjugation. The thin film

conversion process can readily be followed by means of *in situ* UV-Vis spectroscopy. (Figure 4) Upon heating at 120°C, a new absorption band develops which gradually shifts to *circa* 440 nm. This band originates from the π - π^* transition of the extended conjugated system. The energy corresponding to the π - π^* transition is dependent on the extent of delocalisation of the π -electrons. This delocalisation is determined by the effective conjugation length. UV absorption measurements are therefore important as they provide a direct source of detailed information of the effective conjugation. The longer the effective conjugation length is, *i.e.* the longer the conjugated segments are, the more red-shifted λ_{max} will be. For PPV with a maximum effective conjugation length typical λ_{max} values are observed around 440 nm.²⁴ Hence the observed λ_{max} value of 442 nm for the conjugated copolymer **3** at room temperature (*cf.* Figure 4), indicates that true long PPV segments have to present. This observation combined with the previous GPC analyses confirm therefore the presence of PPV blocks in the conjugated copolymer **3**. This makes a further opto-electronic evaluation of this novel copolymer of interest.

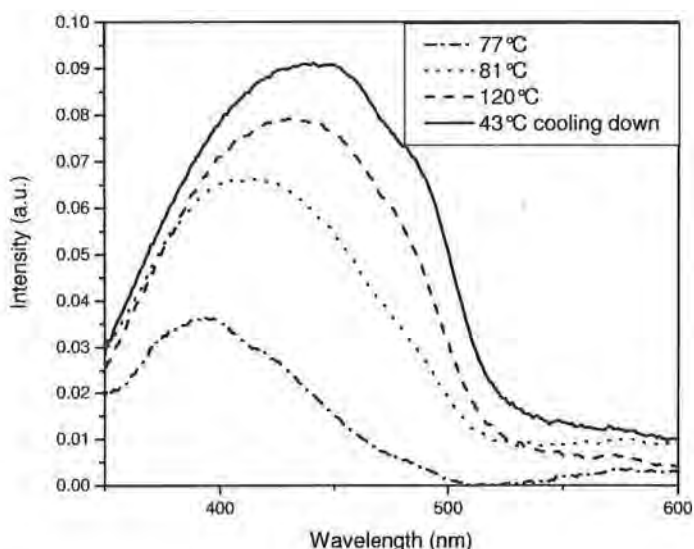


Figure 4. Temperature-dependent UV-Vis spectra of the conversion of precursor copolymer **2** into the conjugated copolymer **3** at selected temperatures.

5.3.2. Device Fabrication and Characterization

In order to test the device performance of the novel copolymer light emitting diodes were fabricated by sandwiching the polymer in between a ITO/PEDOT:PSS anode and barium/aluminum cathode. Figure 5 shows the current density *versus* applied voltage characteristics of a **PPV-co-PnBuA** LED with an active layer thickness of 100 nm. The device shows good diode characteristics and high currents at forward bias indicating excellent charge carrier transport properties. In order to assess the charge carrier mobility of the polymer, a hole only carrier device was fabricated using palladium as an electron blocking top contact. As expected for a PPV-type polymer, the currents of the LED match the currents in a hole only device showing holes to be the dominant charge carrier in the material.

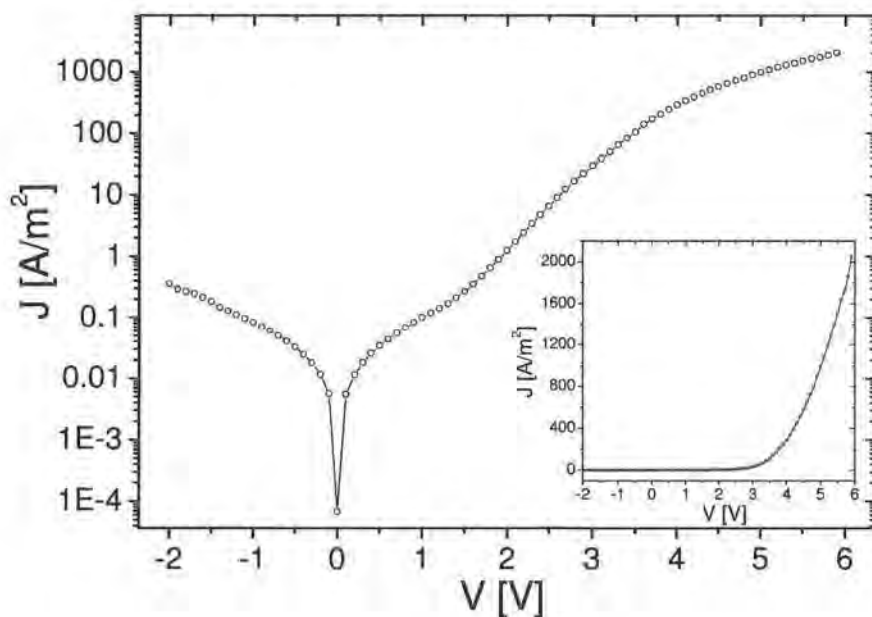


Figure 5. *J-V characteristics of a PPV-co-PnBuA LED on a semi logarithmic and linear (inset) scale.*

Green light emission with a turn-on voltage of 3.0V was observed from a single-layer LED device. Such a low turn-on voltage is remarkable in view of the existing literature data on similar devices obtained from Gilch block copolymers consisting of conjugated PPV segments and a non conjugated polystyrene (PS) segments. The single-layer LED device fabricated from the copolymer **PPV-co-PS**, which was described in the literature, showed an emission of blue light and a turn-on voltage of 8.0 V¹² or 9.0 V.¹³ (Figure 6)

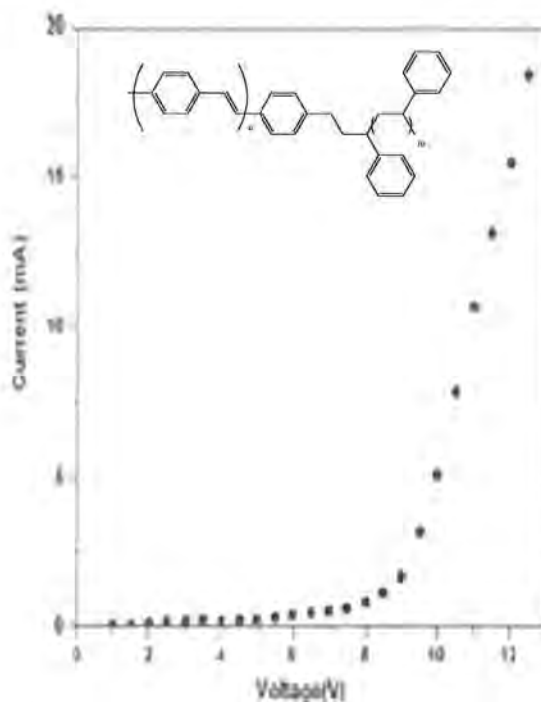


Figure 6. Current-voltage characteristics of the single-layer device with the *PPV-co-PS* copolymer. Inset gives the molecular structure of the *PPV-co-PS* copolymer. Figure taken from reference.¹²

The electronic response of our hole only device can be fitted with a space charge limited current (Figure 8) resulting in a zero field mobility of $4 \times 10^{-9} \text{ m}^2/\text{Vs}$ and a field activation coefficient of $2 \times 10^{-5} (\text{V/m})^{-1/2}$. This high hole mobility is remarkable considering the relatively low mobility of pure PPV of $5 \times 10^{-11} \text{ m}^2/\text{Vs}$ and the fact that a large fraction of the copolymer is not conjugated. An explanation for this might be that the transport characteristics are due to improved interchain interactions by more effective mesoscopic order, similar to what has been previously observed in poly-3-alkylthiophenes.²³

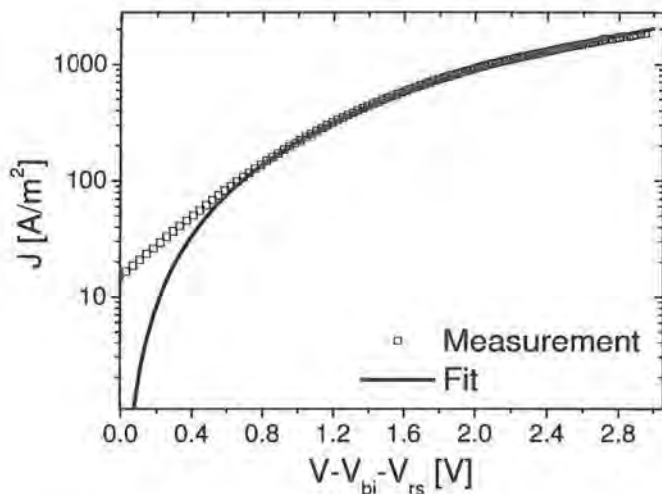


Figure 8. Current density versus voltage, corrected for built in voltage and series resistance of a **PPV-co-PnBuA** hole only device. Data (symbols) is fitted (solid line) using a space charge limited current with a field dependent mobility.

The electroluminescence (EL) spectrum at various voltages is shown in Figure 9. The EL spectrum shows two peaks at 514 and 549 nm, and no dependence on the applied voltage.

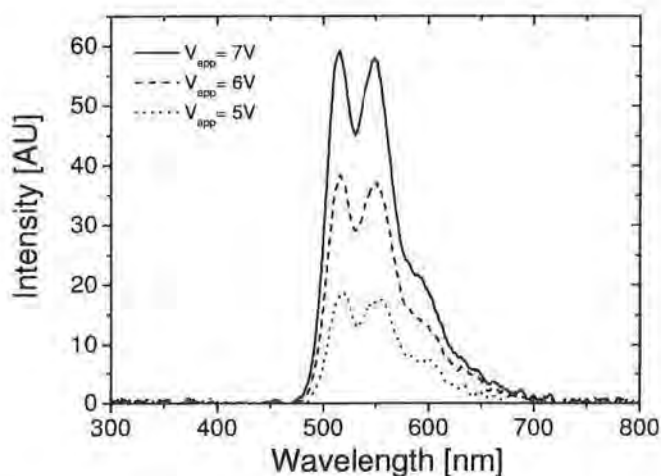


Figure 9. Electroluminescence spectrum of a **PPV-co-PnBuA** LED at different applied voltages.

It should be remarked that unfortunately this high hole mobility was only observed for one batch, albeit in a reproducible manner. Whereas it is possible to reproduce the synthesis of the copolymer **PPV-co-PnBuA**, further experiments are in progress in order to reproduce these increased transport properties. In addition, additional research is needed to investigate the nature of the block-type structure of the copolymer.

5.4. Conclusion

This chapter focuses on an in depth study of the radical polymerization mechanism as is observed for the sulfinyl precursor route. As a representative example, a comparatively simple conjugated polymer, *i.e.* PPV, has been studied. In general, the radical polymerization is responsible for the formation of high molecular weight material. From the study of the

effect of the temperature on the molecular weight for a temperature range from 0°C to 75°C it is clear that the molecular weight decreases upon increasing temperature. This can be interpreted as the result of an increased initiation rate and possibly also an increased termination rate involving molecular oxygen at higher temperatures. Furthermore, a linear dependency is observed for the effect of the monomer concentration on the molecular weight. The experiment to answer the question whether a living radical polymerization is possible was inconclusive, since the experimental conditions under inert atmosphere apparently were insufficiently strict to avoid the termination by traces of oxygen, even during the sequential experiments. An alternative direct approach, by mixing two different monomers, was more successful and a copolymer **PPV-co-PnBuA** has been synthesized. Whereas at this stage all characterizations are in agreement with the proposed formation of a copolymer, they do not allow the conclusive identification of a block-like structure. Notwithstanding, *in situ* UV-Vis spectroscopy of the resulting PPV containing polymer **3** confirm the presence of long PPV segments in view of the observed λ_{\max} of 442 nm. The novel copolymer has also been integrated in devices. Green light emission with a maximum at 514 and 549 nm and a turn-on voltage of 3.0 V were observed from a single-layer device (ITO/PEDOT:PSS/copolymer/Ba/Al). Furthermore, the performed mobility measurements reveal that **PPV-co-PnBuA** has a sufficiently high hole mobility, $\mu_h = 4 \cdot 10^{-9} \text{ m}^2/\text{Vs}$, for use in optoelectronic applications.

5.5. Experimental

5.5.1. General.

NMR spectra were recorded with a Varian Inova Spectrometer ($^1\text{H-NMR}$ 300 MHz). Analytical Size Exclusion Chromatography (SEC) was

performed using a Spectra series P100 (Spectra Physics) pump equipped with two mixed-B columns (10 μm , 2 x 30 cm, Polymer Labs) and a Refractive Index detector (Shodex) at 40 °C or 70 °C. THF or a DMF solution of oxalic acid (1.1×10^{-3} M) was used as the eluent at a flow rate of 1.0 mL/min. Molecular weight distributions are given relative to polystyrene standards.

UV-Vis measurements were performed on a Cary 500 UV-Vis-NIR spectrophotometer (scan rate 600 nm/min, continuous run from 200 to 600 nm). The conversions of the precursor polymers into the corresponding conjugated structures were followed using *in situ* UV-Vis spectroscopy. The *in-situ* UV-Vis measurements in the solid state were performed in a Harrick variable temperature cell, which was for the UV-Vis measurements positioned in the beam of the UV-Vis-NIR spectrometer. The precursor polymer was drop-casted from a CHCl_3 solution on a quartz glass (diameter 25 mm, thickness 3 mm). All measurements were performed under a continuous flow of nitrogen (open system). "Scanning Kinetics software" (Varian) was used to follow the processes.

5.5.2. Copolymerization

Unless stated otherwise, all reagents and chemicals were obtained from commercial sources and used without further purification. Tetrahydrofuran (THF) was purified by distillation from sodium/benzophenone. N-butyl acrylate was dried over calcium hydride, degassed by several freeze-thawing cycles before being distilled under reduced pressure and stored under argon.

The precursor copolymer **2** was synthesized by the following procedure: a solution of NatBuO (80 mg, 0.83 mmol) in THF (6 mL) was added to a solution of the sulfinyl pre-monomer (252 mg, 0.80 mmol; *cf.* Scheme 3)

dissolved in THF (4 ml). After a 5 second delay, n-butyl acrylate (10 ml, 70.4 mmol) was added as the second monomer and stirred under nitrogen for 3 hours. After evaporation of the solvent *in vacuo*, the reaction mixture was poured into water and neutralized with hydrochloric acid. Subsequently, the product was extracted with dichloromethane and after evaporation the crude copolymer was dried. Finally, the crude copolymer was redissolved in chloroform and purified by precipitation in a 50/50 mixture of cold hexane and ether. After filtration and drying, a white polymer **2** was collected (130 mg). SEC in DMF/LiBr, calibration PMMA : $M_w = 106.000$ and $PD = M_w/M_n = 3.3$. $^1\text{HNMR}$ (CDCl_3) : PPV/PnBuA : 5/1.

5.5.3. Device preparation

All devices were made on pre-patterned ITO/Glass samples supplied by Philips. After a standardized cleaning procedure in a wet station, a layer of PEDOT:PSS (Poly(3,4-ethylenedioxythiophene) doped with Poly(styrenesulfonate)) was spin coated on top of the ITO. This layer has a thickness of 50 to 60 nm. The aqueous PEDOT:PSS solution (CLEVIOS P VP AI 4083 by H.C. Starck) was spin coated in exactly the same way for each substrate (10 seconds at 500 rpm followed by 50 seconds at 1500 rpm). The PEDOT:PSS has a better smoothness compared to the ITO and is applied in order to increase the wetting of the active polymer that is spin coated on top. Furthermore, it provides a more stable work function than ITO. On top of the PEDOT:PSS, a layer of precursor copolymer was spin coated inside the glovebox. Table 4 shows the spin procedures and concentrations.

Polymer	Concentration (mg/ml)**	Speed* (rpm; 4 s lid closed)	Speed* (rpm; 60 s lid closed)	Speed* (rpm; 30 s lid open)
Precursor polymer 2	15	500	800	800

* Acceleration: 500 rpm/s

** Precursor polymer dissolved in CHCl₃

Table 4. Spin procedures and concentration for precursor copolymer 2.

For the device manufacturing the precursor polymer had to be used instead of the conjugated polymer, since the conjugated copolymer was insoluble in all common organic solvents tested. Subsequently, the thermal conversion of the precursor copolymer **2** into the conjugated copolymer system **3** was performed in a thin film. During this thermal treatment inside the glove box (185°C on a hotplate for 2 hours) the sulfinyl group is eliminated from the precursor polymer. Finally, as a cathode, a metal top contact was evaporated, consisting of 5 nm barium with 100 nm aluminum on top for LEDs and 20 nm palladium with 80 nm gold on top for hole only devices.

5.5.4. Device measurements

All measurements were performed in a glove box, under a nitrogen atmosphere. Current versus voltage characteristics were determined using a Keithly 2400 Source meter. The device current was registered using a Labview program, while sweeping a voltage across the device, going up from 0 V to a positive voltage of 6 V, then down to -2 V and up again to 0 V. Simultaneously, the photocurrent was determined using a photodiode connected to a Keithly 6514 electrometer. The emission spectra were determined using a USB2000 Miniature Fiber Optic Spectrometer of Ocean

Optics. Thicknesses of all spin coated polymers, including the PEDOT:PSS were determined using a Dektak 6M Stylus Profiler.

5.6. References

- (1) Gilch, H. G. and Wheelwright, W. L. *J. Polym. Sci. A* **1966**, 4, 1337.
- (2) Wessling, R. A.; Zimmerman, R. G. *US Patent* **1968**, 401, 152.
- (3) Louwet, F.; Vanderzande, D.; Gelan, J.; Mullens, J. *Macromolecules* **1995**, 28, 1330.
- (4) Son, S.; Dodabalapur, A.; Lovinger, A. J. and Galvin, M. E. *Science*, **1995**, 269, 376.
- (5) Henckens, A.; Lutsen, L.; Vanderzande, D.; Knipper, M.; Manca, J.; Aernouts, T. and Poortmans, J. *Proc. SPIE Int. Soc. Opt. Eng.* **2004** 5464, 52.
- (6) Lathi, P. M.; Modarelli, D. A.; Denton III, F. R.; Lenz, R. W. and Karasz, F. E. *J. Am. Chem. Soc.* **1988**, 30, 2223.
- (7) Wessling, R. A. *J. Polym. Sci.: Polym. Symp.* **1985**, 72, 55.
- (8) Denton III, F. R.; Lahti, P. M. and Karasz, F. E. *J. Polym. Sci.: Polym. Chem.* **1992**, 30, 2223.
- (9) Cho, B. R.; Kim, Y. K. and Han, M. S. *Macromolecules* **1998**, 31, 2098.
- (10) Issaris, A.; Vanderzande, D. and Gelan, J. *Polymer* **1997**, 38, (10), 2571.
- (11) Gutierrez, J. J.; Luong, N.; Zepeda, D. and Ferraris, J. P. *Polymer Preprints* **2004**, 45, (1), 172.
- (12) Zhang, M.; Guowen, L.; Ma, Y.; Zang, R. and Shen, J. *Materials Letters* **2003**, 57, 4176.
- (13) Qu, G.; Jiang, F.; Zhang, S. and Usuda, S. *Materials Letters* **2007**, 61, 3421.
- (14) Tang, J.; Zhang, R.; Li, G. and Shen, J. *Chem. Mater.* **2003**, 15, 2950.

- (15) Hontis, L.; Lutsen, L.; Vanderzande, D. and Gelan, J. *Synthetic Metals* **2001**, 119, 135.
- (16) Hontis, L.; Vrindts, V.; Vanderzande, D. and Lutsen, L. *Macromolecules* **2003**, 36, 9, 3035.
- (17) Hontis, L.; Van Der Borght, M.; Vanderzande D. and Gelan, J. *Polymer* **1999**, 40, 6615.
- (18) Van Der Borght, M.; Vanderzande, D.; Adriaensens, P. and Gelan, J. *Polymer* **2000**, 41, 8, 2743.
- (19) Adriaensens, P.; Van Der Borght, M.; Hontis, L.; Issaris, A.; van Breemen, A.; de Kok, M.; Vanderzande D. and Gelan, J. *Polymer* **2000**, 41, 7003.
- (20) van Breemen, A. J. J. M.; Issaris, A. C. J.; de Kok, M. M.; Van Der Borght, M. J. A. N.; Adriaensens, P. J.; Gelan, J. M. J. V. and Vanderzande D. J. M. *Macromolecules*. **1999**, 32 ,18, 5728.
- (21) Becker, H.; Spreitzer, H.; Ibrom, K. and Kreuder, W. *Macromolecules* **1999**, 32, 4925.
- (22) Roex, H.; Adriaensens, P.; Vanderzande, D. and Gelan, J. *Macromolecules* **2003**, 36, 15, 5613.
- (23) Siringhaus, H.; Brown, P. J.; Friend, R. H.; Nielsen, M. M.; Bechgaard, K.; Langeveld-Voss, B. M. W.; Spiering, A. J. H.; Janssen, R. A. J.; Meijer, E. W.; Herwig, P. and de Leeuw, D. M. *Nature* **1999**, 401, 6754, 685.

Chapter 6

Poly(thienylene vinylene)

Abstract

*Solar cells based on conjugated polymers are extensively investigated during the last decade. A critical issue for this type of solar cells is the rather narrow absorption of the active layer. Since most of the available conjugated polymers were originally developed for visible-LEDs, they exhibit band gaps > 2 eV. One of the main problems in polymer:fullerene solar cells is the poor overlap between the solar spectrum and the absorption of the used materials. In order to increase the photon harvesting, low band gap polymers offer significant advantages. In this context, two new conjugated polymers, i.e. poly(octyl-thienylene vinylene) **C₈-PTV** and poly(bis-octylphenyl-thienylene vinylene) **BOP-PTV**, have been synthesized. Power conversion efficiencies of 0.80% for **BOP-PTV** and 0.92% for **C₈-PTV** are obtained.*

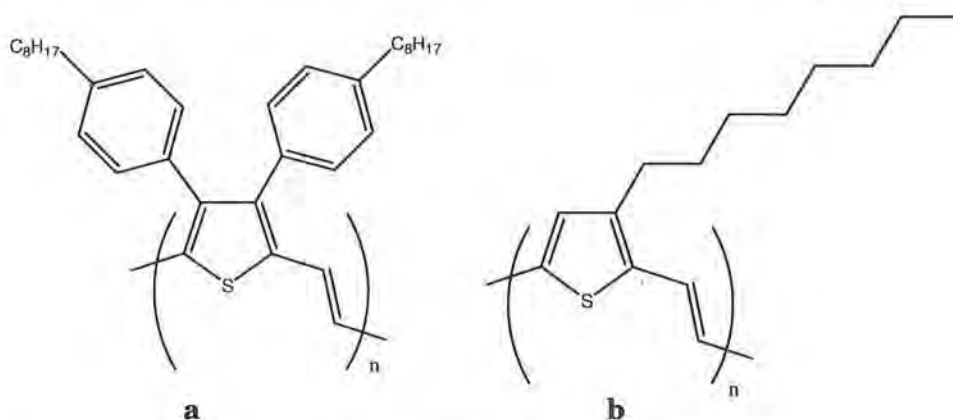


Figure 1. Chemical structures of a) poly(bis-octylphenyl-thienylene vinylene) BOP-PTV and b) poly(octyl-thienylene vinylene) C₈-PTV.

6.1. Introduction

In the field of bulk heterojunction solar cells, over the past decade a lot of work has been done in the design, synthesis and use of low band gap ($E_g < 2$ eV) materials. In Chapter 1 it has been outlined that two common strategies exist to further optimize the solar cell performance, both focusing on an adjustment of the energy levels either on the donor or on the acceptor side. Chapters 2, 3 and 4 have emphasized the design of new n-type materials. This is of interest, since raising the LUMO of the acceptor will directly result in a higher V_{oc} without affecting the absorption of the cell. Alternatively, one can tailor the donor side, by developing novel p-type materials. Upon lowering the LUMO of the donor, and thus lowering the polymer band gap, the absorption is shifted towards lower energy, while maintaining a constant open-circuit voltage. In this way the photocurrent is improved, due to an enhanced overlap between the donor absorption and the solar spectrum.

Hitherto, most of the research in the field of bulk heterojunction solar cells has been devoted to the optimization of cells based on poly(3-

hexylthiophene) (P3HT) as the donor polymer combined with a soluble derivative of C₆₀, (6,6)-phenyl-C₆₁-butyric acid methyl ester (PCBM), as the electron acceptor. Improvements in device fabrication by thermal and solvent annealing have led to power-conversion efficiencies around 4%.¹ Even the band gap of 1.9 eV for P3HT results in a reasonably poor overlap with the solar spectrum, since the absorbance is limited to wavelengths below 650 nm. From the solar spectrum under AM 1.5 conditions depicted in Figure 2 it is clear that conjugated polymers with an even smaller band gap have a huge potential.

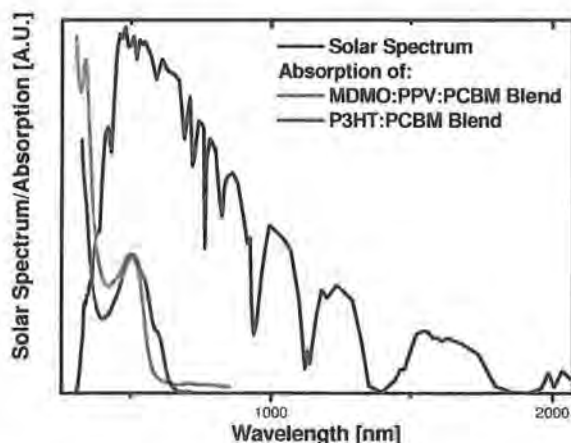


Figure 2. AM 1.5 spectrum, defined as the spectral photon flux on the earth's surface under illumination of 45° (black), compared to the absorption profile of a MDMO-PPV : PCBM (1 : 4) film (red) and the absorption profile of a P3HT : PCBM (1 : 1) film (blue).¹²

For a maximum wavelength of 650 nm only 22.4% of the total amount of photons can be absorbed. Therefore it is not surprising, that in order to increase the photon harvesting there is a quest for new low band gap materials. From models it can be estimated that for a classical bulk

heterojunction with a conjugated polymer as donor in combination with PCBM as the acceptor, a band gap of 1.4 eV for the donor material would be optimal. Since π -conjugated polymers allow endless manipulation of their chemical structure, tuning of the band gap of these materials is a research issue of ongoing interest. It is anticipated that this band gap engineering can give the polymer its desired electrical and optical properties.

In order to circumvent the solubility problems of most unsubstituted conjugated polymers, several precursor routes have been introduced over the last decades.²⁻⁴ Two of these precursor routes were developed in our group, namely the sulfinyl⁵ and the dithiocarbamate^{6,7} precursor routes. These precursor routes involve the formation of an intermediate non-conjugated, soluble and thus processable, precursor polymer, which can be converted into the fully conjugated polymer after processing. Initially, many of these precursor routes were developed for poly(*p*-phenylene vinylene) and its derivatives, as a result of the discovery of electroluminescence for this type of polymers.⁸ However, they can be readily adapted for other conjugated polymers, such as the poly(thienylene vinylene)s (PTV) described in this chapter. PTVs have lower band gaps as compared to polythiophenes because of two effects. The first effect is a decrease in the overall aromatic character, allowing better π -electron delocalization due to less electron confinement. The second effect, which may play a role, is a potential limitation of the rotational disorder due to the presence of ethylene linkages of defined configuration. For PTV a band gap of 1.7 eV¹³ is reported and various structural modifications of PTV led to materials with band gaps as low as 1.2 eV.¹⁴

Previous studies have shown that unsubstituted PTV is a suitable low band gap donor material for polymer:fullerene solar cells. The reported devices containing this polymer were prepared from a soluble precursor polymer synthesized *via* the dithiocarbamate precursor route. The bulk heterojunction photovoltaic devices using PCBM as acceptor showed a

short-circuit current up to 4 mA/cm² and a open-circuit voltage of 0.35 V under AM 1.5 white light illumination. Power conversion efficiencies of around 0.6% were reported.⁹ In this chapter we use two soluble PTVs (**BOP-PTV** and **C₈-PTV**). Due to the better processing capacities better solar cell performance is anticipated.

6.2. Transport properties of C₈-PTV and BOP-PTV

Besides suitable energy levels these two new donor materials should also possess appropriate charge carrier transport properties. To test whether this is the case hole only devices have been made resulting in a hole mobility of 3×10^{-9} m²/Vs for **BOP-PTV** and 5×10^{-9} m²/Vs for **C₈-PTV**, which is slightly lower as compared to the hole mobility of 3×10^{-8} m²/Vs for P3HT,¹⁶ but nevertheless encouraging when compared to other novel low band gap donors (Figure 3). Combined with the good transport properties of PCBM no space charge effects are expected, at least for moderately thick films, similar to those used in MDMO-PPV:PCBM blends.

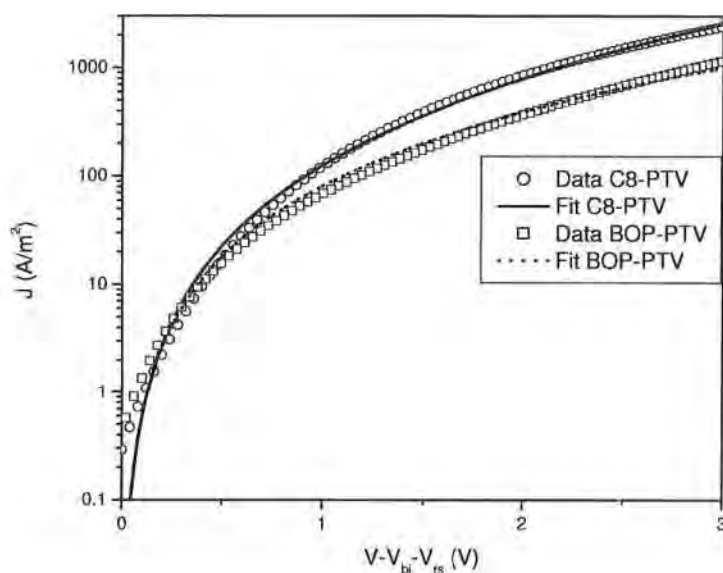


Figure 3. Current density versus voltage, corrected for built in voltage and series resistance of a **BOP-PTV** and **C8-PTV** hole only device. Data (symbols) is fitted (line) using a space charge limited current with a field dependent mobility.

6.3. Cyclic Voltammetry

The cyclic voltammetry data for **BOP-PTV** and **C8-PTV** are not yet available. In Table 1 the HOMO and LUMO levels of previously synthesized comparable PTV derivatives are presented. There is a high similarity for dibutylphenyl-PTV with **BOP-PTV** and for C6-PTV with **C8-PTV**. From the table the low band gap character of these comparable polymers is evident. The differences between the optical and electrochemical band gaps are a result of the fact that during the electrochemical measurements the

electrolyte ion transport through thin films of conjugated polymers with apolar alkyl side groups is somewhat restricted, leading to the requirement of a small overpotential. It should be noted that the optical characterization of **BOP-PTV** and **C8-PTV** has revealed that also these polymers possess a low optical band gap which is comparable to the polymers presented in Table 1 (*vide infra*).

Polymer	HOMO (eV)	LUMO (eV)	Electrochemical Band gap	Optical band gap
Dibutylphenyl- PTV	-5.24	-3.26	1.98	1.8
C6-PTV	-5.17	-3.24	1.93	1.7

Table 1. The HOMO and LUMO energy levels, the electrochemical band gap and the optical band gap.¹⁵

6.4. Solar Cells

Solar cells were made by sandwiching the conjugated polymers in between an ITO/PEDOT:PSS anode and a samarium/aluminum cathode. The best obtained performance for bulk heterojunction solar cells with **BOP-PTV** or **C8-PTV** as donor polymer and PCBM as acceptor material are depicted in Figure 4 and Table 1. For a 1:4 **BOP-PTV**:PCBM solar cell spincoated from chloroform the highest achieved efficiency is 0.80 %. This cell has an open circuit voltage (V_{oc}) of 0.67 V and fill factors of 60% and higher for films with a thickness of more than 200 nm, indicating good charge transport properties of the blend. For a 1:4 **C8-PTV**:PCBM solar cell spincoated from ortho dichlorobenzene the highest achieved efficiency is 0.92 %. The open circuit voltage (V_{oc}) of **C8-PTV** is 0.47 V, this is 0.2 V less compared to **BOP-PTV**. This difference in V_{oc} most likely originates from the differences

in the HOMO levels of both polymers (*cf.* Table 2). Apparently, the introduction of phenyl substituents results in a lowering of the HOMO energy level, which translates itself in a larger V_{oc} . The difference in short circuit currents can be explained by the differences in absorption of both films, which will be discussed in the next section. Notwithstanding, the short circuit currents (J_{sc}) are inferior compared to model systems, which results in the observed efficiencies below 1.0 %.

	V_{oc} (V)	J_{sc} (A/m ²)	Efficiency (%)
1:4 C₈-PTV:PCBM	0.47	52.8	0.92
1:2 BOP-PTV:PCBM	0.67	18.3	0.80

Table 2. Solar cells performance for **BOP-PTV** and **C₈-PTV:PCBM**.

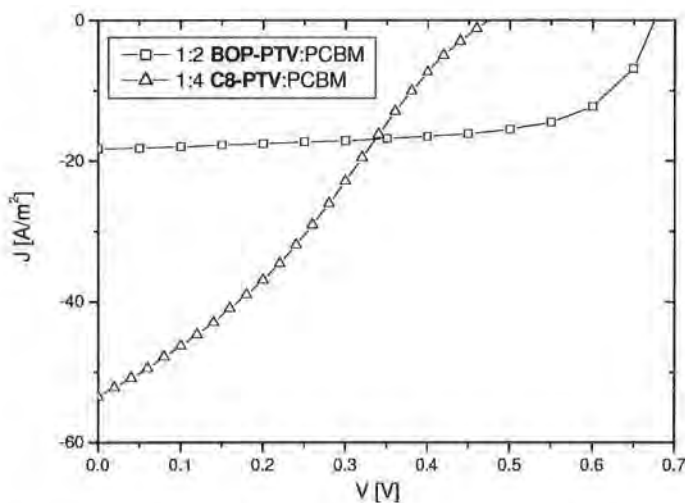


Figure 4. Current density versus voltage of selected **BOP-PTV** and **C₈-PTV:PCBM** solar cells under illumination of a 1000 W/m² simulated solar spectrum.

6.5. Absorption

To understand the moderate efficiencies for these new narrow band gap polymers, the absolute absorption in thin film has been determined. To this end thin films of P3HT, **BOP-PTV** and **C8-PTV** were prepared from the same solvent, *i.e.* chloroform. After measuring the film thickness, the absolute absorbance as a function of the wavelength can be readily determined (Figure 5). Furthermore, the optical band gap can be derived from the low energy side tangent to the π - π^* transition. The band gap and the absolute absorptivity in a thin film are presented in Table 3.

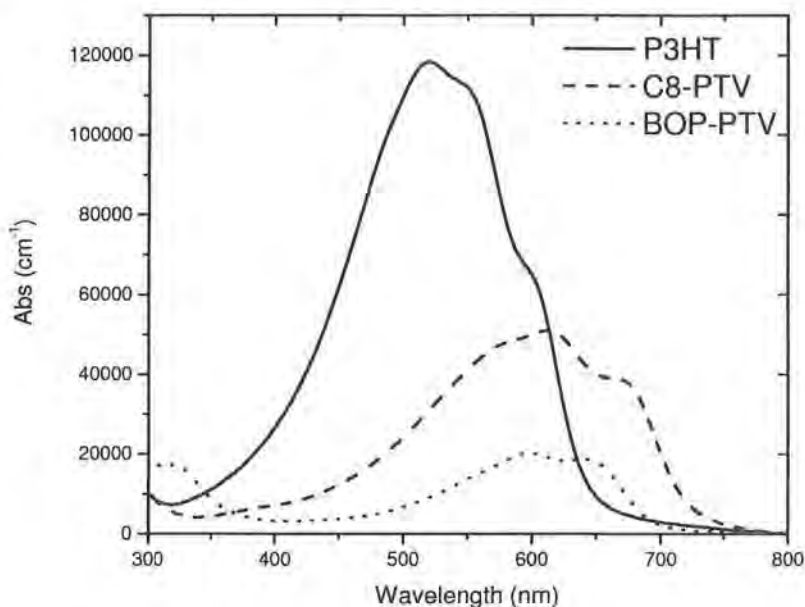


Figure 5. The absolute absorbance in function of the wavelength for spincoated films of P3HT, **BOP-PTV** and **C8-PTV**.

Polymer	Thin film absolute absorptivity (cm ⁻¹)	Solution extinction coefficient (M ⁻¹ cm ⁻¹)	Optical band gap (eV)
BOP-PTV	20135	10453	1.78
C8-PTV	50998	4240	1.70
P3HT	118334	8000	1.90

Table 3. Thin film absolute absorptivities, solution extinction coefficients and optical band gaps of **BOP-PTV**, **C8-PTV** and **P3HT**.

The moderate short circuit currents (J_{sc}) of **BOP-PTV** and **C8-PTV** compared to **P3HT** can be understood in terms of the differences in absolute absorptivities. Since the investigated low band gap polymers have the same backbone, the band gap will depend to a large degree on the rotational disorder around the single bonds between the monomeric units and to a lesser degree probably also on the nature of the side groups.¹⁰ The orbital overlap (and hence E_g) varies approximately with the cosine of the twist angle (θ),¹¹ so that any departure from coplanarity will result in an increase of E_g and a blue shift of the absorption. Potentially, the deviation from planarity is increasing from **C8-PTV** to **BOP-PTV** due to the bigger steric hindrance of the disubstitution of the thiophene unit with octylphenyl groups as compared to monosubstitution with an octyl group. However, from Table 3 it can be seen that these polymers have almost the same optical band gap, with the band gap of **BOP-PTV** indeed being slightly wider. This small difference indicates that the average dihedral angle is not very different for both polymers. Notwithstanding, it can be anticipated that sterically demanding substituents will increase the likelihood of larger steric defects (twists and bends) in the polymer chain. When these defects occur at distances further apart than *circa* 10 repeating units, no effect on

the band gap can be expected (in agreement with the observations). On the other hand the resulting disorder will effect the conjugation significantly and can potentially result in a lowering of the absorptivity. In this case, this would lead to a lower absorptivity for **BOP-PTV** as compared to **C8-PTV**. This is in agreement with our observations in Figure 5. Interestingly, also the extinction coefficients of both polymers in solution have been determined and an opposite behavior is found with the extinction coefficient of **BOP-PTV** being higher than the one found for **C8-PTV**. Apparently, the sterically demanding side groups have a large impact on the density and packing in polymer films and as a result the **C8-PTV** exhibits a better absorptivity in thin film. In contrast, in solution no packing effects are observed, thus explaining the opposite behavior. It is noteworthy that the absorptivity of P3HT in a thin film is higher due to the structural order and even crystalline character of these films.

6.6. Conclusion

In this chapter we introduce two soluble low band gap PTVs (**BOP-PTV** and **C8-PTV**). Due to the better processing capacities we have a better solar cell performance than for the unsubstituted PTV. It is demonstrated that these narrow band gap polymers have a sufficiently high hole mobility. Notwithstanding, the short circuit currents (J_{sc}) are still inferior compared to model systems resulting in low efficiencies. The moderate short circuit currents (J_{sc}) of **BOP-PTV** and **C8-PTV** compared to P3HT can be explained by their low absorptivity in thin films. There should still be quite some room for improvements for this class of materials by manipulation of the side groups. It can be expected that the incorporation of side groups inducing a smaller deviation of the planarity and a better packing, will result in polymers with a lower band gap and, more importantly, a higher thin film absorptivity.

6.7. Experimental

6.7.1. Methods

Ultraviolet visible (UV-Vis) spectroscopy was performed on a VARIAN CARY 500 UV-Vis-NIR spectrophotometer (interval: 1 nm, scan rate: 600 nm/min, continuous run from 200 to 800 nm). Electrochemical properties were measured with an Eco Chemie Autolab PGSTAT 20 Potentiostat/Galvanostat using a conventional three-electrode cell (electrolyte: 0.1 mol/L TBAPF₆ in anhydrous CH₃CN) with an Ag/AgNO₃ reference electrode (0.01 mol/L AgNO₃, 0.10 mol/L TBAPF₆ and CH₃CN), a platinum counter electrode and an Indium-Tin Oxide (ITO) coated glass substrate as working electrode. Cyclic voltammograms were recorded at 50 mV/s under N₂ atmosphere. All electrochemical potentials have been referenced to a known standard, ferrocene/ferrocinium, which is estimated to have an oxidation potential of -4.98 V *vs.* Vacuum.

6.7.2. Device preparation

All devices were made on pre-patterned ITO/Glass samples supplied by Philips. After a standardized cleaning procedure in a wet station, a layer of PEDOT:PSS (Poly(3,4-ethylenedioxythiophene) doped with Poly(styrenesulfonate) was spin coated on top of the ITO. This layer has a thickness of 50 to 60 nm. The aqueous PEDOT:PSS solution (CLEVIOS P VP AI 4083 by H.C. Starck) was spin coated in exactly the same way for each substrate (10 seconds at 500 rpm followed by 50 seconds at 1500 rpm).

On top of the PEDOT:PSS, a layer of either **BOP-PTV** or **C8-PTV** was spin coated inside the glovebox. Table 4 shows the spin procedures and concentrations for both precursor polymers.

Polymer	Solvent	Concentration (mg/mL)	Spin program (lid ,speed (rpm), acceleration (rpm/s),time (s))
BOP-PTV	CHCl ₃	15	Close, 300 , 500, 4 Close, 500, 500, 60 Open, 500, 500, 30
C8-PTV	ODCB	10	Open, 300, 100, 120 Open, 800, 200, 30

Table 4. Utilized spin coating procedures and concentrations for both polymers.

Finally, as a cathode, a metal top contact was evaporated, consisting of 5 nm samarium with 100 nm aluminum on top.

6.7.3. Device measurements

All measurements were performed in a glove box, under nitrogen atmosphere. Current *versus* voltage characteristics were determined using a Keithly 2400 Source meter. The device current was registered using a Labview program, while sweeping a voltage across the device, going up from 0 V to a positive voltage of 3.5 V, then down to -2 V and up again to 0 V. The thicknesses of all spin coated polymers, including the PEDOT:PSS were determined using a Dektak 6M Stylus Profiler.

6.8. References

- (1) Irwin, M. D.; Buchholz, B.; Hains, A. W.; Chang, R. P. H. and Marks, T. *J. Proc. Natl. Acad. Sci. USA* **2008**, 105, 2783.

- (2) Gilch H.G. and Wheelwright, W. L. *J. Polymer Science* **1966**, 4, 1337.
- (3) Wessling R. A. *J. Polymer Science* **1985**, 72, 55.
- (4) Son, S.; Dodabalapur, A.; Lovinger, A. J. and Galvin, M. E. *Science*, **1995**, 269, 376.
- (5) Issaris, A.; Vanderzande, D. and Gelan, J. *Polymer* **1997**, 38, (10), 2571.
- (6) Henckens, A.; Colladet, K.; Fourier, S.; Cleij, T. J.; Lutsen, L.; Gelan, J. and Vanderzande, D. *Macromolecules* **2005**, 38, 19.
- (7) Henckens, A.; Duyssens, I.; Lutsen, L.; Vanderzande, D. and Cleij, T. J. *Polymer* **2006**, 47, 123.
- (8) Burroughes, J. H.; Bradley, D. D. C. and Brown, A. R. *Nature* **1990**, 347, 539.
- (9) Nguyen, L. H.; Günes, S.; Neugebauer, H.; Sariciftci, N. S.; Banishoeib, F.; Henckens, A.; Cleij, T.; Lutsen, L. and Vanderzande, D. *Solar Energy Mat. & Solar Cells* **2006**, 90, 2815.
- (10) Roncali, J. *Chem. Rev.* **1997**, 97, (1), 173.
- (11) Bredas, J. L.; Street, G. B. and Themans, B. *J. Chem. Phys.* **1985**, 83, (3), 1323.
- (12) Winder, C. and Sariciftci, N. S. *J. Mater. Chem.* **2004**, 14, 1077.
- (13) Eckhardt, H.; Shacklette, L. W. and Jen, K. Y. *J. Chem. Phys.* **1989**, 91, (2), 1303.
- (14) Cheng, H. and Elsenbaumer, R. L. *J. Chem. Soc.-Chem. Commun.* **1995**, (14), 1451.
- (15) Fourier, S.; Yperman, J. and Cleij, T. J. *Dissertation Hasselt University* **2007**, 2451, (14), 93.
- (16) Mihailitchi, V. D.; Xie, H.; de Boer, B.; Koster, L. J. A. and Blom, P. W. M. *Adv. Funct. Mater* **2006**, 16, 699.

Summary

Nowadays, most of the energy is derived from fossil fuels and nuclear processes. However, these resources are limited and their use can have a serious environmental and political impact. Hence, a transition in energy consumption and production is desirable. In this respect, renewable energy sources are of considerable interest. However, thus far they make up only a limited part of the total energy production.

In **Chapter 1** it is described how organic photovoltaics offer significant technological potential as an alternative renewable source for electrical energy. Solar cells based on conjugated polymeric materials have several advantages, such as potential flexibility, low manufacturing costs and straightforward processing. In current examples of such solar cells, which can already reach efficiencies as high as 5.15%, a p-type conjugated polymer is combined with a soluble derivative of C₆₀, PCBM, as the electron acceptor. However, an n-type polymeric alternative for PCBM is of interest to facilitate the formation of an optimal and stable morphology. Moreover, the use of polymer-polymer solar cells will lead to a significant increase of the photon harvesting, which in turn may improve the overall efficiency. A further improvement of the efficiency can also be achieved by an adjustment of the energy levels either on the donor or on the acceptor side. For example, raising the LUMO of the acceptor will directly result in a higher V_{oc} without affecting the absorption of the cell. Hence, an n-type conjugated material with a polymeric nature with a higher LUMO than PCBM is of considerable interest, since this would combine both above mentioned aspects.

In **Chapter 2** an overview of existing n-type conjugated polymers as well as an outline of our search for a novel class of n-type conjugated polymers are presented. In general, the n-type polymers reported in literature can be divided into two different classes. In the first class the n-type behavior is

introduced by electron accepting substituents like cyano groups attached to the polymer backbone. In the second class, the enhanced electron affinity is related to the aromatic building blocks containing electron withdrawing groups like N or/and S, which are incorporated into the conjugated backbone. The aim of the research presented in this dissertation is the design and development of an entirely new class of n-type conjugated polymers. It was proposed by us that this goal could be achieved by introducing non-alternant cyclopenta-fused polycyclic aromatic hydrocarbon repeating units into the conjugated polymer backbone. A first example of such a polymer, poly(fluoranthene vinylene) (PFV), is presented in this chapter. Recent progress in the synthesis of substructures of C_{60} has provided us with an opportunity to create this novel polymer. PFV exhibits unusual n-type behavior. The straightforward synthesis towards this novel polymer as developed in our laboratory provides the opportunity to use PFV as a platform for further functionalization, thus allowing for a further adjustment of the optoelectronic properties.

In **chapter 3**, a universal synthesis route is presented towards alkyl derivatives of PFV, *i.e.* hexyl-PFV and dodecyl-PFV, which display enhanced solubility. The introduction of solubilizing alkyl side chains, leads to a significantly enhanced purity and processability as compared to unsubstituted PFV. Additional CELIV mobility measurements on dodecyl-PFV, a typical representative of this novel class of polymers with a high purity, reveal an excellent electron mobility, $\mu_e = 1.4 \cdot 10^{-8} \text{ m}^2/\text{Vs}$, confirming the excellent n-type characteristics of this novel class of conjugated polymers. Notwithstanding, the position of the energy levels is not yet optimal to facilitate charge transfer in a typical bulk-heterojunction solar cell. Hence, in the future further tuning of the energy levels will be required for organic solar cell applications.

In **chapter 4**, it is proven that the non-alternant character of fluoranthene ($C_{16}H_{10}$) is indeed responsible for the n-type behavior. For this proof an

additional conjugated polymer (PPyV) containing an alternant PAH, i.e. pyrene ($C_{16}H_{10}$), has been synthesized and the transport properties of this polymer have been compared to those of dodecyl-PFV. While dodecyl-PFV exhibits typical n-type behavior, PPyV is a normal p-type conjugated polymer. It is demonstrated that PPyV has a hole mobility of $\mu_h = 1.5 \cdot 10^{-10} \text{ m}^2/\text{Vs}$. It can be concluded that non-alternant cyclo-penta fused polycyclic aromatic hydrocarbons are efficient structural elements to achieve n-type characteristics in conjugated polymers, whereas alternant structural elements induce p-type behavior.

Chapter 5 focuses on a more in depth studied of precursor routes towards conjugated polymers. Special attention is focused on the question whether it is possible to manipulate such routes to obtain well-defined block-type copolymers, which well may generate a more organized morphology. Such enhanced morphologies are of interest for improving the performance of conjugated polymer based devices. In this chapter various aspects of the radical polymerization found for the sulfinyl precursor route are studied and the question is addressed to what extent a living polymerization for this type of polymerization is realistic. In addition, the radical copolymerization of 1-(chloromethyl)-4-[(n-octylsulfinyl)methyl] benzene and n-butyl acrylate was investigated and the obtained PPV and PnBuA based copolymer was tested in devices. Green light emission and a turn-on voltage of 3.0 V were observed from a single-layer device. Furthermore, mobility measurements reveal that PPV-co-PnBuA has a sufficiently high hole mobility, $\mu_h = 4 \cdot 10^{-9} \text{ m}^2/\text{Vs}$, for use in optoelectronic applications.

Finally, **Chapter 6** focuses on another strategy for increasing the solar cell performance. Whereas chapters 2, 3 and 4 have emphasized the design of new n-type materials, which may result in a favorable adjustment of the energy levels at the acceptor side, chapter 6 focuses on the tailoring of the energy levels at the donor side, by developing novel p-type materials. Upon

lowering the LUMO of the donor, and thus narrowing the polymer band gap, the absorption is shifted towards lower energy, while maintaining a constant open-circuit voltage. In this way the photocurrent is improved, due to an enhanced overlap between the donor absorption and the solar spectrum. The opto-electronic characterization of two of these low band gap PTV derivatives, *e.g.* BOP-PTV and C8-PTV, are presented in this chapter. The enhanced processability of these novel polymers results in an improved solar cell performance as compared to unsubstituted PTV. Although these narrow band gap polymers have a sufficiently high hole mobility, the observed solar cell efficiencies are relatively low compared to P3HT, the most widely used polymer in this regard. This can be explained by the low absolute absorbance in thin films of these materials. It can be expected that the incorporation of side groups inducing a smaller deviation of the planarity and a better packing, will result in polymers with a lower band gap and, more importantly, a higher thin film absorptivity.

Finally, it is worth mentioning that the commercialization of organic photovoltaics is determined by three factors, *i.e.* efficiency, lifetime and cost. Polymer bulk heterojunction solar cells have the potential to score well on all of these issues, giving them significant market potential. However, several issues remain and it is clear that new and improved materials are necessary. The work described in this thesis certainly contributes to this goal by presenting several novel conjugated polymers. The best example is our discovery of a novel class of n-type conjugated polymers. These polymers are based on non-alternant cyclo-penta fused polycyclic aromatic hydrocarbons, which prove to be efficient structural elements to achieve n-type characteristics in conjugated polymers. As can be clearly seen in this thesis, our integrative research approach focusing on design, synthesis, characterization, device manufacturing and testing can provide valuable insights into the various possible improvements of organic photovoltaics.

Samenvatting

Vandaag de dag wordt het merendeel van onze energie opgewekt uit fossiele en nucleaire brandstoffen. Slinkende olievoorraden en een groeiend milieubewustzijn vormen de aanleiding voor een toename in het onderzoek naar goedkope en milieuvriendelijke energiebronnen. Ondanks deze problematiek is de productie via groene energiebronnen nog beperkt.

Na het lezen van **hoofdstuk 1** zal het potentieel van organische zonnecellen als alternatieve energiebron duidelijk zijn. Zonnecellen gebaseerd op geconjugeerde polymeren hebben volgende voordelen: buigbaarheid, een lage productiekost en een eenvoudige verwerkbaarheid. Dergelijke zonnecellen bestaan uit een p-type polymeer en een oplosbaar derivaat van C_{60} namelijk PCBM als elektron acceptor. De best werkende fotovoltäische cel van dit type heeft een efficiëntie van 5,15%. Voor de verdere commercialisatie van deze innovatieve techniek is er een zoektocht naar een n-type polymeer alternatief voor PCBM. Een n-type alternatief kan de vorming van een optimale en stabiele morfologie vereenvoudigen. Anderzijds kan het gebruik van een polymeer:polymeer zonnecel leiden tot een verhoogde absorptie van fotonen wat direct zal leiden tot een verbeterde efficiëntie. Een verdere verhoging van de efficiëntie kan bereikt worden door het verder tunen van de energieniveau's van zowel de donor als de acceptor. Zo zal een verhoging van de LUMO van de acceptor leiden tot een hogere V_{oc} zonder de absorptie van de cel te beïnvloeden. Indien men bovenstaande aspecten in acht neemt is het duidelijk dat er een sterke interesse bestaat voor een n-type geconjugeerd polymeer met hogere LUMO dan PCBM.

In **hoofdstuk 2** wordt er een historische achtergrond geschetst van de bestaande n-type geconjugeerde polymeren. In het algemeen wordt dit type polymeren onderverdeeld in 2 klassen. In de eerste klasse wordt het n-type gedrag veroorzaakt door elektronenzuigende groepen zoals CN te plaatsen

op de backbone van het polymeer. In de tweede klasse wordt de verhoogde elektronenaffiniteit verkregen door ingebouwde aromatische bouwstenen die elektronegatieve groepen zoals N of/en S bevatten. De doelstelling van het onderzoek, voorgesteld in deze thesis, is de ontwikkeling en het ontwerp van een totaal nieuwe klasse van elektron accepterende geconjugeerde polymeren. Recente vooruitgang in de synthese van substructuren van C_{60} heeft ons op het idee gebracht om niet-alternerende polycyclisch aromatische koolwaterstoffen (PAH) in te bouwen in de hoofdketen van het geconjugeerde polymeer. Een eerste voorbeeld van een dergelijk polymeer, poly(fluorantheen vinyleen) (PFV) wordt gegeven in dit hoofdstuk. De wijze waarop dit nieuwe n-type polymeer wordt gesynthetiseerd laat verdere functionalisatie en een nauwkeurige instelling van de opto-elektronische eigenschappen toe.

In **hoofdstuk 3** wordt een universele syntheseroute naar deze oplosbare PFV-derivaten voorgesteld. Functionalisatie met oplosbare C_6 en C_{12} zijstaarten leidt tot een verhoogde zuiverheid en verwerkbaarheid vergeleken met de niet-gesubstitueerde PFV. CELIV mobiliteitsmetingen van het C_{12} derivaat bevestigen het ongewone n-type gedrag van deze nieuwe klasse van geconjugeerde polymeren. Ook werd een hoge elektronenmobiliteit, $\mu_e = 1.4 \cdot 10^{-4} \text{ cm}^2/\text{Vs}$ vastgesteld. Toch is de positie van de LUMO niet optimaal voor ladingsoverdracht in organische zonnecellen. Verdere optimalisatie van de energieniveau's van deze interessante n-type materialen door chemische modificatie zal nodig zijn alvorens ze kunnen worden gebruikt in fotonvoltaïsche cellen.

In **hoofdstuk 4** wordt bewezen dat het niet-alternerende karakter van fluorantheen ($C_{16}H_{10}$) verantwoordelijk is voor het elektron accepterend n-type gedrag. Om tot deze conclusie te komen werd er ook een geconjugeerd polymeer (PPyV) gesynthetiseerd dat een sterk gelijkend, maar alternerende PAH bevat, namelijk pyreen ($C_{16}H_{10}$). Van deze beide

polymeren waarvan de aromatische kernen structurele isomeren zijn werden de transporteigenschaften vergeleken.

Terwijl dodecyl-PFV een n-type polymeer is, is PPyV een normaal p-type geconjugeerd polymeer. Het is dus duidelijk dat niet-alternerende polycyclisch aromatische koolwaterstoffen efficiënte structurelementen zijn voor het verkrijgen van n-type gedrag in geconjugeerde polymeren.

In **hoofdstuk 5** worden meerdere aspecten van de radicalaire sulfinyl precursor polymerisatie van dichterbij bekeken. Ook werd er gekeken worden bij welke condities een levende polymerisatie voor dit soort polymerisaties mogelijk is. Het uiteindelijke doel van dit hoofdstuk is om deze polymerisatiemethode zo te beïnvloeden dat blokachtige copolymeren mogelijk worden. Zulke copolymeren leiden tot een meer geordende morfologie, wat op zijn beurt aanleiding kan geven tot verbeterde device eigenschappen. Als voorbeeld van een dergelijk copymeer werd er een radicalaire copolymerisatie uitgevoerd van 1-(chloromethyl)-4-[(n-octylsulfinyl)methyl] benzeen en n-butyl acrylaat. Het verkregen copolymeer PPV-co-PnBuA werd onderzocht en getest in devices. Een gefabriceerde enkel laagse LEDs emiteerde groen licht en ging aan bij 3.0V. Uit mobiliteitsmeting volgt dat het copolymeer een gaten mobiliteit heeft van $4 \cdot 10^{-9} \text{ m}^2/\text{Vs}$. Deze hoge waarde in vergelijking met normaal PPV maakt gebruik in optoelektronische toepassingen mogelijk.

Het onderzoek in **hoofdstuk 6** spitst zich toe op het verhogen van de zonnecel efficiëntie door het verlagen van de bandgap van het geconjugeerde polymeer. De strategie die gebruikt werd in hoofdstukken 2, 3 en 4 was de ontwikkeling van nieuwe n-type materialen met een verhoogde LUMO. Door verlaging van de LUMO van de donor krijgt het polymeer een kleinere band gap en verschuift de absorptie naar lagere energie terwijl de V_{oc} onveranderd blijft. Door de verbeterde overlapping tussen de donorabsorptie en het zonnenspectrum gaat de fotostroom omhoog. In dit hoofdstuk worden de opto-elektronische eigenschappen van

twee low band gap polymeren, te weten BOP-PTV en C8-PTV, gepresenteerd. Deze gesubstitueerde PTV's vertonen een betere verwerkbaarheid in zonnecellen vergeleken met het ongesubstitueerde PTV. Ondanks de hoge gatenmobiliteit zijn de zonnecefficiënties relatief laag in vergelijking met de modelverbinding P3HT. Dit kan verklaard worden door de lage absolute absorptie van deze materialen in dunne film. Door verdere chemische ontwikkeling kan de afwijking van planariteit potentieel verminderd worden, hetgeen kan leiden tot een betere polymeer pakking en een verhoogde licht absorptie.

Tot slot is het belangrijk te vermelden dat de commercialisatie van organische zonnecellen pas mogelijk is indien er een optimaal evenwicht bestaat tussen een drietal factoren, te weten efficiëntie, levensduur en kostprijs. Bulk heterojunctie zonnecellen die volledig gebaseerd zijn op polymeren hebben zeer veel potentieel om de markt te veroveren. Echter om deze commercialisatie teweeg te brengen is een verdere zoektocht naar nieuwe materialen met verbeterde eigenschappen van groot belang. Het werk beschreven in deze thesis draagt zeker aan deze zoektocht bij gezien het feit dat een nieuwe klasse van geconjugeerde polymeren is ontwikkeld, op basis van niet-alternerende polycyclisch aromatische koolwaterstoffen. Het is bewezen dat deze structurelementen gebruikt kunnen worden om n-type karakter in geconjugeerde polymeren te creëren.

Het is duidelijk dat ons interdisciplinair onderzoek, dat gericht is op zowel de ontwikkeling, synthese en karakterisatie van nieuwe geconjugeerde polymeren als de toepassing van deze polymeren in devices, belangrijke inzichten heeft verschaft met betrekking tot de verschillende strategieën om tot verbeterde organische zonnecellen te komen.

Dankwoord

In de komende pagina's zal ik mijn dank proberen te betuigen, voor de samenwerking met tal van mensen, bij het tot stand komen van deze thesis. Maar ik weet nu al dat dit een zeer moeilijke taak is. Want welke superlatieven ik ook gebruik, ze zullen niet volstaan om jullie te bedanken voor deze fantastische periode.

Gedurende deze vier jaren kreeg ik de kans om mezelf te ontplooien en om samen te werken met mensen uit andere landen en uit andere vakgebieden. Ik ben ervan overtuigd dat ik door deze internationale ervaring vaardigheden heb ontwikkeld die mij in de toekomst dan ook verder zullen helpen.

De eerste persoon die ik wil danken is mijn pas overleden grootvader, "Pa", (2 mei 2008). Dit woord van dank is dan ook een eerbetoon aan hem. Pa ik wil je bedanken voor de onvergetelijke tijd die ik met jou mocht en kon doorbrengen. Ik zal al deze momenten koesteren en er met een glimlach naar terug kijken. Zonder jou had ik nooit gestaan waar ik nu sta. Je hebt me zoveel geleerd over het leven, je stond altijd voor me klaar, maar nu ben je er niet meer. Ik draag ook deze thesis op aan jou.

Ik wil Thomas Cleij bedanken voor de excellente invulling van de taak van promotor. Iedere (niet) wetenschappelijke babbel gaf me inzicht en inspiratie voor een volgende stap. Dank voor de fijne trip naar de USA. Hopelijk kunnen we onze passie voor lekker eten verder blijven delen.

Mijn copromotor Dirk Vanderzande wil ik danken voor de kans die ik kreeg om in deze groep te mogen doctoreren. Vanaf het begin van mijn opleiding kreeg ik een passie voor synthese, het creëren van nieuwe dingen vanuit bestaande elementen, klinkt voor mij als iets groots. Bedankt voor je synthetische kennis, voor de onvergetelijke zeiltrip en de gewone pint aan de toog.

Peter Adriaensens en Jan Gelan wil ik bedanken voor de NMR-karakterisatie. Jullie zijn onmisbaar en zorgen voor een sterke ondersteuning van deze synthese groep.

I got the opportunity to do research in several other groups in Europe. Laurence Lutsen, I would like to thank you for helping me with this visits. This decision for going abroad was one of the most important steps during my Ph.D.

Ik ben het Fonds Wetenschappelijk Onderzoek-Vlaanderen (FWO) en de "European Science Foundation" (ESF) erkentelijk voor de financiële steun. Via mijn FWO beurs kon ik genieten van enorme vrijheid in de keuze van mijn onderzoek. Via het ESF was het mogelijk om als gast onderzoeker ontvangen te worden in de groep van Prof. dr. ir. Serdar Sariciftci in Linz en in de groep van Prof. dr. ir. Paul Blom en Prof. dr. Bert de Boer in Groningen. Deze buitenlandse verblijven waren over de hele lijn positief en hebben een grote invloed gehad op de inhoud van deze thesis.

I want to thank Prof. dr. ir. Serdar Sariciftci for giving me the opportunity for visiting LIOS. Thanks to Christoph, Almantas, Anita and Robert, I learnt a lot about device preparation and spectroscopic techniques during my lovely stay in Linz.

Zo kom ik bij het hoogtepunt van mijn doctoraat, mijn verblijf in Groningen. Welke woorden ik ook zal gebruiken ze zullen niet volstaan om mijn dank uit te spreken. Prof. dr. ir. Paul Blom en Prof. dr. Bert de Boer bedankt dat ik de MEPOS groep mocht vervolledigen gedurende 9 maanden. Het onderzoek dat ik bij jullie heb gedaan heeft van mijn thesis een compleet verhaal gemaakt van synthese tot device karakteristie. Ik wil graag de voltallige MEPOS groep bedanken voor de enorme goede werksfeer.

Graag een specifieke vermelding voor de volgende personen: Lenes, Kuik, Porné, Hylke, Herman, Auke, Steve, Johan, Jan H., Eek en Krisztina. Jullie stonden letterlijk 24 uur per dag klaar voor mij.

Daarnaast heb ik ook nog de kans gehad om kunnen samen te werken met verschillende mensen uit andere onderzoeksgroepen. Zo wil ik dr. Dirk Veldman en Prof. dr. René Janssen van de TUEindhoven danken voor de spectroscopische metingen. I would like to thank dr. Antoine Debuigne and Prof. dr. Christophe Detrembleur from the Univesité de Liège for the hospitality during my visits. Antoine thanks for the good working conditions and the nice discussions we had in this collaboration.

Natuurlijk ben ik ook mijn eigen collega's van organische dankbaar voor de fijne werksfeer en alle andere activiteiten. Anja, Kristof, Jérôme, Lien, Ine, Iris, Steven, Veerle, Jan, Wouter, Bert, Jimmy, Wibren, Raoul, Joke, Zarina, Juliette, Ans, Fré, Sarah, Hanne, Fateme, Sylvain, Sofie, Burak en Lydia bedankt voor de wetenschappelijke hulp, de voetbalwedstrijdjes, de kooklessen, het labo-weekend, de gezellige terrasjes, het leven zoals het is (de bevalling, bob de bouwer, de trouwerij), en nog zoveel meer waar ik nu niet zo direct aan denk. Ook dank aan de mensen van anorganische en het IMO . Tevens wil ik de mensen achter de schermen Jos, Christel, Koen, Huguette, Jan en het voltallige SBG secretariaat bedanken.

Tot slot wil ik mijn ouders bedanken voor alle steun en kansen die ik gekregen heb om mij breed te kunnen ontplooien. Ik heb de luxe gehad om op te groeien in een gezin van vier broers. Ik ben ook absoluut trots dat al mijn broers het goed doen.

Bedankt allemaal!!!

